

Sandra Pérez Rodríguez

# Macrophage-bacteria interactions: a 3D microfluidics-based approach

Director/es

García Aznar, José Manuel  
Gonzalo Asensio, Jesús Ángel

<http://zaguan.unizar.es/collection/Tesis>

© Universidad de Zaragoza  
Servicio de Publicaciones

ISSN 2254-7606



**Universidad**  
Zaragoza

Tesis Doctoral

**MACROPHAGE-BACTERIA INTERACTIONS: A 3D  
MICROFLUIDICS-BASED APPROACH**

Autor

**Sandra Pérez Rodríguez**

Director/es

García Aznar, José Manuel  
Gonzalo Asensio, Jesús Ángel

**UNIVERSIDAD DE ZARAGOZA**  
**Escuela de Doctorado**

Programa de Doctorado en Ingeniería Biomédica

2022





**Universidad**  
Zaragoza



Instituto Universitario de Investigación  
**en Ingeniería de Aragón**  
**Universidad Zaragoza**

# MACROPHAGE-BACTERIA INTERACTIONS: A 3D MICROFLUIDICS- BASED APPROACH



Dissertation presented by

**Sandra Pérez Rodríguez**

for the degree of *Doctor of Philosophy in Biomedical Engineering*

Faculty advisors

**José Manuel García Aznar**

**Jesús Ángel Gonzalo Asensio**



*A mis padres y hermano*





# CONTENT

Agradecimientos / Acknowledgements .....	v
Abstract .....	vii
Resumen .....	ix
List of figures .....	xi
List of tables.....	xii
List of abbreviations .....	xiii
<b>1. INTRODUCTION .....</b>	<b>1</b>
1.1. Background.....	3
1.1.1. Pathogen bacteria and immune system .....	3
1.1.1.1. The role of macrophages in immunity.....	5
1.1.1.2. Salmonella typhimurium infection .....	7
1.1.1.3. Mycobacterium tuberculosis infection.....	10
1.1.2. <i>In vitro</i> bacterial research * .....	12
1.1.2.1. Traditional methods .....	13
1.1.2.2. Microfluidics .....	14
1.1.2.3. Bacteria in microfluidics .....	14
i. Device with linear channels .....	17
ii. Devices with mixing channels .....	17
iii. Devices with multiple floors.....	18
iv. Porous devices .....	18
v. Topographic devices .....	19
vi. Droplet microfluidics.....	19
1.1.2.4. Comparison between traditional methods and microfluidics.....	20
i. Reproducibility of results .....	20
ii. Calculating migration rates .....	21
iii. Versatility of materials and designs .....	21
iv. Small size and volume .....	22

v.	Single platform.....	23
vi.	PDMS absorption .....	24
vii.	Absence of standardized protocols.....	24
viii.	Absence of cell cocultures.....	25
1.2.	Objectives.....	26
1.3.	Thesis overview .....	27
<b>2.</b>	<b>MONOCYTE EXTRAVASATION .....</b>	<b>29</b>
2.1.	Abstract * .....	31
2.2.	Introduction.....	32
2.2.1.	Monocyte extravasation.....	32
2.2.2.	Role of hemodynamics in extravasation .....	33
2.2.3.	Role of surrounding stiffness in extravasation .....	34
2.2.4.	Models to study extravasation .....	34
2.3.	Methods .....	36
2.3.1.	Cell Culture.....	36
2.3.2.	Fabrication of Microfluidic Devices .....	36
2.3.3.	Formation of the Endothelial Vessel .....	37
2.3.4.	Extravasation Assays.....	38
2.3.5.	Inmunofluorescence .....	39
2.3.6.	Image acquisition and analysis .....	39
2.3.7.	Permeability assays.....	40
2.3.8.	Collagen hydrogel characterization .....	41
2.3.9.	Determination of hydraulic permeability .....	41
2.4.	Results .....	42
2.4.1.	Microfabricated blood vessels that mimic physiologic vasculature....	42
2.4.2.	Fluid shear stress increases monocytes adherence to the vessel wall but decreases extravasation .....	43
2.4.3.	Increased collagen matrix concentration decreases vascular barrier integrity and increases extravasation .....	48
2.5.	Discussion.....	52

<b>3. MACROPHAGE MIGRATION .....</b>	<b>55</b>
3.1. Abstract * .....	57
3.2. Introduction.....	58
3.3. Methods .....	59
3.3.1. Cell culture .....	59
3.3.2. Bacteria culture and fractions preparation .....	59
3.3.3. Manufacturing of microfluidic device.....	60
3.3.4. Migration assays .....	60
3.4. Results .....	62
3.4.1. Macrophage migration and velocity are inversely proportional to collagen concentration in the microfluidic device .....	62
3.4.2. 2.5 mg/ml collagen hydrogels allow gradient of all molecules of the bacterial fractions.....	64
3.4.3. Macrophages show directional migration towards bacterial fractions of <i>S. typhimurium</i> 66	
3.4.4. Macrophages show directional migration towards bacterial fractions of <i>M. tuberculosis</i> .....	69
3.4.5. Macrophages migrate towards fractions of non-pathogenic <i>E. coli</i> and <i>M. smegmatis</i> 71	
3.5. Discussion.....	73
<b>4. CONCLUSIONS .....</b>	<b>75</b>
4.1. Conclusions.....	77
4.1.1. Monocytes extravasation .....	77
4.1.2. Macrophage migration in response to bacterial fractions.....	78
4.2. Conclusiones.....	80
4.2.1. Extravasación de monocitos .....	80
4.2.2. Migración de macrófagos en respuesta a estímulos bacterianos .....	81
<b>5. FUTURE WORK .....</b>	<b>83</b>
<b>6. BIBLIOGRAPHICAL NOTE .....</b>	<b>87</b>
6.1. Publications obtained from this PhD Dissertation .....	89
6.2. Participation in conferences and congresses.....	89

6.3. Research stay .....	90
6.4. Teaching activities .....	90
<b>APPENDIX .....</b>	<b>93</b>
A.1. Selection of cell lines .....	95
A.2. Genetic modification .....	95
A.2.1. Selection of plasmids.....	95
A.2.2. Primers design .....	96
A.2.3. Gibson Assembly Protocol.....	97
A.2.4. Cloning in monocyte.....	98
A.3. Microfluidic device .....	99
<b>REFERENCES.....</b>	<b>101</b>

## Agradecimientos / Acknowledgements

Tras cuatro años termina esta etapa de mi vida llamada doctorado y no imaginaba la realización personal que sentiría al escribir la última página del primer borrador. Esto no habría sido posible sin el apoyo y conocimiento de mis dos directores, el Dr. José Manuel García Aznar y el Dr. Jesús Ángel Gonzalo Asensio. Gracias por confiar en la propuesta de colaboración que os propuse allá por el 2017, que demuestra los bonitos resultados que se obtienen al fusionar la ingeniería y la microbiología. Agradecer también la financiación concedida a los proyectos del Ministerio de Educación, Cultura y Deporte (FPU16/04398) y al Ministerio de Ciencia e Innovación (RTI2018-094494-B-C21 y PID2019-104690RB-I00), sin los que hubiera sido imposible realizar esta tesis.

También quiero agradecerles a todos los que han estado día a día conmigo en el laboratorio, siempre aportando e intercambiando ideas para ayudarme a continuar cuando me atascaba. Gracias a los que habéis estado desde el principio: a Nieves por preocuparte tanto, de mi tesis y de mí, has sido más que una mentora para mí; a Yago y Pilar por ser mis iguales y entender en todo momentos los altibajos de ilusión y sufrimiento que conlleva el doctorado. También agradecer a las nuevas incorporaciones: Pedro, Soraya y Paula, todos habéis aportado un granito de arena en esta tesis. Y por supuesto a los que estuvieron, pero se marcharon a mitad de camino: Cris, Esther y Vanesa, gracias por hacer el laboratorio un lugar tan agradable para trabajar. Y no me olvido de los que no están en el laboratorio, Carlos, sin ti habría sido imposible conseguir unos resultados y figuras tan chulas.

Además de mi grupo de investigación, esta tesis no habría sido lo mismo sin las colaboraciones realizadas. Gracias al grupo de investigación de genética micobacterias de la Universidad de Zaragoza, por siempre echarme una mano y dejarme usar sus cepas de bacterias, Juan, Elena y Ana Belén. También al grupo de William Polacheck de la University of North Carolina at Chapel Hill donde realicé mi estancia. Thank you so much Bill, for accepting me for my research stay with your group and teaching me so much in only five

months. It gave me an indescribable work and personal experience. I would also like to thank Stephanie for or training me upon arrival and for her contribution to my research.

Finalmente, agradecer a todas las personas fuera del ámbito científico que han estado durante esta etapa. Gracias a mis padres y mi hermano, que han tenido que aguantarme horas hablando sobre mis experimentos y haciendo de público para practicar mis exposiciones. Habéis sido mi mayor apoyo y sin vosotros no podría haber llegado donde estoy. Al resto de mi familia, gracias por estar apoyándome desde la distancia y celebrar cada nueva publicación que conseguía. También agradecer a mis amigos, que me habéis apoyado durante todo este camino, alegrándoos por mis éxitos y animándome en mis desilusiones. En especial, gracias a mi mejor amiga Anyi por estar siempre disponible para contarnos nuestros dramas doctorales en interminables audios o para ser mi compi de mesa otra vez en clase.

Gracias a todas las personas que formáis parte de mi vida y habéis hecho de esta experiencia algo único.

## Abstract

Bacterial infections cause numerous deaths annually, so it is essential to understand the infection processes in order to develop prevention and cure strategies. Usually, *in vitro* studies are performed with traditional methods that, despite providing great knowledge, do not realistically recreate physiological environments and the results obtained do not always agree with *in vivo* studies. Therefore, in this thesis we propose microfluidic devices as a novel *in vitro* model for the study of these processes. Microfluidics allows the incorporation of three-dimensionality, flow and co-cultures, among others, to achieve scenarios that are more realistic. Since pathogenic infections are long multistage processes, in this thesis, we focused on the macrophage-pathogen interaction.

First, the extravasation of monocytes from the endothelial lumen into the extracellular matrix was studied. This process is necessary for immune cells to reach bacteria. For this purpose, a microfluidic device was used that allowed the development of an endothelial vessel through which monocytes were passed, allowing the quantification of adherent and extravasated monocytes after 24 hours. The effect of mechanical stimuli on this process was analyzed: the application of oscillatory flow and environmental stiffness. It was determined that flow increased the membrane integrity of the vessel, hindering monocyte extravasation. However, higher stiffness of the extracellular matrix, due to high collagen concentration, reduced the barrier integrity of the vessel, increasing monocyte extravasation.

Second, macrophage migration was studied in response to bacterial fractions obtained from pathogenic bacteria, *Salmonella typhimurium* and *Mycobacterium tuberculosis*, and non-pathogenic bacteria, *Escherichia coli* and *Mycobacterium smegmatis*. The results show that macrophages migrate directionally attracted to fractions of all bacteria, both pathogenic and non-pathogenic, suggesting the existence of pathogen-associated molecular patterns in the sample molecules.





## Resumen

Las infecciones bacterianas causan numerosas muertes anualmente, por lo que es esencial entender los procesos de infección para desarrollar estrategia de prevención y cura. Habitualmente, los estudios *in vitro* se realizan con métodos tradicionales que, a pesar de aportar un gran conocimiento, no recrean de manera realista los entornos fisiológicos y los resultados obtenidos no siempre concuerdan con los estudios *in vivo*. Por tanto, en esta tesis proponemos los dispositivos microfluídicos como un modelo *in vitro* novedoso para el estudio de estos procesos. La microfluídica permite incorporar tridimensionalidad, flujo y cocultivos, entre otros, para conseguir escenarios más realistas. Dado que las infecciones patógenas son procesos largos de múltiples etapas, en esta tesis, nos hemos centrado en la interacción macrófagos-patógenos.

En primer lugar, se estudió la extravasación de monocitos del lumen endotelial a la matriz extracelular. Este proceso es necesario para que las células inmunes alcancen las bacterias. Para ello, se utilizó un dispositivo microfluídico que permitía el desarrollo de un vaso endotelial a través del cual se hacían pasar monocitos, permitiendo la cuantificación de los monocitos adheridos y extravasados al cabo de 24 horas. Se analizó el efecto de estímulos mecánicos en este proceso: la aplicación de flujo oscilatorio y la rigidez del entorno. Se determinó que el flujo aumentaba la integridad de membrana del vaso, dificultando la extravasación de los monocitos. Por otro lado, una mayor rigidez de la matriz extracelular, debido a un aumento en la concentración de colágeno, reduce la integridad de barrera del vaso, aumentando la extravasación de los monocitos.

En segundo lugar, se estudió la migración de macrófagos en respuesta a fracciones bacterianas obtenidas de bacterias patógenas, *Salmonella typhimurium* y *Mycobacterium tuberculosis*, y no patógenas, *Escherichia coli* y *Mycobacterium smegmatis*. Los resultados muestran que los macrófagos migran direccionalmente atraídos hacia las fracciones de todas las bacterias, tanto patógenas, como no patógenas, sugiriendo la existencia de patrones moleculares asociados a patógenos en las moléculas de las muestras.



## List of figures

Figure 1.1. Basic components of the innate and adaptive immunity. ....	4
Figure 1.2. Stages of differentiation to macrophage. ....	5
Figure 1.3. Ligands of Toll-Like Receptors (TLR) and NOD-Like Receptors (NLR).....	6
Figure 1.4. <i>Salmonella typhimurium</i> infection. ....	8
Figure 1.5. Peyer’s patch structure. ....	9
Figure 1.6. <i>Mycobacterium tuberculosis</i> infection. ....	11
Figure 1.7. Experimental stages in clinical trials.....	12
Figure 2.1. Stages of leukocyte extravasation and the molecules involved. ....	33
Figure 2.2. Microfluidic platform for investigating monocyte extravasation. ....	38
Figure 2.3. Image processing. ....	40
Figure 2.4. Endothelial vessels embedded in 2.5 and 6 mg/ml collagen gels within the microfluidic device. ....	43
Figure 2.5. Effect of the fluid flow stimulation on extravasation.....	46
Figure 2.6. Correlation of the diameter of each vessel and the number of monocytes adhered to the endothelial lumen.....	47
Figure 2.7. Correlation of the diameter of each vessel and the number of monocytes extravasated from the endothelial lumen into the surrounding matrix. ....	47
Figure 2.8. Storage shear modulus of 2.5 (white) and 6 mg/ml (black) collagen hydrogels. ....	49
Figure 2.9. 3D structure and hydraulic permeability of 2.5 and 6 mg/ml collagen gels.....	50
Figure 2.10. Effect of the collagen concentration on vascular permeability and monocyte extravasation. ....	52
Figure 3.1. Microfluidic device .....	61
Figure 3.2. Macrophage migration in collagen gels of different concentrations: 2.5 mg/ml (blue), 4 mg/ml (orange) and 6 mg/ml (yellow). ....	63
Figure 3.3. Macrophage facing <i>S. typhimurium</i> stimuli.....	68
Figure 3.4. Macrophage facing <i>M. tuberculosis</i> stimuli. ....	70
Figure 3.5. Macrophage facing <i>E. coli</i> stimuli.....	71

Figure 3.6. Macrophage facing <i>M. smegmatis</i> stimuli. ....	72
Figure 5.1. Graphical representation for the device proposed for the study of the monocyte-bacteria extravasation and interaction.....	86
Figure A.1. Structure of plasmids 17448 and pcDNA-CD68. ....	96
Figure A.2. Visual map of primer design. ....	97
Figure A.3. Final plasmid after genetic modification .....	98

## List of tables

Table 1.1. Summary of different articles that used microfluidics-based approaches to study different phenomena. ....	16
Table 1.2. Summary of microfluidic advantages and limitations .....	20
Table A.1. Primers sequences.....	97

## List of abbreviations

2D	two-dimensional
3D	three-dimensional
Ag85	antigen 85
ATCC	American Type Cell Culture
BSA	bovine serum albumin
CCL2	C-C motif chemokine ligand 2
CCR2	chemokine receptor 2
CM	cytomegalovirus early gene
CSF-1	colony-stimulating factor 1
DAMPs	damage-associated molecular patterns
DAPI	4',6-diamino-2-phenylindole
ECM	extracellular matrix
FBS	fetal bovine serum
FITC	fluorescent dextran fluorescein
FRAP	fluorescence recovery after photobleaching
FT	Fourier Transform
GA-100	gentamicin sulfate/amphotericin
GFP	green fluorescent protein
hEGF	human epidermal growth factor
HSCs	haematopoietic stem cells
HUVECs	human umbilical vein endothelial cells
ICAM-1	intercellular adhesion molecule 1
IL	interleukin
INF- $\gamma$	interferon gamma

LAM	lipoarabinomannan
LB	Luria-Bertani
LM	lipomannan
LPS	lipopolysaccharides
M cells	microfold cells
MCP-1	monocyte chemoattractant protein-1
MSD	Mean Squared Displacement
MyD88	myeloid differentiation primary response protein 88
NK	Natural Killer
NLR	NOD-like receptors
PAMPs	pathogen-associated molecular patterns
PBS	phosphate-buffered saline
PBS++	PBS + 0.5 mM MgCl <sub>2</sub> + 1 mM CaCl <sub>2</sub>
PCR	polymerase chain reaction
PDIM	phthiocerol dimycocerosates
PDL	poly-D-lysine
PDMS	polydimethylsiloxane
PFA	paraformaldehyde
PIM	mannosylated phosphatidylinositol
PLL	poly-L-lysine
PMA	phorbol 12-myristate-13-acetate
PPR	pathogen pattern receptors
PSGL-1	P-selectin Glycoprotein Ligand 1
R3 IGF-1	R3 insulin-like growth factor 1
Sip	<i>Salmonella</i> invasive proteins
Sop	<i>Salmonella</i> outer proteins
SPI	pathogenicity islands

T3SS	type III secretion system
T7SS	type VII secretion system
TCA	trichloroacetic acid
TLR	Toll-like receptors
TNF	tumor necrosis factor
VCAM-1	vascular cell adhesion molecule 1
VEGF	vascular endothelial growth factor
WHO	World Health Organization
$\beta$ 2M	beta-2-microglobulin





# 1. INTRODUCTION

---



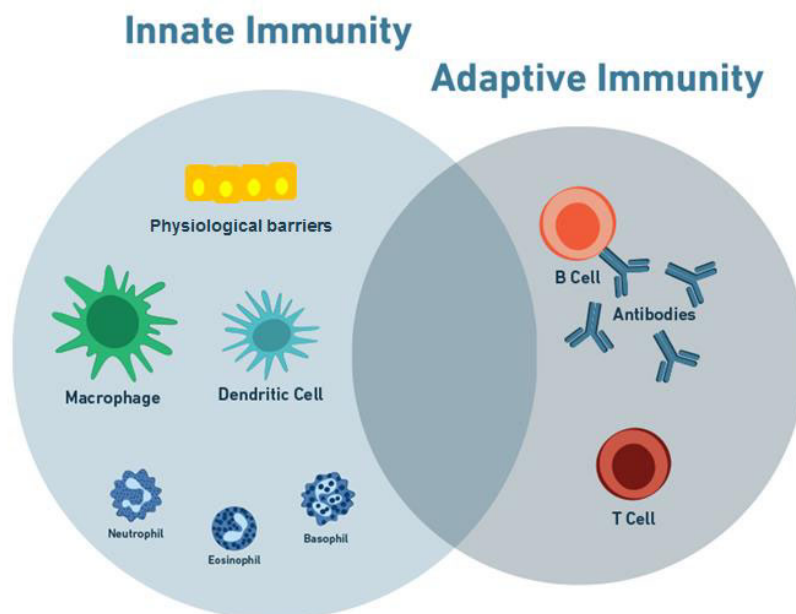
## 1.1. Background

Infections caused by pathogenic bacteria cause numerous deaths each year worldwide. Therefore, research focused on understanding the mechanisms involved in these processes is of vital importance in order to develop drugs capable of combating them. In this section, we describe the specific role of macrophages as immune cells in the eradication of infection, focusing on our bacteria of interest, *Salmonella typhimurium* and *Mycobacterium tuberculosis*. Finally, a state of the art on the *in vitro* methodologies used for the investigation of bacterial phenotypes is shown, highlighting the advantages and limitations between traditional techniques and the emerging methodology known as microfluidics.

### 1.1.1. Pathogen bacteria and immune system

A pathogen is defined as a microorganism that is capable of causing disease in the host it inhabits [1]. There are an estimated 1400 species of pathogens for the human species, and although this may seem like a large number, human pathogens do not represent even 1% of the world's microbial species [2]. However, pathogens continue to emerge constantly. A current example of this fact is COVID-19 [3]. At least 50 new pathogens have been identified in the last 45 years, 10% being bacteria [4]. Some of the causes of this continuous emergence of infectious agents are mutations that modify the genome of innocuous microorganisms, providing them with virulence or resistance mechanisms [5]; the continuous development of biomolecular analysis techniques that have allowed the characterization of new prokaryotic species, including some pathogens [6,7]; or the zoonotic transmission of diseases from animals to humans [8]. These pathogens present a wide taxonomic biodiversity, including viruses, fungi or protozoa, although the most common are bacteria [9]. This diversity of pathogenic bacteria implies numerous possible infections. Bacteria can enter the body by various pathways such as the respiratory tract, by foodborne, or through open wounds [10]. Thus, infection can develop at different sites in the system depending on the type of bacteria infecting the system.

The immune system is responsible for protecting the organism against pathogens. For this purpose, it presents mechanisms that are distinguished between innate and adaptive immunity (Figure 1.1). Innate immunity includes strategies that are possessed from birth and constitutes the body's first line of defense. The main components are physical barriers, such as the intestinal or alveolar epithelium, and phagocytic cells, such as macrophages and dendritic cells. However, the adaptive response is threat-specific. This is achieved by the presentation of antigens to lymphocytes that are capable of preparing an individual response to these epitopes. This response can be cellular, with the expression of surface receptors on T lymphocytes, or humoral through the secretion of antibodies by B lymphocytes [11]. Both immunities are interrelated and it is their fusion that successfully eradicates the pathogen. Innate immunity is immediate and contains the infection until adaptive immunity starts up. In addition, phagocytes are the main cells that digest microbes and present their molecules to lymphocytes for activation [11].



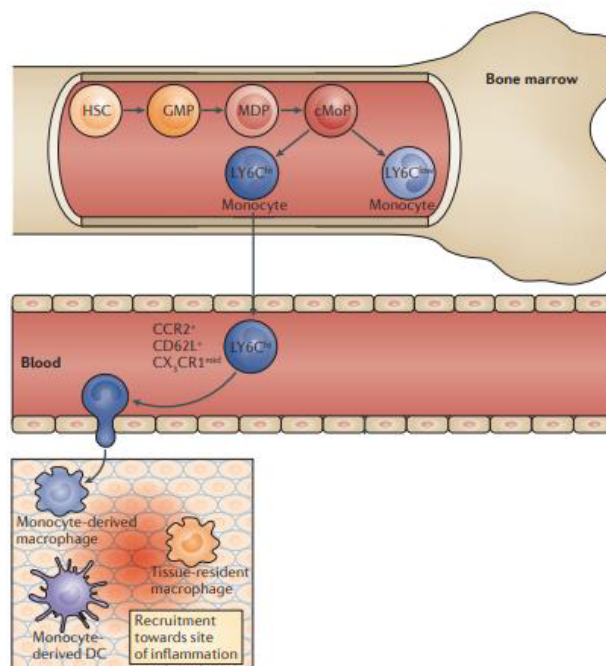
**Figure 1.1. Basic components of the innate and adaptive immunity.**

The adaptive immune system is mainly composed of physiological barriers, which act as physical barriers in the body, phagocytic cells such as macrophages and dendritic cells, and other immune cells like neutrophils, eosinophils or basophils. However, the adaptive immune system can have a humoral component by which antibodies are secreted, and a cellular component by which B cells differentiate to express different antimicrobial receptors on their surface. Both responses are interrelated. Adapted from [12].

Despite the great importance of all stages of the immune system, in this project we have focused on the innate response, specifically the role of macrophages. As foodborne and respiratory infections exceeds one million deaths annually [13–15], in this thesis we have focused our attention on pathogenic bacteria causing these infections, *Salmonella typhimurium* and *Mycobacterium tuberculosis*, as intestinal and respiratory bacteria, respectively.

### 1.1.1.1. The role of macrophages in immunity

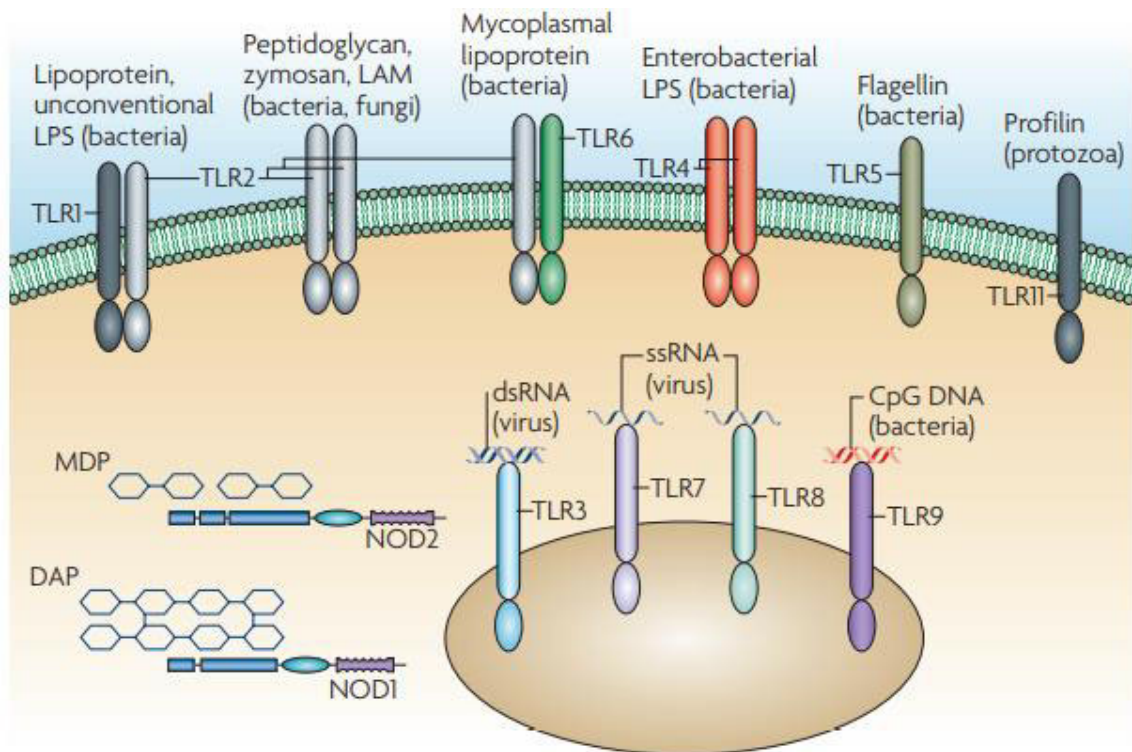
Among the immune cells that fight bacterial infections, macrophages play an essential role as the largest phagocytic cell family [16]. Macrophages are derived from monocytes, whose precursors are bone marrow from hematopoietic stem cells. Monocytes are in continuous circulation in the peripheral blood until they are recruited and extravasate into damaged and swollen tissues. There, monocyte differentiate into mononuclear phagocytes, including macrophages (Figure 1.2) [17].



**Figure 1.2. Stages of differentiation to macrophage.**

Monocytes derive from haematopoietic stem cells (HSCs) that are found in bone marrow. monocytes pass into the circulatory system and eventually extravasate into the extracellular matrix (ECM) where they differentiate into macrophages, or dendritic cells. Adapted from [17].

Macrophages migrate towards pathogens, attracted by immunoglobulins and chemokines released in situations of inflammation and infection, being the first cells to interact with microbes [18]. Macrophages possess a series of receptors that allow them to sense their environment and recognize the presence of pathogens (Figure 1.3). To do so, they interact with the pathogens themselves or their secreted products, which are characterized by pathogen-associated molecular patterns (PAMPs) and damage-associated molecular patterns (DAMPs). There are six groups of pathogen sensors: Toll-like receptors (TLR), NOD-like receptors (NLR), receptors for intracellular RNA, receptors for intracellular DNA, C-type lectins and scavenger receptors. Activation of these receptors generates a signaling cascade that results in changes in macrophage behavior [19].



**Figure 1.3. Ligands of Toll-Like Receptors (TLR) and NOD-Like Receptors (NLR).**

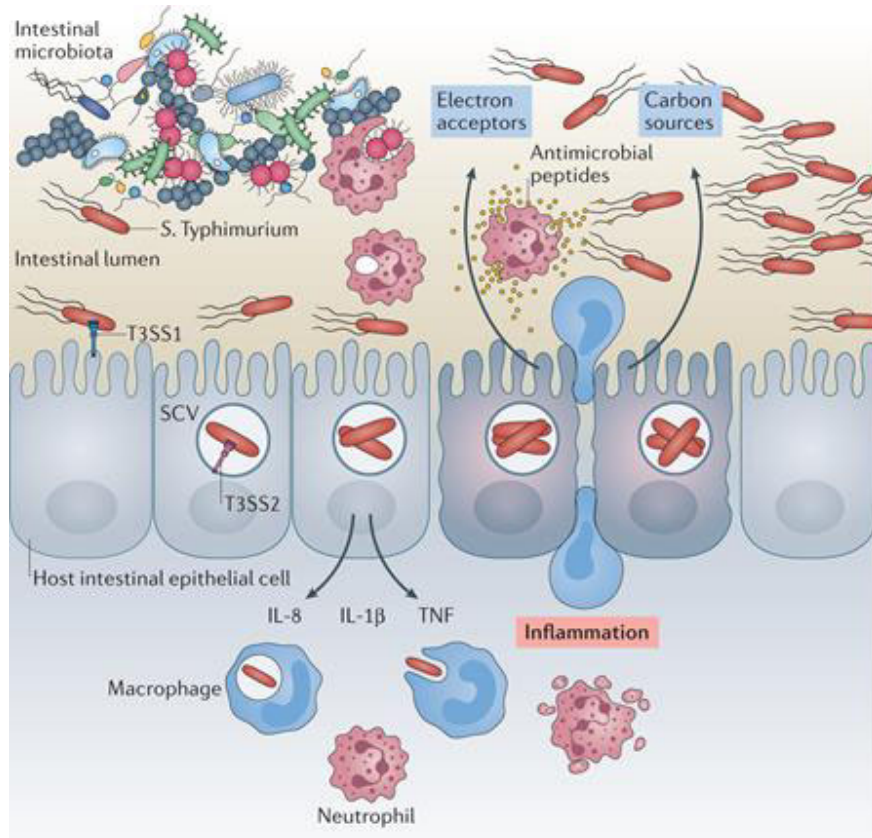
TLR and NLR are pathogen pattern receptors (PPR) that recognized pathogen-associated molecular patterns (PAMPs). This figure shows the different microbial ligands that can interact with the TLR receptors. Some TLR are presented on the macrophage surface and recognize, for example, lipid components of the bacterial wall that interact with TLR1, TLR2 and TLR4. Other TLR, such as TLR3 and TLR7-9, and NLR are intracellular receptors and interact with genetic components of pathogens. Taken from [20].

Macrophages phagocytose bacteria and start up antimicrobial mechanisms that include granule proteins, reactive oxygen and nitrogen species, and sequestration of iron molecules. They also secrete cytokines and chemokines that recruit more inflammatory phagocytes, especially neutrophils, which reinforce the defense at the site of infection [18]. Finally, they are able to present antigens on their surface to activate lymphocytes, giving way to the initiation of the adaptive immune response [21]. All this together, the final goal of the immune system is the complete elimination of the invading microorganism.

#### 1.1.1.2. *Salmonella typhimurium* infection

*Salmonella typhimurium* is a Gram - bacteria belonging to the *Enterobacteriaceae* family, *enterica* species and serotype *typhimurium*. *S. typhimurium* is one of the two most important and abundant serotypes causing salmonellosis in humans [22]. This bacterium usually enters the body orally, through ingestion of contaminated food or water, until it reaches the small intestine, where it replicates and invades the intestinal cells (Figure 1.4). This invasion is mediated by the type III secretion system (T3SS), by which, through a syringe mechanism, it injects effector proteins into the cytosol of host cells with the capacity to modulate several processes. Among the most significant changes that the infected cell undergoes is a reorganization of the cytoskeleton to internalize the bacterium. *S. typhimurium* is able to alter the structure and metabolism of the vacuoles in which it is found, generating a niche in which it can survive and replicate [23]. Furthermore, it destabilizes E-cadherin junctions between neighboring cells, increasing the permeability of the intestinal monolayer and favoring the invasion of the pathogen through it [24]. Finally, it induces an increase in the expression and production of proinflammatory molecules, such as prostaglandins that induce the secretion of water and electrolytes into the intestine, causing diarrhea [25], or cytokines, such as interleukin 8 (IL-8), interleukin 1 $\beta$  (IL-1 $\beta$ ) and tumor necrosis factor (TNF), that recruit immune system cells to the infected area. The presence of immune cells leads to an increased release of antimicrobial compounds, which affect both the pathogenic bacteria and the host microbiota [23]. Together, this generates

an inflammation of the intestine accompanied by pain, which together with the previously described diarrhea, are the main symptoms of salmonellosis [26].



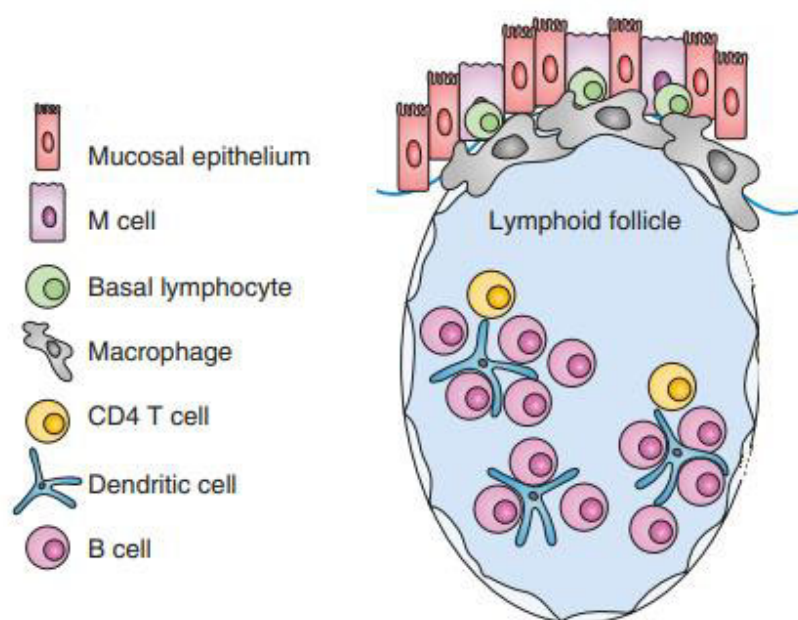
**Figure 1.4. *Salmonella typhimurium* infection.**

*S. typhimurium* enters the body orally until it reaches the intestinal epithelium. Through its type 3 secretion system (T3SS) it injects effector proteins into the epithelial cells. This leads to changes, such as internalization of the bacteria into vacuoles or secretion of inflammatory cytokines (IL-8, IL-1 $\beta$  and TNF) that recruit immune cells (macrophages and neutrophils). The immune cells phagocytize the bacteria and secrete antimicrobial products. This inflammatory situation induces the secretion of water and electrolytes into the intestinal lumen, leading to diarrhea. Adapted from [23].

The body has numerous mechanisms for containment and eradication of pathogens. The first defense strategy is the physical barrier, such as the intestinal epithelium, which has a selective permeability to capture nutrients or water, but avoiding the passage of microorganisms [27]. Above this barrier inhabits a bacterial community in a symbiotic relationship, known as the intestinal microbiota [28], which modifies niche conditions and secretes bacteriocins to prevent pathogens from colonizing the intestine [29]. The intestinal



epithelium is composed of different cell types, among which microfold (M) cells cover aggregated lymphoid follicles, known as Peyer's Patch (Figure 1.5). M cells act as antigen presenters, transporting pathogen particles or even whole microorganisms from the lumen of the intestine to the subendothelial dome of the Peyer's Patch, where B lymphocytes and mononuclear phagocytes, such as dendritic cells or macrophages, are found [30]. B lymphocytes are activated upon recognition of antigens and produce antibacterial antibodies [31]. Dendritic cells phagocytize the bacteria to present their antigens to other lymphocytes and induce further activation of the immune system [32]. Finally, macrophages phagocytize bacteria into vacuoles that fuse with lysosomes to digest them [33].



**Figure 1.5. Peyer's patch structure.**

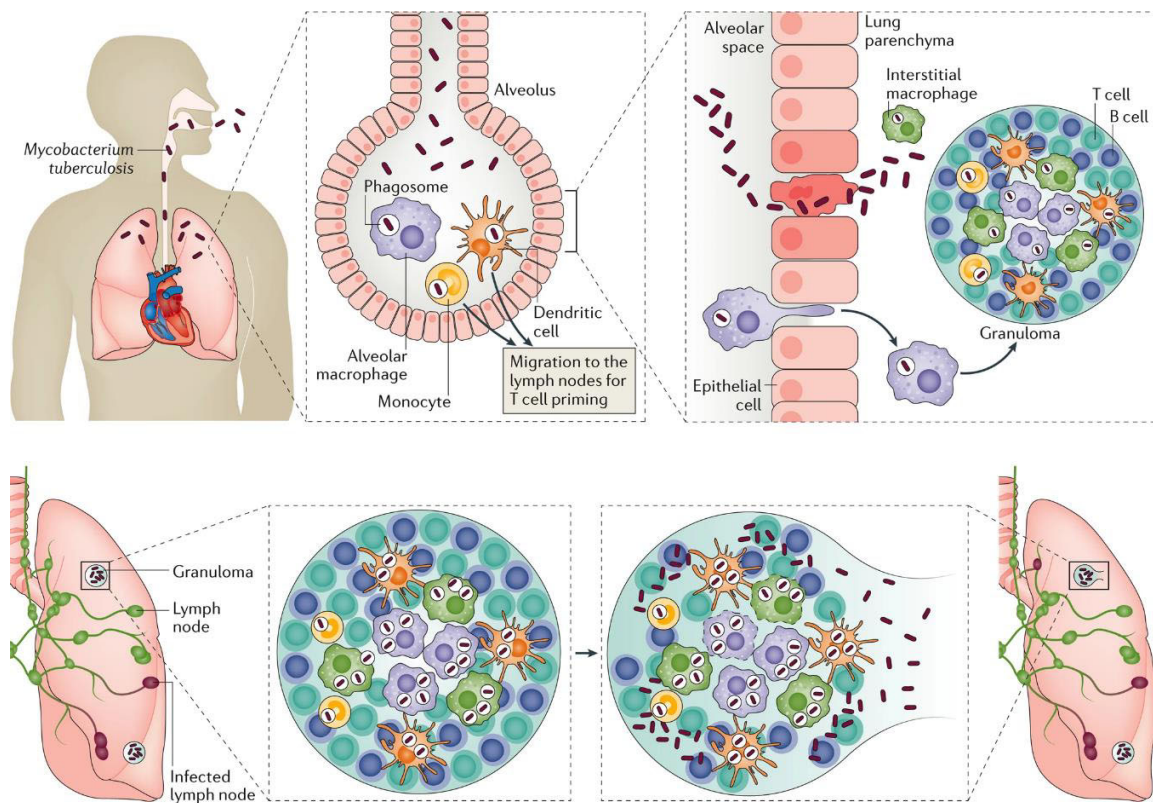
Peyer's patch are aggregated lymphoid follicles covered by intestinal cells and in contact to microfold (M) cells. A wide variety of immune cells are found in the follicle, including phagocytes such as macrophages or dendritic cells and basal, B and T lymphocytes. Adapted from [34].

However, *S. typhimurium* also has defense and survival strategies. For example, it uses induced inflammation to its own advantage to compete with the host's natural microbiota. Inflammation inhibits the growth of gut flora bacteria, allowing the pathogen to colonize the lumen, replicate, and increase bacterial load [35]. It can also use the same antigen presentation pathway of M cells to cross the intestinal barrier and colonize the

subepithelium [36]. In addition, Knodler *et al.* described a subpopulation of *S. typhimurium* with hyper-replicative capacity that is found in the cytosol of epithelial cells, rather than contained in vacuoles [37]. Finally, *S. typhimurium* is able to escape from immune system and survive phagocytosis, for example, by avoiding vacuole-lysosome fusion [38].

#### 1.1.1.3. Mycobacterium tuberculosis infection

Tuberculosis in humans is caused by the bacterium *Mycobacterium tuberculosis*. The most common form of infection is by inhalation of droplets containing the bacterium (Figure 1.6). Once in the lungs, alveolar macrophages phagocytize and eliminate the bacteria. Monocytes and pulmonary dendritic cells also phagocytize the bacteria and transport it to the pulmonary lymph nodes, where antigen-presenting cells activate lymphocytes. If this defensive line fails, *M. tuberculosis* colonizes the lung tissue [39]. *M. tuberculosis* presents mechanisms to survive inside phagocytic cells. This leads to a proliferation of the bacterium within dendritic cells and alveolar macrophages, which induces the release of proinflammatory cytokines, such as IL-1. In turn, *M. tuberculosis* is capable of producing cell death of the cells containing it by secretion of effector proteins. In this way it exits into the ECM and can infect neighboring cells, causing a pulmonary dysfunction [40]. To contain the infection, the infected cells aggregate with other immune cells such as macrophages, dendritic cells, neutrophils or T cells, forming a confining structure called a granuloma. However, granulomas are dynamic structures and when the bacteria load becomes too great, both infected macrophages and free bacteria can escape and spread the infection to other parts of the body [41].



**Figure 1.6. *Mycobacterium tuberculosis* infection.**

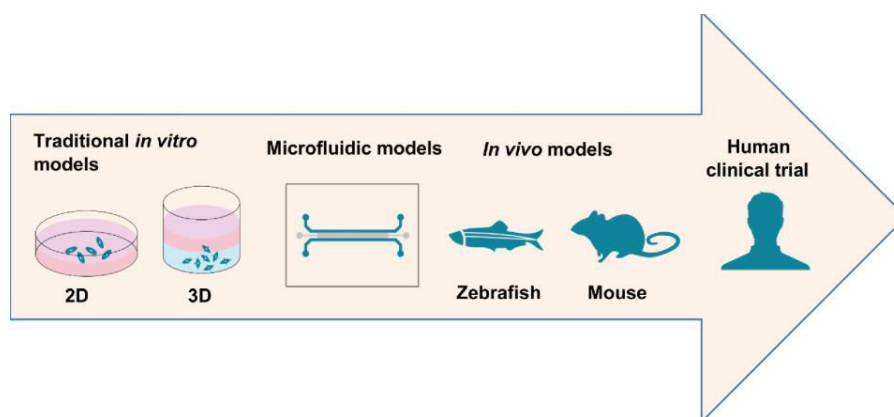
*M. tuberculosis* enters the body by the respiratory route until it reaches the pulmonary alveoli. There, the bacterium is phagocytized by macrophages that eliminate it, and by monocytes and dendritic cells that transport it to the lymph nodes for presentation to lymphocytes and activation of the adaptive response. This line of defense can fail, allowing the bacteria to gain access to lung tissue. To contain the infection, a cluster of immune cells aggregate to form a granuloma that confines the bacteria within. However, *M. tuberculosis* can escape again by colonizing lung tissue. Taken from [39].

For survival and escape from the immune system, *M. tuberculosis* has a number of characteristic virulent features. On the one hand, it possesses a bacterial wall containing peptidoglycan, arabino-galactan and mycolic acid layers. Its components include phthiocerol dimycocerosates (PDIM) that are able to mask bacterial epitopes and thus go unnoticed by macrophages [42]. On the other hand, it is able to compromise the integrity of the phagosome thanks to effector proteins secreted by the type VII secretion system (T7SS). Among them, ESAT-6 and CFP:10 stand out, which in dimeric form acidify the phagosome preventing its maturation and rupture its membrane to escape to the cytosol [43]. Other mechanisms that *M. tuberculosis* relies on include inhibiting the oxidative and

nitrosative stresses mediated by Acr chaperones [44], promoting wall integrity thanks to cyclopropane rings [45] or releasing anti-apoptotic factors, like katG and sodA, [46].

### 1.1.2. *In vitro* bacterial research \*

The study of bacterial infections to understand the mechanisms involved in the process and to be able to develop and test effective drugs is a long, multi-stage process (Figure 1.7). It starts with *in vitro* assays in laboratories, to obtain the knowledge base. This allows experimental models to be developed and animal tests to be carried out *in vivo*. This is known as the preclinical phase, and if the results obtained are satisfactory, it moves on to the clinical trials, where it is tested in humans [47]. In this section, we will focus on *in vitro* methods, standing out the advantages that microfluidics offer.



**Figure 1.7. Experimental stages in clinical trials.**

The experimental part of clinical trials start with the use of traditional *in vitro* methods, until reaching *in vivo* models, and finally human trials. Microfluidic models provide an intermediate *in vitro* strategy between traditional methods and animal models. Adapted from [48].

\* This section of chapter 1.2 is an adaptation from the article already published as: **Pérez-Rodríguez, S.;** García-Aznar, JM.; Gonzalo-Asensio, J. **Microfluidic devices for studying bacterial taxis, drug testing and biofilm formation.** *Microbial Biotechnology.* 2021. doi: 10.1111/1751-7915.13775.

### 1.1.2.1. Traditional methods

Understanding bacterial interactions with cells under physiological conditions is essential to study certain bacterial phenotypes. Traditional microbiological *in vitro* techniques include microscopy, cell infection models and recent molecular, cellular and immunological assays [49,50]. Microscopy has advanced over the years, allowing at first, the testing of the effect of different bactericides and bacteriostats of intracellular infections through quantification by fluorescent microscopy [51], to being able to visualize the composition of the internal and external membranes of bacteria at high resolution with expansion microscopy [52]. *In vitro* co-culture of bacteria with host and immune system cells has enabled the development of numerous intracellular infection models [53,54]. Finally, there are numerous molecular approaches, such as mass spectrometry to determine cell-bacteria protein interactions [55], or the use of microarrays to analyze gene expression changes that bacteria undergo in response to different stimuli [56]. These methods have provided and continue to provide inestimable information, contributing to gaining insight into the molecular and cellular microbiology of the host-bacteria interplay.

However, traditional methodologies have some limitations. On the one hand, although culture procedures have improved with time, bacteria still exist that cannot be cultured under *in vitro* conditions [57,58]. On the other hand, *in vitro* and *ex vivo* models are not able to fully recreate the physiological environment, such as gastric acidity, whose pH increases while digestion occurs [59]. Consequently, *in vitro* and *in vivo* results do not always correlate. In addition, some phenotypes, such as biofilm formation, are traditionally studied under simplistic environments that do not mimic complex physiological scenarios [60]. Nevertheless, the recent advent of microfluidics can help to solve some of these limitations, to not only advance fundamental microbiological research but also help in the development of therapeutic interventions.

### 1.1.2.2. Microfluidics

Microfluidics is known as the technique that handles microscale fluid flows [61], allowing the integration, miniaturization and automation of several processes [62]. Working with manufactured microdevices involves the use of small volumes (on the microliter scale), assuring better control of environmental conditions and saving reagents, biological material, residues and space [63]. However, the main advantage of these microfluidic devices is the possibility of recreating biological environments more realistically than traditional macroscopic cultures in flasks, well plates or dishes [62]. This approximation can be implemented by three-dimensional (3D) cultures of microorganisms embedded in hydrogels that simulate the ECM, or by introducing a flow to mimic interstitial fluid flow that transports nutrients and other microorganisms [64]. In addition, the physical (rigidity, pressure forces, fluid flows, etc.) and chemical (pH, attraction and repulsion factors, etc.) conditions can be modified to study adaptations to the changing environment [65].




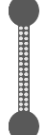


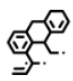







The materials used in the pioneering microfluidic devices were silicon and glass. Nevertheless, the opacity of silicon makes it incompatible with microscopy studies. Moreover, both glass and silicon are characterized by their fragility, difficult bonding protocols and high cost. Altogether, their use has been limited, paving the way for the use of new materials [61]. Since the 90s, the most utilized material has been polydimethylsiloxane (PDMS), a mineral-organic polymer from the siloxane family [66]. PDMS presents numerous beneficial properties: optical transparency, gas permeability, flexibility, chemical inertness, biocompatibility, ease of bonding and unbonding to other materials, the possibility of making its surface more hydrophilic and low cost [67]. Thus, PDMS has been considered a great candidate for microfluidics studies. Other materials used for this application are thermoplastics, paper and wax [61].

### 1.1.2.3. Bacteria in microfluidics

There are numerous researches in which microfluidics has been applied to the study of bacterial phenotypes, mainly encompassing three approaches: bacterial taxis, drug

testing and biofilm formation ([Table 1.1](#)). Taxis processes are defined as directed bacterial movement towards or away from an external stimulus or gradient [68]. Depending on the external stimulus, different taxis can be stimulated. If there is a chemical compound, it is chemotaxis; an oxygen gradient, aerotaxis; a flow current, rheotaxis; a light stimulus, phototaxis; a magnetic field, magnetotaxis; a temperature stimulus, themotaxis; and a pH stimulus, pH taxis. Drug testing studies consist of bacterial growth assays under different environments, in the presence of diverse compounds. Finally, biofilms are known as microbial communities established in the self-produced extracellular substances [69].

The versatility offered by microfluidics in terms of design provides different device configurations. Each of them is useful for the recreation of specific environments and the study of different phenotypes. The diverse patterns found in the literature have been divided into six groups: a) devices with linear channels, subdividing for one, two and three parallel channels; b) devices with mixing channels; c) devices with multiple floors; d) porous devices; e) topographic devices; and f) droplet microfluidics ([Table 1.1](#)).

Linear channels		[74-77]	[81-83]	[92, 93]	[95-97]	[100-102]	[103, 104]	[111-118]	[102]
Mixing channels		[72,73]	[79, 80]						
Multiple floors			[78]			[98,99]		[110]	
Porous devices		[70,71]		[90, 91]					[124]
Topographic devices				[84-89]	[94]			[108,109]	[87,88,122,123]
Droplet microfluidics								[105-107]	[119-121]
		Chemo taxis	Aero taxis	Rheo taxis	Magneto taxis	Thermo taxis	pH taxis	Growth tests	Biofilm formation
									

**Table 1.1. Summary of different articles that used microfluidics-based approaches to study different phenomena.**

Research topic icons were constructed by Freepik (chemotaxis, aerotaxis, magnetotaxis, pH taxis, growth tests and biofilm formation), Good Ware (rheotaxis) and fps web agency (thermotaxis) from www.flaticon.com



### i. Device with linear channels

Devices with linear channels are the most basic design and consist of straight channels, connected or separated from each other, and with openings at each end. Multiple channels can be added in parallel to create more versatile devices. Different conditions are used to study a behavioral comparison. This difference in environments can occur in the same channel, with different conditions at each end, or with homogeneity within the channel, but different conditions between channels. Thanks to this strategy, multiple gradients have been generated in order to study migratory responses in response to chemical molecules [74–77], oxygen availability [81–83], fluid flow [92,93], magnetic fields [95–97] or temperature [100–102], pH [103,104]. For example, when confronted with *E. coli* to the chemoattractants  $\alpha$ -methylaspartate and L-serine, it was determined that their speed increased by 35% [74]. These devices also allow to study the growth ration in presence of antibiotics and toxic substances [111–118]. For instance, *Pseudomonas aeruginosa* was cultured inside four independent channels, each containing different dilutions of an antimicrobial compound. The results correlated with standard antimicrobial susceptibility tests and produced results within 3 hours. Finally, biofilm formation was also studied in two connected channels device with two inputs that converge into only one outlet. Gashti *et al.* entered *Streptococcus salivarius* through a single inlet, managing to develop a biofilm only at the upper part of the central channel. The channels contained fluorescein, a pH indicator that showed a decrease in environmental pH in the biofilm area [102].

### ii. Devices with mixing channels

Microfluidic devices with mixing channels are more complex than those explained above since they require a network of channels, which is challenging in terms of both device design and fabrication. They consist of a series of interconnected microchannels that allow diffusive mixing. This channel network is used to generate a linear concentration gradient and has been used to determine that *E. coli* was attracted to low concentrations of L-

aspartate and deterred from high concentrations of L-aspartate and Ni<sup>2+</sup> [72]. With an oxygen mixture, these devices have been also used to recreate specific microenvironments whose conditions require precise control to grow several bacteria, such as *Streptococcus mutans* (anaerobe) and *Fusobacterium nucleatum* (anaerobe) [80].

### iii. Devices with multiple floors

Different layers of PDMS, with the same or distinct designs, can be successively bonded to create a microfluidic device with more than one floor. This allows the study of the relationship between two conditions at the same time or to recreate 3D conditions between different tissues. These devices have been used to generate temperature [98,99] or oxygen [78] circuits in a different plane than that of the bacterial culture, to study their migration and behavior under these conditions. This configuration also allows the arrangement of independent culture chambers on one floor, connected by a permeable membrane to a common chamber on another floor, allowing the study of intercellular communication. For example, *Azotobacter vinelandii*, *Bacillus licheniformis* and *Paenibacillus curdlanolyticus* colonies were unstable, and their population size decreased or were maintained at the initial levels over time when grown individually, but when they were connected, these colonies were stable with increasing population sizes [110].

### iv. Porous devices

The versatility of microfluidics designs permits the use of non-flat surfaces, increasing the scope of studies and allowing the possibility to recreate more realistic environments. For example, porous devices are characterized by a surface full of tiny holes on which bacteria adapt to grow or migrate. These designs are typically utilized to evaluate chemo- [70,71] and rheotaxis [90]. Hole distribution can be homogenous (same diameter and same separation distance), the microfluidic device simulates ideal flows in porous surfaces [90], or heterogenous (pore sizes and distances vary), recreating more realistic environment, such as soil surroundings [91,124].

#### v. Topographic devices

Topographic devices are characterized as showing an irregular design. Using a non-linear channel, Rusconi *et al.* evaluated *Pseudomonas aeruginosa* biofilm formation. Bacterial aggregation tended to be the more linear possibility, occupying the center of the channels and touching only the inner corners, without distinguishing between round or sharp corners [85]. These devices have also been used to observe how bacteria avoid obstacles to move forward. Yazdi *et al.* printed different flat and curved patterns on the surface of a device. They observed that against curved obstacles, *Magnetospirillum magneticum* maintained its axial direction, whereas when it faced flat obstacles, it switched its direction to backwards until it overcame the obstacle [94].

#### vi. Droplet microfluidics

Droplet-based microfluidics are characterized for their isolation and confinement of a single bacteria or small populations into individual droplets. These devices include an immiscible two-phase system: an organic liquid, usually oil, that fills the channel, and an aqueous liquid that breaks into droplets when it is introduced into the system [125]. Poisson statistics govern the ratio of organism encapsulation, determining the probability of isolating one or more cells per drop as a function of the starting concentration and occupied fraction of the droplets [126]. Droplet-based microfluidics is the most recent and innovative approach among microfluidic devices, still in an optimization phase, with several studies determining the optimal parameters for growing bacteria. The predominant assays are oriented to grow tests and biofilm formation. Kaushik *et al.* designed a device to determine antibiotic effects on bacteria. It consisted of two inlets to generate drops with a single bacterium, followed by a serpentine where bacteria reproduced a couple of times and a camera for fluorescence detection at the end. Through fluorescence analysis, the droplets were characterized as positive or negative depending on the presence or absence of bacteria, respectively. *E. coli* was tested with 4 µg/ml gentamycin, and the positive droplet ratio significantly decreased [106]. On the other hand, biofilm formation has been

studied inside droplets using *B. subtilis* as a model bacterium. It was described that these bacteria first swam individually, started to aggregate in 12 hours around the drop edges, and finally sporulated in 48 or 72 hours [119].

#### 1.1.2.4. Comparison between traditional methods and microfluidics

Both the use of traditional methods and microfluidic techniques provide a great contribution to scientific knowledge. However, microfluidics has a number of advantages over traditional methods (Table 1.2), which will be the reason why we have opted for this technique in this thesis.

Advantages	Limitations
Reproducibility of results obtained with traditional methods	PDMS absorption
Calculation of new data: migration rates	Absence of standardized protocols
Great variety of materials and designs: three dimensionality	Absence of cell cocultures
Small size and volume: high control and money savings	
Integration of processes in a single platform: times shortened	

**Table 1.2. Summary of microfluidic advantages and limitations**

##### i. Reproducibility of results

Microfluidics is a versatile technique that is gaining momentum in the field of microbiological research. The reproducibility of results previously obtained by traditional methods provides confidence and robustness to this tool. A clear example of this fact is the migration assays in which the chemotactic response of *E. coli* to different compounds is studied. Traditional methods are based on inoculating bacteria onto agar plates to analyze the kinetics of colony formation over time. The chemoattractant may be contained in the agar plate itself or may have been used to pretreat the bacterial sample following the method proposed by Adler [127]. This method consists of introducing a capillary with

chemoattractant into a bacterial solution that is subsequently deposited on an agar plate, and after its incubation, the number of colonies is quantified. By means of this methodology, Mesibov and Adler demonstrated that *E. coli* was attracted to several amino acids, including L-aspartate, showing a peak at a concentration of 10 mM [128]. Wolfe and Berg used the strategy of incorporating L-aspartate into agar plates and determined that *E. coli* shows maximum attraction at 10  $\mu$ M [129]. On the other hand, through the individual monitoring of bacteria grown in microcapillaries, both Roggo's and Cheng's teams corroborated the attraction of *E. coli* to L-aspartate at such concentrations, also highlighting migratory responses at intermediate concentrations such as 0.1 and 1 mM [76,77]. Thus, the similarity and reproducibility of the results obtained by both methods make microfluidics a reliable tool.

## ii. Calculating migration rates

However, although both methods are capable of determining optimal concentrations of chemoattractant, agar methods have limitations, such as the impossibility of calculating migration rates. This calculation is unfeasible since individual cells cannot be followed; instead, colony growth is evaluated. Partridge *et al.* decided to transfer colonies on agar plates to liquid cultures. They inoculated part of the cultures in small crystal chambers in order to monitor the bacteria individually, determining a migration speed of approximately 20-25  $\mu$ m/s [130]. Nevertheless, this approach is incompatible with the generation of chemical gradients. Therefore, it was necessary to rely on microfluidic techniques, such as a single-channel device designed by Ahmed and Stocker, with which they created gradients of  $\alpha$ -methylaspartate in a range of concentrations between 0.1 and 1 mM and obtained migration speeds between 0.6 and 13.8  $\mu$ m/s [74].

## iii. Versatility of materials and designs

While traditional methods are limited to working on flat two-dimensional (2D) surfaces, such as culture flasks, Petri dishes or well plates, microfluidics offers a new variety of materials with promising properties, among which PDMS stands out. Due to its

biocompatibility and gas permeability, it is ideal for cellular and microbiological cultures, but in addition, its optical transparency allows visualization and analysis by microscopy. However, its major advantage is the possibility of combining it with other materials, resulting in great versatility in device design. Thus, microfluidics offers the option of working in heterogeneous or even three-dimensional conditions, on which different stimuli, such as fluid flow or tactic gradients, can be applied. This advantage in culture conditions has been exposed by comparing two strategies to grow bacteria. On the one hand, following a traditional method, Bible *et al.* isolated *Pantoea sp.* from the rhizosphere of *Populus deltoides* and grew it on an agar plate [131]. On the other hand, Aufrecht *et al.*, after isolating *Pantoea sp.*, cultured it on a surface with heterogeneous pores that simulate a more realistic soil distribution [124]. In addition, Aufrecht applied a flow stream over the system to recreate rainwater filtration. While *Pantoea sp.* grew homogeneously on the agar plate and formed colonies [131], in the microfluidic device, it tended to grow by selecting preferential routes depending on the availability of nutrients provided by the stream flows [124]. Altogether, it is tempting to conclude that microfluidics offers the possibility of replicating more realistic environments than those offered by traditional methods.

#### iv. Small size and volume

The difference in volume and bacterial numbers used in microfluidics as opposed to conventional methods is also an aspect to consider. Microfluidics uses volumes in the microliter range, while traditional methods usually use volumes in the milliliter range. This small size turns microfluidic devices into portable tools and offers a number of advantages, such as economic savings in reagents, materials and space or a more accurate control of the biological and physical conditions of the study. From a biological perspective, macroscopic cultures contain a high number of bacteria, in the thousands or millions, giving rise to inevitable heterogeneity in the study population. In microfluidic assays, the number of bacteria is reduced to hundreds or even individual bacteria, achieving results that are more precise on the single-cell scale. In the physical environment, specific conditions can be achieved, making the growth of several bacteria possible, including oligotrophic bacteria,

which are still a challenge for traditional 2D cultures [132]. In addition, microfluidics allows almost instantaneous changes in environmental conditions within the device, allowing the study of bacterial adaptation. Lambert and Kussel designed a microfluidic device composed of a central channel and lateral culture chambers of  $25 \mu\text{m}^3$ . By adding a flow current through the main channel, they were able to generate transitions in the media conditions in less than 250 milliseconds. As a result, they studied the adaptive response of *E. coli* to fluctuating changes in glucose- or lactose-enriched broth media on a time scale of 1 to 10 generations [117]. On the other hand, Phillips *et al.* studied the same adaptive response in 1 ml of *E. coli* cultures, making daily inoculations to perform the media changes. They conducted these experiments over approximately 3,000 generations [133]. In this way, the greater control over the studied condition results is reflected in the reduced duration of the experiments.

#### v. Single platform

Experimental times can also be shortened by integrating several experimental processes into a single platform, thus also reducing the number of manipulations by researchers and therefore the risk of contamination and technical variability [62]. A clear example of the power of integration from microfluidics is droplet-based devices. This can be demonstrated by comparing the approach of these devices to traditional methods in the study of antimicrobial susceptibility. In 1966, the antibiotic susceptibility test was established by means of the standardized disk diffusion method [134], colloquially named the antibiogram, which is still used today [135]. This method consists of inoculating a bacterial culture onto an agar plate and placing it on a paper disk containing antibiotics that radially diffuse in the agar. After an incubation period, in the case where the bacteria are susceptible to the antibiotic, a growth inhibition zone appears whose diameter correlates with the antimicrobial power of the antibiotic tested. Kaushik *et al.* proposed a droplet-based microfluidic device in which they integrated the incubation of the bacteria in contact with the antibiotic in microdrops with the detection and analysis of its susceptibility (*figure 8b*) through the fluorescence produced by resazurin when reduced by the bacterial

metabolic activity [106]. While the standardized method requires several manipulations, including inoculation, deposition of the antibiotic disk or measurement of the diameter of the inhibition zone, the microfluidic device integrates all steps in a continuous flow system where the only manipulation is the initial load of the components to be studied. In addition, the antibiogram requires at least 24 hours of incubation, while microfluidic devices allow testing of antimicrobial susceptibility after 1 hour. Undoubtedly, this time-saving and minimal technical manipulation are valuable considerations for the use of microfluidic devices in a clinical context, where proper treatment of infected patients requires reliable and instant results.

#### vi. PDMS absorption

Nevertheless, microfluidics still has a long way to go to overcome several of the challenges it presents. For example, despite the numerous advantages described above for PDMS, we also have also found some drawbacks. Its major limitation in the cellular field is its capacity to absorb small hydrophobic molecules or biomolecules, such as proteins, interfering with the results of the assays. This demonstration was performed by van Meer *et al.*, comparing the absorption of four cardiac drugs when incubated in standard tissue culture grade polystyrene (TCPS) 96-well and PDMS wells. While the adsorption in the TCPS wells was negligible, PDMS adsorbed between 20 and 80% of the compounds within 3 hours [136]. PDMS is a porous material that not only absorbs molecules but also allows the passage of organic solvents that can modify the dimensions of the channels. Dangla *et al.* observed that when filling 50  $\mu\text{m}$ -high channels with the solvent hexadecane, the channels were deformed by sinking the ceiling parabolically by approximately 7  $\mu\text{m}$  [137]. As a result, protocols are being developed that modify the surface of PDMS to avoid these phenomena [138–140].

#### vii. Absence of standardized protocols

Due to its recent appearance, the absence of standardized protocols in microfluidics-based research is evident. Bacteria are mainly visualized using microscopy



techniques, which require reporter-labeled bacteria and/or specialized microscopy facilities [141]. This restricts microfluidics assays to visual analysis and model microorganisms, which frequently do not reflect the virulent traits of pathogenic species. The assays carried out are mostly focused on the study of migration trajectories and growth rates, and it is clear that there is a lack of molecular characterization. The development of devices based on droplets has led to a great advance in this field, giving the possibility of studying bacteria at a single cell level. In addition, some protocols for the extraction of nucleic acids and proteins from samples confined within microfluidic devices have been published [142–145]. Nevertheless, microfluidics is far from assessing molecular changes at the intracellular level, and new techniques have to be improved to allow genomic, transcriptomic, proteomic and metabolomic research at the same level as established methods. Once these limitations are overcome, microfluidics might become an indispensable technique for research and commercial applications.

#### viii. Absence of cell cocultures

Most microfluidic studies involving bacteria have been performed using environmental or nonpathogenic species. This fact shows a knowledge gap in the biomedical field regarding the interaction between host cells and bacteria, both symbiotic and pathogenic. Some researchers have developed more complex microfluidic devices, integrating several tissues to mimic organs, which is known as organ-on-a-chip. Some of the organs that have been simulated thanks to microfluidics are the gut [146], lung [147], liver [148], endothelial vessels [149] and brain [150]. The application of bacteria in these systems would not only result in a more complete and realistic approach to recreate complex bacterial interactions with some human organs, but would also allow for a more detailed study of the host-bacterial interplay *in vitro*.

## 1.2. Objectives

The main objective of this thesis is to apply microfluidic devices to recreate bacterial infection processes more realistically than traditional methods. Specifically, stages involving macrophages and their interaction with pathogens. For this purpose, a series of sub-targets were proposed, focusing on two processes under study: monocyte extravasation and macrophage migration in response to bacterial stimuli.

Regarding monocyte extravasation, the following subobjectives were proposed:

- Develop a functional endothelial vessel that allows quantification of extravasation.
- Determine the effect of oscillatory flow on the process of monocyte extravasation.
- Determine the effect of environmental stiffness on the process of monocyte extravasation.

Regarding macrophage migration in response to bacterial stimuli, these other subobjectives were proposed:

- Determine the optimal conditions for macrophage tracking.
- Analyze changes in macrophage migration patterns in the presence of pathogenic bacteria
- Analyze changes in macrophage migration patterns in the presence of non-pathogenic bacteria.

### 1.3. Thesis overview

This thesis is structured in 6 chapters. This initial chapter is dedicated to a basic explanation of the immune system and the infections produced by the bacteria of interest, *Salmonella typhimurium* and *Mycobacterium tuberculosis*. In addition, a review of the state of the art is presented on bacterial behavior studies with traditional methods and microfluidic techniques, offering a comparison of the advantages and limitations of both. Then, chapters 2 and 3 are focused on two different stages of infection.

In chapter 2, we show a microfluidic device that allows the study of monocyte extravasation. In addition, the effect of oscillatory flow and environmental stiffness on the extravasation process is determined.

In chapter 3, the migration of macrophages in response to a gradient of molecules obtained from bacterial fractions is studied. The bacteria studied were *Salmonella typhimurium*, *Mycobacterium tuberculosis*, *Escherichia coli* and *Mycobacterium smegmatis*. The macrophage tracking during 24 h allows us to deduce the presence of immunogenic and attractant molecules.

Chapter 4 contains the global conclusions of the thesis, both in English and Spanish, future work and contributions from this PhD Dissertations.

The PhD dissertation finishes with two chapters that include future work and contributions from this PhD Dissertations, an appendix with methodology developed from future work, and references.



## 2. MONOCYTE EXTRAVASATION

---



## 2.1. Abstract \*

Extravasation of circulating cells is an essential process that governs tissue inflammation and the body's response to pathogenic infection. To initiate anti-inflammatory and phagocytic functions within tissues, immune cells must cross the vascular endothelial barrier from the vessel lumen to the subluminal extracellular matrix. In this work, we present a microfluidic approach that enables the recreation of a three-dimensional, perfused endothelial vessel formed by human endothelial cells embedded within in a collagen-rich matrix. Monocytes are introduced into the vessel perfusate, and we investigate the role of luminal flow and collagen concentration on extravasation. In vessels conditioned with flow, increased monocyte adhesion to the vascular wall was observed, though fewer monocytes extravasated to the collagen hydrogel. Our results suggest the lower rates of extravasation are due to the increased vessel integrity and reduced permeability of the endothelial monolayer. We further demonstrate that vascular permeability is a function of collagen hydrogel mass concentration, with increased collagen concentrations leading to elevated vascular permeability and increased extravasation. Collectively, our results demonstrate that extravasation of monocytes is highly regulated by the structural integrity of the endothelial monolayer. The microfluidic approach developed here allows for the dissection of the relative contributions of these cues to further understand the key governing processes that regulate circulating cell extravasation and inflammation.

\* This chapter 1 correspond to the article already published as: **Pérez-Rodríguez, S.**; Huang, S.A.; Borau, C.; García-Aznar, JM.; Polacheck, W.J. **Microfluidic model of monocyte extravasation reveals the role of hemodynamics and subendothelial matrix mechanics in regulating endothelial integrity.** *Biomicrofluidics*. 2021, 15(5):054102. doi: 10.1063/5.0061997.

## 2.2. Introduction

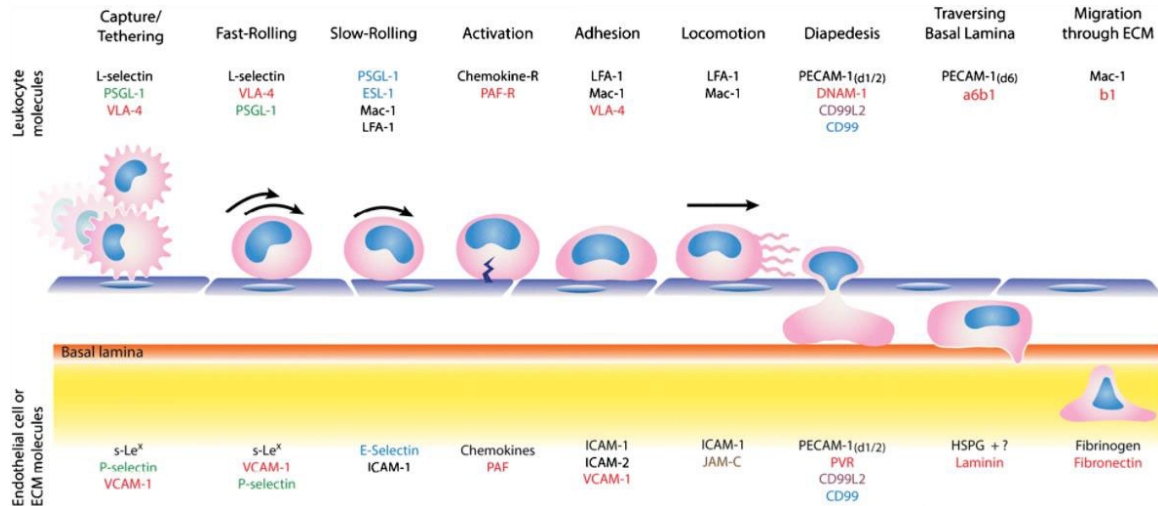
### 2.2.1. Monocyte extravasation

Extravasation is the process by which cells and proteins traverse the endothelial barrier from the intravascular cannula into surrounding tissue [151]. During an inflammatory injury or bacterial infection, immune cells extravasate in response to mechanical and chemical stimuli secreted by damaged tissues [152]. In this work, we focus specifically on monocyte extravasation due to its essential role in homeostasis and the development of innate and adaptive immune responses to pathogens [153]. While a number of cellular and molecular regulators of extravasation have been identified using conventional *in vitro* approaches [154], interpreting these results in the context of the native microenvironment is challenging due to limitations to *in vitro* culture systems, including the lack of physiologic tissue architecture and mechanics. Here, we seek to address these shortcomings through the implementation of a microfluidic multi-cell culture system that more closely mimics the native architecture and mechanics of the microvasculature.

Monocyte extravasation is initiated through the coordination of receptor-mediated interactions between the apical surface of vascular endothelial cells and monocytes (Figure 2.1). First, immune cells from damaged tissue secrete inflammatory cytokines that induce the expression of adhesion molecules in endothelial cells. E- and P-selectin, intercellular adhesion molecule 1 (ICAM-1) and vascular cell adhesion molecule 1 (VCAM-1) have been specifically implicated in monocyte-endothelial interactions [155]. ICAM-1 and VCAM-1 contribute to monocyte adhesion [156], and VCAM-1 reduces rolling speed and enhances firm arrest [157]. Additionally, monocytes have basal expression of P-selectin Glycoprotein Ligand 1 (PSGL-1), which interacts with endothelial selectins, allowing for the attachment and rolling of monocytes [158]. Once monocytes attach to the endothelial wall, an increase in endothelial RhoA GTPase-mediated actomyosin contractility in endothelial cells induces intercellular junction disassembly and the formation of transient gaps in the monolayer



[159]. Finally, monocytes generate protrusions to probe the endothelial surface and cross the endothelial barrier [160,161].



**Figure 2.1. Stages of leukocyte extravasation and the molecules involved.**

Leukocytes (pink cells) circulating in the blood system come into contact with endothelial cells (blue cells) and slow down until they adhere to them. They then generate a series of protrusions that allow them to sense the environment and cross the barrier between the endothelial cell junctions until they reach the basal lamina (red) and the extracellular matrix (yellow). Numerous molecules are involved in this process, such as P- and E-selectins, or the adhesins VCAM-1 and ICAM-1, on the part of the endothelial cells, or PSLG-1 on the part of the leukocytes. Taken from [162].

### 2.2.2. Role of hemodynamics in extravasation

Hemodynamics play a critical role in extravasation through modulating protein expression and signaling in endothelial cells. Fluid shear stress between 2 and 10 dynes/cm<sup>2</sup> upregulates the expression of E-selectin, P-selectin, ICAM-1 and VCAM-1 on endothelial cells, leading to an increase in monocyte arrest at the endothelial wall [163–165]. Conversely, endothelial cells exposed to physiological shear stress, in a range between 3 and 5 dynes/cm<sup>2</sup>, suppress RhoA signaling and upregulate Rac1 signaling, resulting in adherens junction assembly and cytoskeletal alignment [166–168]. Therefore, hemodynamic shear stress imparts competing signals on the extravasation process by increasing monocyte arrest to the endothelium, but strengthening the vascular barrier. Further dissection of these mechanisms necessitates the development of a platform in

which vascular endothelial cells and monocytes can be cultured in a hemodynamic environment and observed in real time.

### 2.2.3. Role of surrounding stiffness in extravasation

Signals from the basal surface of the endothelium, including the perivascular extracellular matrix, have also been shown to play a role in extravasation. Vascular endothelial cells are highly sensitive to the stiffness of the underlying matrix [169], and pathologically increased matrix stiffness drives increases in vascular permeability [170]. Substrate mechanics also play a role in monocyte adhesion. For example, Mackay and Hammer observed increased monocyte attachment to hydrogels coated with E-selectin as a function of stiffness, but they found no stiffness-dependence for gels coated with P-selectin [171], highlighting the complex interplay between biochemical and biophysical cues in extravasation. Moreover, stiffer substrates are required to properly recruit and stabilize ICAM-1 on endothelial cells [172]. Collectively, these studies demonstrate that investigation of the key factors and molecular mediators that govern extravasation requires recapitulation of native perivascular matrix mechanics.

### 2.2.4. Models to study extravasation

A variety of model systems have been developed to investigate the key molecular mechanisms that govern extravasation. Key chemokines secreted by monocytes, including IL-8 and monocyte chemoattractant protein-1 (MCP-1) which regulate firm monocyte adhesion and extravasation from the vascular endothelium, have been identified by molecular binding assays [173,174]. Electrophoresis, microarrays, and polymerase chain reaction (PCR) techniques have allowed for the evaluation of monocyte and endothelial gene and protein expression that correlate with extravasation events in response to inflammatory factors. For example, lipopolysaccharides (LPS) induce E-selectin, VCAM-1 and ICAM-1 gene expression [175], whereas interferon gamma (INF- $\gamma$ ) and IL-4 upregulate MCP-1 mRNA and protein expression [176,177]. In addition, electron microscopy has provided spatial resolution for key signaling pathways including IL-8, which, after being

secreted by monocytes, is concentrated at the apical surface of endothelial cells prior to internalizations [178]. Furthermore, the combination of these data with animal models and computational simulations has elucidated possible models of paracellular and transcellular migration of leukocytes across endothelial barriers [179], [180,181]. Despite enabling significant progress in identifying key governing pathways, these approaches have limitations, including a lack of physiological architecture and mechanics in *in vitro* systems [182], and divergent mechanisms in mouse and human models [183], [184]. For example, the commonly used mice strain C57B1/6 exhibits cell-mediated immunity and Natural Killer (NK) cell activity that is significantly higher than other mice strains [185], and which is not representative of humans [186].

Microfluidic systems address some of these key limitations, particularly the need for more physiologic, three dimensional microenvironments *in vitro* [187], [61]. Recently, a number of microfluidic approaches have been developed for the study of extravasation [188–190], as recently reviewed Ma *et. al* [191]. However, the majority of these approaches are used to study cancer cell extravasation during metastasis, while the study of leukocytes and immune cell extravasation has received less attention. A few experimental approaches have been developed to study leukocyte extravasation in microfluidic devices, including endothelial cells cultured as a monolayer on a porous membrane [183,192,193], vascular networks embedded within collagen hydrogels [189], and endothelial monolayers attached to a rectangular PDMS channel [194]. Studies using these platforms have contributed to a fundamental and critical understanding of the mechanisms of extravasation, such as the relation between cancer cell extravasation and the expression of adenosine receptors [189] and late metastatic markers [194] or the inability of leukocytes to extravasate when treated with pertussis toxin [183]. However, there exist significant limitations in the physiological relevance of these approaches, including the lack of three-dimensional native architecture and/or physiologic substrate mechanics and hemodynamics.

Here, we present a microfluidic device and an approach that allows the formation of a continuous, lumenized, cylindrical monolayer of endothelial cells embedded within a collagen type-I matrix [195]. The diameter of this vessel varies between 150-250  $\mu\text{m}$ ,

resembling physiological arterioles and venules [196,197]. In vessels of this size, mechanotransduction of hemodynamic shear stresses facilitate interactions between immune and endothelial cells and immune cell extravasation [186,198]. Using this platform, we demonstrate key aspects of physiological monocyte extravasation, including arrest to the apical vascular endothelial surface, crossing of the vascular endothelial barrier, and 3D migration through the hydrogel matrix. We further investigate the effect of hemodynamic shear stress and perivascular collagen concentration on extravasation, and the results of these studies demonstrate a critical role for biophysical stimuli in extravasation.

## 2.3. Methods

### 2.3.1. Cell Culture

Human umbilical vein endothelial cells (HUVECs) were grown in EGM-2 medium supplemented with 2% of fetal bovine serum (FBS), hydrocortisone, vascular endothelial growth factor (VEGF), R3 insulin-like growth factor 1 (R3 IGF-1), ascorbic acid, human epidermal growth factor (hEGF), gentamicin sulfate/amphotericin (GA-1000) and heparin (medium EGM-2, Lonza, Basel, Switzerland). Cells were used from passage number 2 to 10, consistent with manufacturer recommendations to assure the viability and an adequate metabolism of cells.

THP-1 is a commercial cell line of monocytes isolated from peripheral blood from the American Type Cell Culture (ATCC TIB202™, Manassas, VA, Unites States). THP-1 were grown in suspension in RPMI-1640 media supplemented with L-glutamine, 2% of FBS and ampicillin/streptomycin (RPMI-1640, Gibco, Gaithersburg, MD, United States), and THP-1 were used from passage number 0 to 7.

### 2.3.2. Fabrication of Microfluidic Devices

Microfluidic devices ([Figure 2.2](#)) were prepared following the protocol developed by Polacheck *et al.* [167], with minor modifications. Briefly, PDMS molds were generated by the mixture and degasification of the curing agent of Sylgard 184 silicone elastomer and the

base in a 1:10 ratio, poured onto plastic molds replica molded from silicon master molds patterned by photolithography, and incubated at 60 °C for 24 h. Next, PDMS mold was separated from the plastic molds, and devices were individually cut and autoclaved. PDMS devices and glass coverslips (22 x 40 mm cover slips, Menzel-Gläser, Brunswick, Alemania), pretreated with iso-2-propanol, were treated with oxygen plasma for 30 s to surface activate the PDMS and promote glass-PDMS bonding. Sealed devices were incubated at 100 °C for 10 minutes then treated with 1 mg/ml poly-D-lysine (PDL) (Sigma, St Louis, MO, United States) for one-channel devices or 0.01% w/v poly-L-lysine (PLL) (Sigma, St Louis, MO, United States) for two-channel devices, for at least 1 hour at room temperature. Then, washed with deionized water, treated with 1% glutaraldehyde for 15 min, and washed with deionized water for 24 hours on a shaker. For faster device turnaround, the PDMS can be treated with 2 mg/ml dopamine hydrochloride (Millipore Sigma) in 10 mM Tris buffer pH 8.5 (bioWORLD, Dublin, OH) for two hours, followed by a wash with deionized water [199].

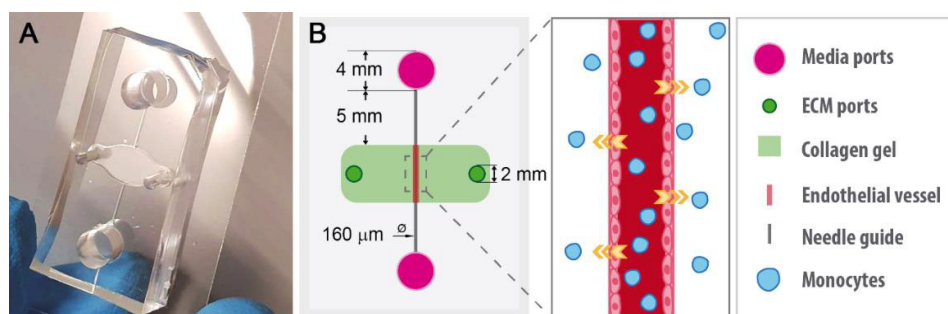
### 2.3.3. Formation of the Endothelial Vessel

After fabrication, bonding, and surface treatment, the devices were sterilized in a 70% ethanol solution for 30 minutes. A 0.16 mm diameter acupuncture needle ( $\Phi$  0.16 x 40 mm, Seirin, Shizuoka, Japan), pretreated with 0.01% bovine serum albumin (BSA) in phosphate-buffered saline (PBS) for 30 min, was inserted into the device and sterilized with ultra violet light for 15 min. Subsequently, reconstituted type-I collagen derived from rat tail (Corning, Glendale, AZ, United States), was buffered to a pH of 7.5 with 1 N NaOH in sterile H<sub>2</sub>O, 10x dPBS with phenol (Euroclone, Milan, Italy) and EGM-2 medium, was introduced in the central region of the device. Two different collagen concentrations were tested, 2.5 and 6 mg/ml, starting from stock concentrations at 4.33 and 9.44 mg/ml, respectively. Devices were moved to a humidified incubator at 37 °C for at least 2 h, and device reservoirs were filled of EGM-2 media to avoid dehydration of the hydrogel. Next, the needle was removed, and the device was sealed with vacuum grease (Millipore Sigma, Saint Louis, MO, United States). For two-channel devices, the same procedure was performed with two needles inserted into each device.

Fresh EGM-2 was introduced into devices, and devices were moved to a laboratory rocker within a humidified incubator to wash devices for 24 hrs. The next day, a HUVECs suspension with a final concentration of  $2 \cdot 10^6$  cells/ml in EGM-2 was introduced into the device reservoirs, and cell adherence to the central channel in the collagen gel was observed by phase contrast microscopy (Nikon D-Eclipse C1 Confocal Microscope, 10x lens, Nikon Instruments, Tokyo, Japan). As previously described, when the cylindrical space was covered by an adequate density of HUVECs [167], cell-containing media was replaced with fresh media and devices were incubated at 37 °C for 24 hours on a rocker at 30 degrees and 5 cycles/min to introduce oscillatory, reciprocating flow through the vessel lumen.

#### 2.3.4. Extravasation Assays

For the extravasation assays, a solution of  $7.5 \cdot 10^5$  cell/ml of THP-1 monocytes were resuspended in EGM-2 media and introduced into device ports. Devices were incubated at 37 °C for 24 hours prior to analysis (Figure 2.2). To study the influence of flow in the extravasation process, devices were pretreated with oscillating flow for 24 hours before adding the monocytes, while static devices were maintained on a shelf of the same incubator for 24 hours too. To analyze the role of collagen density, extravasation assays were conducted with 2.5 and 6 mg/ml collagen hydrogels as described above.



**Figure 2.2. Microfluidic platform for investigating monocyte extravasation.**

A) Photograph of device bonded to (24 mm x 40 mm coverslip). B) Graphical representation of the device (not to scale) that consists of a central chamber with two ports (dark green) through which the collagen gel (light green) is introduced and polymerized. A channel formed by an acupuncture needle connects two reservoirs filled with medium (bright pink) to the collagen gel region. HUVECs line the channel in the collagen gel (pink), and hydrostatic pressure gradients induced by the rocker induce flow through the channel. Monocytes (blue) are flowed through the vessel, and extravasation from the lumen into the collagen hydrogel is investigated using light microscopy.

### 2.3.5. Immunofluorescence

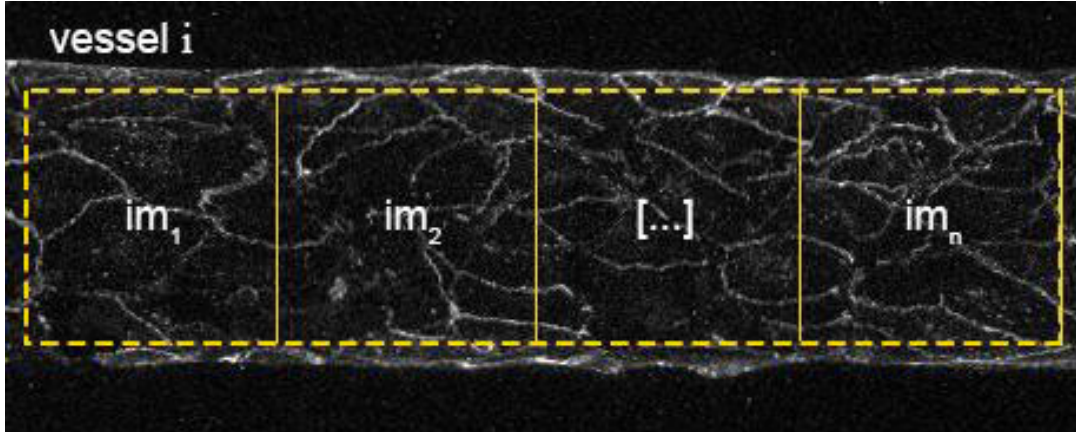
Devices were washed with PBS + 0.5 mM MgCl<sub>2</sub> + 1 mM CaCl<sub>2</sub> (PBS++), fixed with 4% paraformaldehyde (PFA) at 37 °C for 20 min on the oscillatory rocker, and washed again with PBS++. Samples were permeabilized with 0.1% Triton X (Calbiochem, Darmstadt, Alemania) for 20 minutes and washed with PBS++. Subsequently, devices were rocked with 4',6-diamino-2-fenilindol (DAPI) (1:1000) (Invitrogen, Carlsbad, CA, United States) and rhodamine phalloidin (1:200) (Thermo Fisher Scientific, Madrid, Spain) in 2% BSA in PBS++ at room temperature for 20 min. After washing with 2% BSA, devices were incubated with primary antibody against VE-cadherin (1:200) (Santa Cruz Biotechnology, Santa Cruz, CA, Unites States) in 2% BSA in PBS++ at 4 °C overnight. Next, anti-goat Alexa Fluor 647 secondary antibody (1:250) (Thermo Fisher Scientific, Madrid, Spain) in 2% BSA in PBS++ was added at room temperature for 2 hours while protected from light. Finally, devices were washed with 2% BSA and stored at 4 °C. Maximum intensity projections were synthesized from Z-stack series obtained with a laser scanning confocal microscopy (FV3000, Olympus) at 20x magnification (20x C Plan fluor 0.7 NA air objective, Olympus).

### 2.3.6. Image acquisition and analysis

Data for extravasation assays were obtained from the analysis of fixed immunofluorescence images taken as described above with a 20x objective. The number of extravasated and adhered monocytes, the monocyte migration distance, and diameters were measured manually using Fiji [200]. Monocytes were identified and differentiated from HUVECs by their small size, rounded shape and different cell refractive index, which gave them a different shade of gray under the bright-field microscope [201,202].

Alignment of phalloidin and VE-cadherin networks was determined by analyzing the maximum intensity projection of seven independent assays. After the projection, vessel images were split in square patches and their walls were removed to avoid bias in the main direction of the vessel (Figure 2.3). The alignment index ( $\alpha$ ) was estimated using a discrete

Fourier Transform (FT) method as described previously [203,204]. This index ranges from 0 to 1, with 1 meaning a complete alignment of the network and 0 a random orientation.



**Figure 2.3. Image processing.**

Sample images demonstrating the process by which a maximum intensity project was processed to measure an alignment index parameter. Projections were split in square blocks to perform the alignment analysis to ensure lateral vessel boundaries did not contribute to alignment index calculations.

### 2.3.7. Permeability assays

Diffusive permeability ( $P_d$ ) of vessels was quantified as previously described [167]. Briefly, EGM-2 supplemented with 70-kDa fluorescent dextran TexasRed (200  $\mu\text{g}/\text{ml}$ ) (Sigma-Aldrich, Saint Louis, MO, United States) was introduced into the vessel, and images were taken at 10x magnification every 5 s for 50 cycles at the median transversal plane of the vessel. Total flux of dextran transported across the vascular wall was quantified by measuring the total intensity within the vessel for each time point ( $I_0$ ), and the total intensity outside of the vessel ( $I$ ) as a function of time. The radius of the vessel ( $r$ ), intensity within the vessel ( $I_0$ ), and rate of change of intensity outside of the vessel ( $\delta I/\delta t$ ) were used to determine  $P_d$  through the following relation:

$$P_d = \left(\frac{2r}{I_0}\right)\left(\frac{\delta I}{\delta t}\right)$$



### 2.3.8. Collagen hydrogel characterization

Collagen hydrogels at mass concentrations of 2.5 and 6 mg/ml were prepared as described above and frozen in liquid nitrogen overnight prior to lyophilization (ScanVac CoolSafe 110-4, Labogene, Lynge, Denmark) for 44 hours. Samples were then deposited in holders on carbon tape and coated with a 14 nm layer of palladium to increase conductivity. The gels were visualized and photographed using a field scanning electron microscope (CSEM-FEG INSPECT F50, FEI Company, Hillboro, OR, United States) at resolutions of 10, 20, 50 and 100K.

### 2.3.9. Determination of hydraulic permeability

Following removal of needles in a two-channel device, all device reservoirs were emptied and filled with 70-kDa fluorescent dextran fluorescein (FITC) (200  $\mu\text{g/ml}$ ) (Sigma-Aldrich, Saint Louis, MO, United States) in PBS. These devices were then incubated overnight at 37  $^{\circ}\text{C}$  to allow the dextran to permeate the collagen hydrogel. The reservoirs were then emptied, and glass capillary tubes were inserted into the reservoirs of one channel. Any gaps between the PDMS and glass were sealed using vacuum grease, and the 70-kDa FITC solution was added to the glass reservoirs to apply a hydrostatic pressure of 5, 10, or 20  $\text{mmH}_2\text{O}$ . Fluorescence recovery after photobleaching (FRAP) was performed by finding the median transversal plane of the vessel and photobleaching a 50 pixel circle in the collagen gel between the two channels for 3 seconds, followed by continuous imaging of the bleached circle every second for 30 seconds. The velocity of the interstitial flow induced by the hydrostatic pressure was calculated using a custom Matlab code (Mathworks, Natick, CA, USA) that fit a circle to the bleached region and determined circle displacement across the time series.

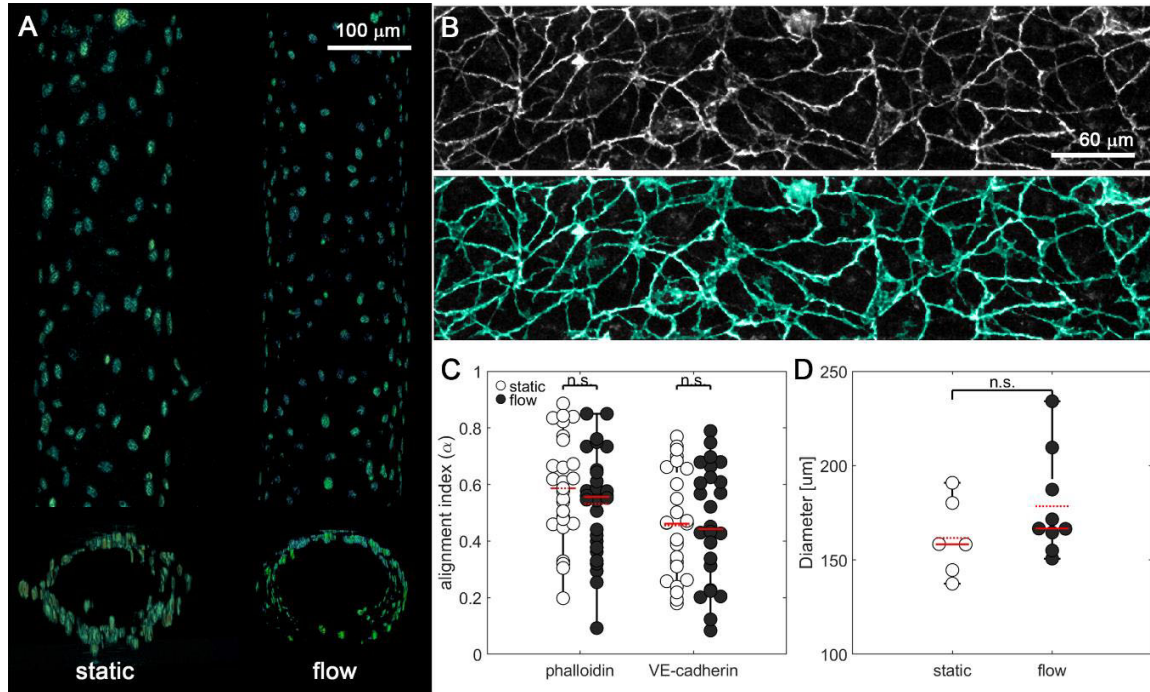
## 2.4. Results

### 2.4.1. Microfabricated blood vessels that mimic physiologic vasculature.

We fabricated a microfluidic cell culture system to develop microfabricated blood vessels, consisting of a perfusable channel lined with HUVECs embedded in 3D collagen hydrogel (Figure 2.4). After seeding with endothelial cells, these devices were cultured with oscillatory flow or under static conditions for 24 hours. To characterize endothelial cell distribution within devices, we fixed the devices, stained them with DAPI, and performed a three-dimensional reconstruction of the spatial arrangement of the nuclei of endothelial cells forming the vessel (Figure 2.4A). These reconstructions reveal a continuous cylindrical endothelial monolayer embedded within the collagen type I hydrogel. It has been shown previously that application of physiologic hemodynamic shear stress leads to alignment of the actin cytoskeleton [205]. To measure the alignment of filamentous actin fibers, we stained fixed devices with rhodamine phalloidin and anti-VE-cadherin antibodies. VE-cadherin is an adherent junction protein that in part regulates endothelial permeability [206], and assembly of VE-cadherin-containing junctions indicates the establishment of endothelial barrier function [207].

By performing a simple threshold segmentation of the VE-cadherin staining, we observed that all pixels were connected in a lattice of cell-cell junctions as a single object (Figure 2.4B). This suggests that there are no gaps between the HUVECs forming the vessel and that it is in fact composed by a continuous monolayer of endothelial cells. We then computed an alignment index using a Fourier transform analysis of max intensity projections from z-stacks acquired with confocal microscopy. With this approach, we observed that the cytoskeleton presents an alignment index slightly greater than 0.5, and that VE-cadherin alignment was approximately 0.5. In both cases, there were no significant differences between vessels cultured under static and flow conditions (Figure 2.4C). This index value indicates that the fibers are aligned mostly parallel to the vessel, in the same direction as flow. We further used devices stained with phalloidin to measure vessel

diameter, which ranged from 125 to 250  $\mu\text{m}$  (Figure 2.4D) and is comparable to the diameter of human arterioles and venules [196], [197].



**Figure 2.4. Endothelial vessels embedded in 2.5 and 6 mg/ml collagen gels within the microfluidic device.**

A) Three-dimensional reconstruction from nuclei staining with DAPI, showing a longitudinal (upper) and transverse (lower) view from a static and a flow vessel. B) First row shows a grayscale example of the VE-cadherin staining of a vessel (maximum intensity projection) while second row shows, superimposed in cyan, the segmentation of the former performed by simple thresholding. C) Phalloidin and VE-cadherin alignment index ( $\alpha$ ) of the maximum fluorescence projection of an endothelial vessel, with 1 being the complete alignment parallel to the vessel. D) Diameters of each static and flow endothelial vessel. For all plots, each data point represents data from an individual device, and solid and dashed red lines represent the median and mean values, respectively. ANOVA tests were performed to determine statistical significance. \* $p < 0.05$ .

### 2.4.2. Fluid shear stress increases monocytes adherence to the vessel wall but decreases extravasation

Physiologically, fluid shear stresses stimulate monocytes and endothelial cells by increasing their expression of adhesion proteins, including E-selectin and ICAM-1, and by reorganizing the cytoskeleton of endothelial cells [163,193]. To investigate the role of endothelial response to hemodynamic shear stress on monocyte attachment and

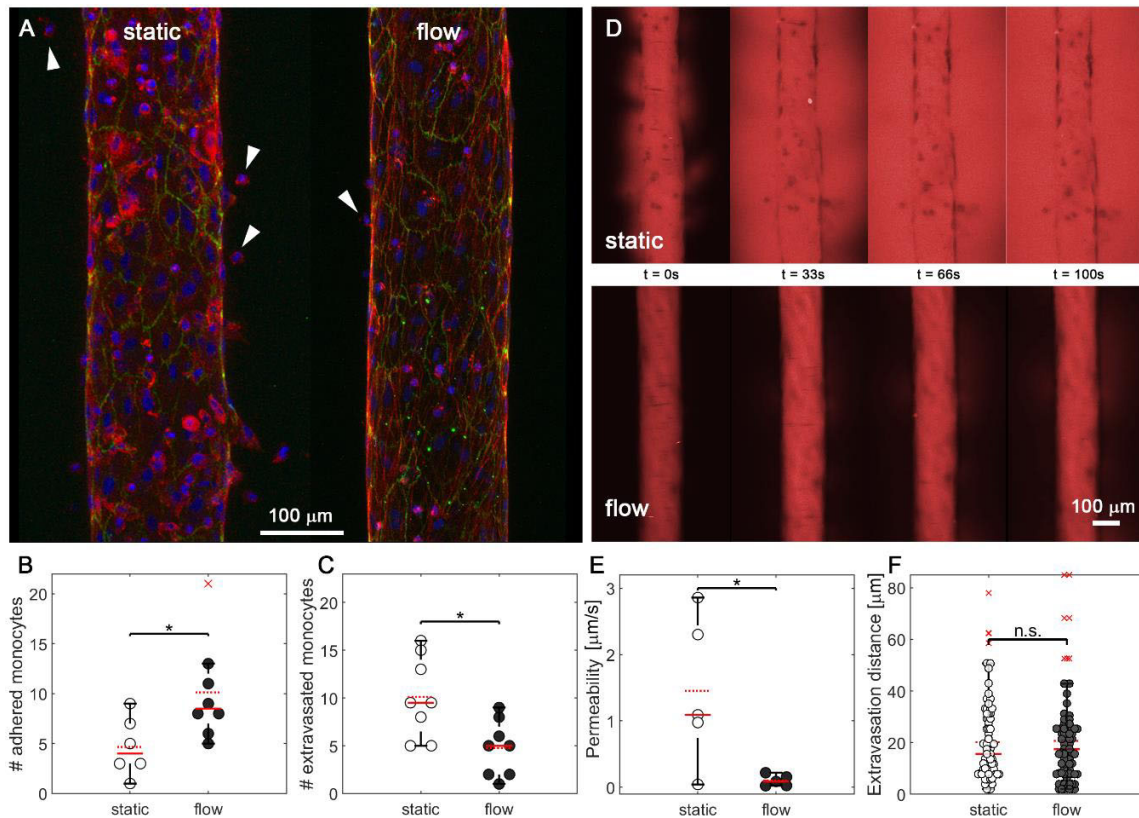
extravasation, endothelial vessels were pretreated with 24 hours of oscillatory flow or were cultured in static conditions. After this differential treatment, monocytes were added to one of the reservoirs to introduce a hydrostatic pressure gradient resulting in flow of monocytes through the endothelial lumen for 24 hours.

Treatment of vessels with flow resulted an increase in adherent monocytes and a decrease in extravasated monocytes (Figure 2.5A). To quantify this observation, monocyte nuclei stained with DAPI were counted in image stacks acquired with a laser-scanning confocal. Vessels pretreated with flow demonstrated between 5 and 20 adherent leukocytes per vessel (counted along the entire vessel), while static vessels did not exceed 10 monocytes per vessel (Figure 2.5B). This statistically significant effect of flow is supported by previous work demonstrating that flow increases expression of proteins involved in monocyte adherence, including E-selectin and ICAM-1, in vascular endothelial cells [163]. Despite the increase in monocyte adherence to the lumen of flow-stimulated vessels, we found a decrease in the number of monocytes that traversed the endothelial barrier and migrated into the collagen hydrogel. As quantified from confocal z-stacks, extravasated monocytes in static vessels ranged from 5 to 20 per vessel, whereas when treated with flow, the range is reduced to 1 to 10 (Figure 2.5C). We hypothesized that the decreased rate of extravasation could be due to the effects of flow on vascular endothelial barrier integrity, as permeability of endothelial cell monolayers decreases with applied flow [193].

To test this hypothesis and to determine whether flow impacts barrier function of the vascular endothelial monolayer, we quantified the diffusive flux of fluorescently tagged 70 kDa dextran from the vessel lumen into the hydrogel using time lapse confocal microscopy. After 100 seconds of dextran perfusion, we observed a stark difference between the distribution of dextran throughout the hydrogels, with the levels of dextran within the subluminal matrix nearly equivalent to those in the lumen for vessels cultured in static conditions (Figure 2.5D). To quantify this observation, we measured the diffusive permeability of vessels, a measure of the barrier to diffusive flux in response to discrete changes in concentration across a membrane, in this case the endothelial monolayer. We

found a significant difference in the diffusive permeability of vessels cultured in static vs. flow conditions, with the mean permeability more than 10 times higher in static vessels (mean = 1.45  $\mu\text{m/s}$ ) than in flow-treated vessels (mean = 0.10  $\mu\text{m/s}$ ) (Figure 2.5E), consistent with previous observations [208]. Previous work has demonstrated that a flow-mediated reduction in vascular permeability is driven by the assembly of VE-cadherin-containing adherens junction complexes [168], and we hypothesize that this junctional assembly presents a barrier to monocyte migration and extravasation. This hypothesis is further supported by work demonstrating that VE-cadherin expression levels are increased with flow [209] and is an essential part of a mechanosensory complex that plays a role in the establishment and maturation of tight junctions [210], [211], and that mature adherens junctions present a barrier to monocyte extravasation [153].

Interestingly, once monocytes have crossed the endothelial barrier, there is no difference in the total migration distance through the collagen gel. In both conditions, monocytes travel around 20  $\mu\text{m}$  from the vessel wall (Figure 2.5F). These results are similar to previously published data by Boussohier-Calleja et al., which indicated that after extravasation, monocytes tended to migrate between 10-20  $\mu\text{m}$  [212]. Our longer migration distances might be explained by differences in the hydrogels used. Boussohier-Calleja worked with 3 mg/ml fibrin collagens, whereas we use 2.5 mg/ml collagen gels. In addition, fibrin gels present different fiber organization, with smaller pore sizes [213]. It has also been demonstrated that cells encounter greater steric hindrance in their advance and migrate shorter distances when traversing fibrin gels compared to collagen gels [214].

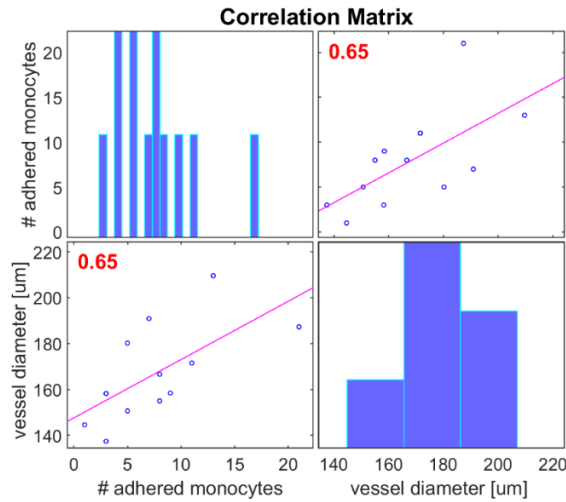


**Figure 2.5. Effect of the fluid flow stimulation on extravasation.**

A) Endothelial vessels in 2.5 mg/ml hydrogels in static (left) and flow-pretreated (right) conditions. Vessels are stained for actin (red), VE-cadherin (green) and nucleus (blue). Extravasated monocytes are indicated with white arrows. B) Number of monocytes adhered to the endothelial lumen in static (white) and flow-pretreated (black) vessels. C) Number of monocytes extravasated from the lumen to the surrounding hydrogel in static (white) and flow-pretreated (black) vessels. D) Permeability assay with 70 kDa fluorescent dextran (red) added to the endothelial lumen. Images are single confocal slices taken after the addition of dextran in a static (upper) and a flow-pretreated (lower) vessel. E) Permeability of static (white) and flow-pretreated (black) vessels. F) Distance migrated by monocytes from the endothelial wall to the collagen gel in static (white) and flow-pretreated (black) vessels. For all plots, each data point represents data from an individual device, solid and dashed red lines represent the median and mean values, respectively. Red crosses represent outliers. ANOVA tests were performed to determine statistical significance. \* $p < 0.05$ .

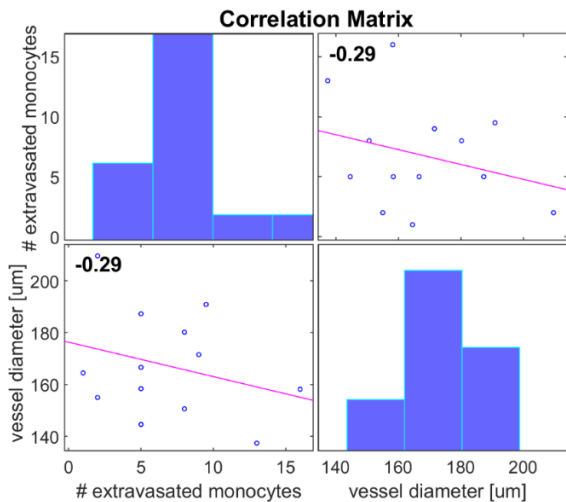
The diameter of vessels formed in microfluidic devices was variable and appeared to be weakly a function of flow. In [Figure 2.4D](#), it is shown that flow-conditioned vessels have slightly larger diameters, though differences are not statistically significant. To determine whether vessel diameter has an effect on monocyte adherence or extravasation, a correlation analysis was run to determine the number of monocytes that adhered or extravasated correlated with the magnitude of vessel diameter. The results demonstrate a

positive correlation between monocyte adherence and vessel diameter (Figure 2.6), and a negative correlation between extravasation and diameter (Figure 2.7). However, these data are still no significant.



**Figure 2.6. Correlation of the diameter of each vessel and the number of monocytes adhered to the endothelial lumen.**

Each data point represents data from an individual device. Data from static and flow experiments are included. Red lines represent the trend line of the data associated with a linear equation, and the red number indicates the slope.



**Figure 2.7. Correlation of the diameter of each vessel and the number of monocytes extravasated from the endothelial lumen into the surrounding matrix.**

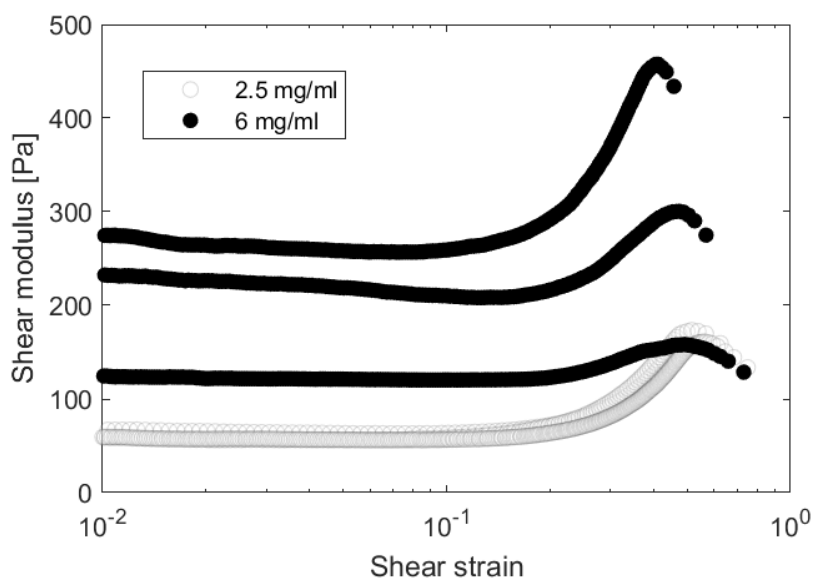
Each data point represents data from an individual device. Data from static and flow experiments are included. Red lines represent the trend line of the data associated with a linear equation, and the black number indicates the slope.

### 2.4.3. Increased collagen matrix concentration decreases vascular barrier integrity and increases extravasation

The physical properties of the endothelial basement membrane and intimal tissue are known to modulate vascular barrier function and inflammation [215]. Previous work demonstrated that increased intimal stiffness results in increased vascular permeability and immune cell extravasation through activation of Rho-mediated contractility in endothelial cells [216]. To elucidate the role of collagen matrix concentration on permeability and extravasation in our microfluidic model, we synthesized vessels in 2.5 and 6 mg/ml collagen type I hydrogels. It has been previously demonstrated that a change in collagen concentration impacts the biophysical properties of hydrogels. Our group previously analyzed the storage shear modulus ( $G'$ ), which indicates the elastic response of a material to shear stress, as a function of collagen mass concentration. We found that 2.5 mg/ml hydrogels were characterized by a  $G'$  of  $62.14 \pm 4.87$  Pa, while 6 mg/ml hydrogels were characterized by a  $G'$  of  $254.05 \pm 29.06$  Pa (Figure 2.8) [217]. Oliveros *et al.* performed a computational spatial characterization of the collagen fibers that comprise the solid phase of the hydrogel, and determined that increasing collagen concentration resulted in a decrease in pore size and porosity of the material. In addition, they found that increasing collagen concentration resulted in an increase in the number of fibers, while the length and radius of the fibers decreased [218]. We examined the structure of collagen hydrogels with SEM (Figure 2.9A). Consistent with previous results, at lower magnifications, we found that the 2.5 mg/ml hydrogels by increased void space when compared to the 6 mg/ml hydrogels, and increased suggests the 6 mg/ml gels are comprised of thicker fibers with more junctions between fibers (Figure 2.9A). Together these data indicate that the increase in collagen concentration results in changes in the spatial distribution of collagen fibers, which we expect to impact mechanical properties. To determine whether these structural differences presented differential functional barriers to migration, in collaboration with Polacheck's group, we determined the hydraulic permeability, which is related to the effective pore size. The hydraulic permeability of the different collagen compositions was determined by applying a hydrostatic pressure of 5, 10, or 20 mmH<sub>2</sub>O using 70-kDa FITC dextran across a

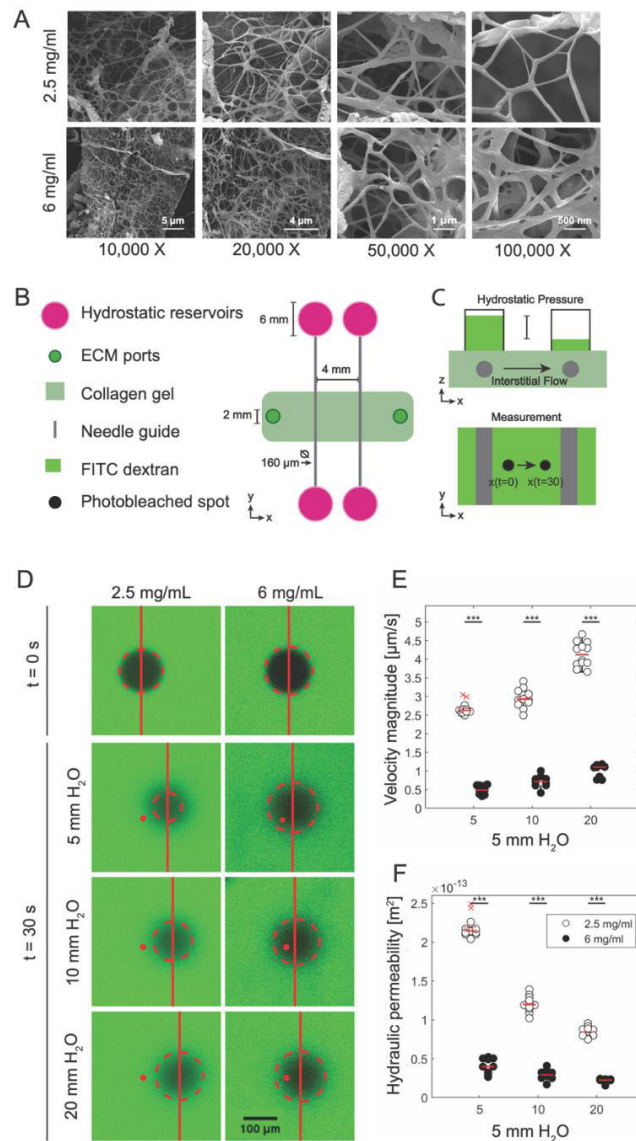


two-channel device and measuring the resulting velocity across the collagen between the two channels (Figure 2.9B). FRAP was performed by photobleaching a spot between the channels and imaging the displacement of the circle over time (Figure 2.9C). This displacement was used to calculate the velocity of fluid (Figure 2.9D) due to the applied hydrostatic pressures and used to calculate the hydraulic permeability in each condition, and statistically significant decreases in hydraulic permeability were found between the two hydrogel compositions (Figure 2.9E).



**Figure 2.8. Storage shear modulus of 2.5 (white) and 6 mg/ml (black) collagen hydrogels.**

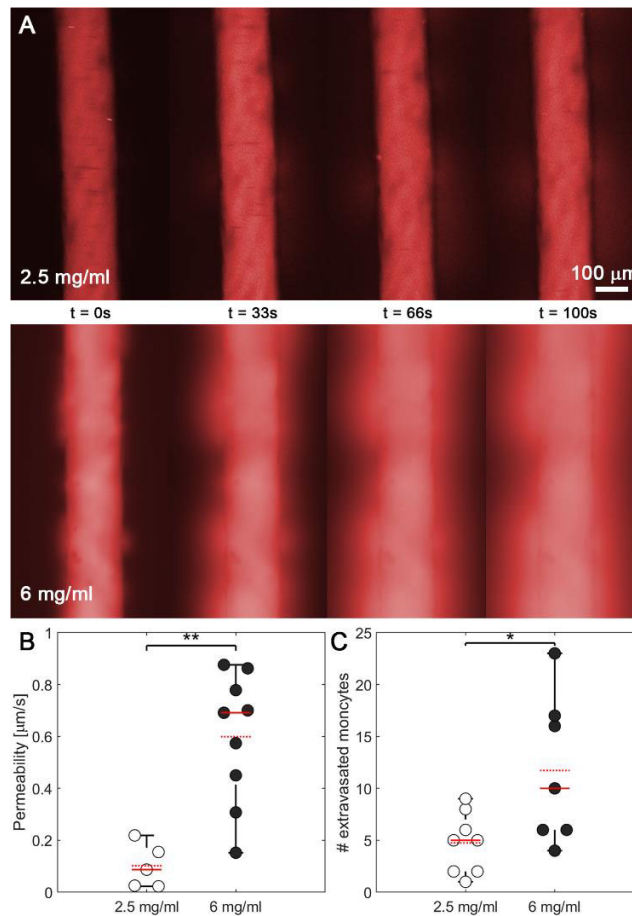
The graph has been plotted from the results obtained by Valero *et al.* in rheology assays [217]. The higher concentration collagen hydrogels are characterized by increased stiffness and variability in effective modulus.



**Figure 2.9. 3D structure and hydraulic permeability of 2.5 and 6 mg/ml collagen gels.**

A) Scanning electron microscope (SEM) images of 2.5 mg/ml and 6 mg/ml gels at resolutions of 10, 20, 50 and 100K. B) Diagram of two-channel device used to measure hydraulic permeability. Reservoirs are connected to the media ports to allow application of a defined pressure gradient across the collagen hydrogel. C) Experimental setup of fluorescence recovery after photobleaching (FRAP) method used to measure the hydraulic permeability. A known pressure gradient is applied to hydrogels immersed in dextran-containing medium, and the velocity magnitude of a photobleached circle is measured with timelapse fluorescence microscopy. D) Sample FRAP data demonstrating spot displacement in response to an applied hydrostatic pressure gradient. E) Measured velocity of fluid flow between two channels. F) Hydraulic permeability of collagen hydrogels as a function of applied pressure gradient calculated from Darcy's law. For all plots, each data point represents data from an individual device, solid and dashed red lines represent the median and mean values, respectively. ANOVA tests were performed to determine statistical significance. \*\*\* $p < 0.001$ .

To determine the impact of collagen concentration on vascular barrier function and monocyte extravasation, we repeated the diffusive permeability assay in vessels synthesized in 2.5 mg/ml vs. 6 mg/ml collagen hydrogels and exposed to flow. Increased collagen concentration resulted in significant increases in vascular permeability (Figure 2.10A). Quantitatively, the average permeability in high collagen concentration gels (mean = 0.60  $\mu\text{m/s}$ ) is six times higher than the mean obtained in lower collagen concentration gels (mean = 0.10  $\mu\text{m/s}$ ). In 2.5 mg/ml gels, the permeability ranges from 0 to 0.2  $\mu\text{m/s}$ , while in 6 mg/ml gels, it ranges from 0.1 to almost 0.9  $\mu\text{m/s}$  (Figure 2.10B). Interestingly, despite the decreased pore size of the 6 mg/ml collagen gels, there were nearly twice as many extravasated monocytes in the 6 mg/ml hydrogels compared to the 2.5 mg/ml hydrogels. (Figure 2.10C). Our data suggest that the integrity of endothelial vessels plays an essential role in monocyte extravasation, and is more impactful than the steric hindrance caused by the higher collagen concentrations.



**Figure 2.10. Effect of the collagen concentration on vascular permeability and monocyte extravasation.**

A) Diffusive permeability assay with fluorescent dextran (red) diffusing from the vessel lumen through the endothelial monolayer at different times ( $t= 0, 33, 66,$  and  $100$  seconds) in vessels formed in  $2.5$  mg/ml (upper) and  $6$  mg/ml collagen hydrogels (lower). B) Diffusive permeability of vessels embedded in  $2.5$  mg/ml (white) and  $6$  mg/ml collagen hydrogels (black). C) Number of monocytes extravasated from the lumen into the surrounding hydrogel in  $2.5$  mg/ml (white)  $6$  mg/ml collagen hydrogels (black). For all plots, each data point represents data from an individual device, solid and dashed red lines represent the median and mean values, respectively. ANOVA tests were performed to determine statistical significance. \*  $p < 0.01$ ; \*  $p < 0.05$ .

## 2.5. Discussion

Here, we introduce a microfluidic model of a monocyte-laden perfusable 3D blood vessel and demonstrate the ability to recapitulate monocyte arrest, extravasation, and 3D migration through a subluminal matrix. Importantly, this model system improves upon traditional assays by allowing for modulation of key hemodynamic parameters, including

pressure and flow, for vessels embedded within a 3D extracellular matrix with varying density. We demonstrate that both flow and matrix density play key roles in adhesion, extravasation, and migration, and interestingly, our data demonstrate a complex interplay among biophysical parameters that govern monocyte-endothelial interactions. While flow promotes adhesion of monocytes to the vascular wall, the number of cells that extravasate into the subluminal matrix decreases with flow, suggesting that extravasation, rather than adhesion, is the rate limiting step for immune cell trafficking in the presence of flow. This idea is supported by vascular permeability data, which demonstrates increased barrier to diffusion of 70 kDa dextran in the presence of flow, and further suggests that targeting vascular permeability could be an effective strategy for screening the passage of molecules or other cells through the endothelial wall, such as drugs that must diffuse to their target organ or pathogen, or metastatic cells in cancer progression.

Devices fabricated in a similar manner, by casting a hydrogel around a needle to ultimately form a perfusable vessel embedded within a 3D hydrogel, have been used for numerous applications to study the impact of the biochemical and biophysical microenvironment on microvascular morphogenesis and function. Such devices have been implemented to screen the effects of pro-angiogenic cocktails on neovascularization [219], to define the role of matrix degradability in angiogenesis [220], and to determine the role of inflammatory factors in governing lymphatic drainage [221]. Yet, in most of these studies (reviewed in [222]), cell culture media is used as a blood surrogate, and the contributions of circulating cells towards microvessel function are not considered, despite increasing evidence that leukocytes and immune cells play critical roles in microvascular development, homeostasis, and dysfunction [223]. Our results demonstrate that such platforms are compatible with circulating cells and suggest that mechanistic studies enabled by these devices could allow for dissection of key signals involved in pathologies such as fibrosis and cancer, where changes in ECM composition and mechanics occur concomitantly with changes in hemodynamics, to identify and screen therapeutic interventions.

While the application of flow impacted the rate of monocyte adherence and extravasation, the migration distance of monocytes into the collagen hydrogel was not

dependent on the application of flow. Given that tissues demonstrate varying degrees of infiltration by monocytes and other circulating cells *in vivo*, it is likely that the platform described here does not recapitulate sufficient complexity to investigate mechanisms that lead to differences in cell migration behaviors beyond extravasation. By focusing only on the extravasation process, we neglect the events that occur before and after the extravasation and that may influence the final outcome. The addition of external chemical and biological stimuli, such as chemokines or molecules derived from microorganisms, would allow us to include in the study the recruitment of monocytes to the damaged tissue [158] and their subsequent differentiation into macrophages in the ECM [224,225]. In this way, a more complete and realistic model would be optimized and achieved. Recent work introducing epithelial ducts into lumenized vascular devices [226] and coculturing diverse bacterial colonies on chip [227] together illustrate the potential to recapitulate complex inflammatory responses *in vitro* through the integration of these approaches.

# 3. MACROPHAGE MIGRATION

---





### 3.1. Abstract \*

Macrophages play an essential role in the process of recognition and containment of microbial infections. These immune cells are responsible for migrating to infectious sites to reach and phagocytose pathogens. Specifically, in this article, bacteria from the genus *Mycobacterium*, *Salmonella* and *Escherichia*, were selected to study directional macrophage migration towards different bacterial fractions. We recreated a three-dimensional environment in a microfluidic device, using a collagen-based hydrogel that simulates the mechanical microarchitecture associated to the ECM. First, we showed that macrophage migration is affected by the collagen concentration of their environment, migrating greater distances at higher velocities with decreasing collagen concentrations. To recreate the infectious microenvironment, macrophages were exposed to lateral gradients of bacterial fractions obtained from the intracellular pathogens *S. typhimurium* and *M. tuberculosis*. Our results showed that macrophages migrated directionally towards the sites where bacterial fractions are located, suggesting the presence of attractants molecules in all the samples. Finally, we also observed that macrophages migrate towards fractions obtained from non-pathogenic bacteria, such as *Escherichia coli* and *M. smegmatis*. In conclusion, our microfluidic device represents a useful tool to study directional macrophage migration towards different stimuli, and opens new perspectives to study the recognition of specific antigens by innate immune cells.

\* This chapter 3 correspond to an adaptation of the article under review as: **Pérez-Rodríguez, S.**; Borau, C.; García-Aznar, JM.; Gonzalo-Asencio, J. **A microfluidic-based analysis of 3D macrophage migration after stimulation by *Mycobacterium*, *Salmonella* and *Escherichia*.**

## 3.2. Introduction

The latest World Health Organization (WHO) report indicates that lower respiratory infections and diarrheal diseases remain one of the top 10 causes of death globally, and people living in low-income countries are far more likely to die from these diseases [14]. Both diseases are frequently caused by microorganisms. Specifically, according to the WHO, more than 420.000 people die annually from foodborne, with bacteria such as *Salmonella typhimurium* or *Escherichia coli*, being the most typical causative agents. These pathogens contaminate spoiled food which, when ingested, lead to the development of diarrheal diseases. These infections lead to more than half of the global deaths from foodborne, reaching 550 million affected and 230.000 deaths [13]. Among respiratory infections, Tuberculosis, which is mainly caused by *Mycobacterium tuberculosis* remains today as the deadliest bacterial disease accounting for more than 1.5 million deaths in 2020, having higher prevalence in low-income countries. Tuberculosis is aggravated by the alarming emergence of drug resistant strains, and co-infection with Human Immunodeficiency Virus [15].

Both in the intestine and in the lungs there are innate immune cells, as macrophages, responsible for containing bacterial infections. Macrophages possess a series of receptors that allow them to sense their environment and recognize the presence of pathogens. These receptors interact with the pathogens themselves or their secreted products [228], and activate a series of signaling cascades that generate changes in the cytoskeleton, so that the macrophage migrates towards the invading microorganism and is able to phagocytize it [229].

Therefore, since the outcome of the infection is strongly determined by the interplay between macrophages and bacteria, in this article we have focused on the study of the macrophage migration towards different bacterial stimuli. For this purpose, we have used 3D cultures on microfluidic devices. In this case, we used a three-channel device, in which we embedded macrophages in a collagen hydrogel in the central channel. In this way, we recreated a more realistic physiological situation as the hydrogel mimics the ECM through

which these innate cells must migrate to interact with pathogens. The side channels allow the generation of chemical gradients by adding different conditions in each of them [230]. Therefore, here we generated a chemotactic gradient by means of adding different bacterial fractions in different spatial locations. In this way, we were able to quantify the directional migration of macrophages to assess whether they were attracted to different fractions from representative bacteria.

### 3.3. Methods

#### 3.3.1. Cell culture

We used THP-1 monocytes from the ATCC that came from peripheral blood of one year infant human. THP-1 were cultured in suspension in RPMI-1640 supplemented with L-glutamine, 2% FBS and Ampicillin/Streptomycin. For monocyte differentiation to macrophages, THP-1 were resuspended at  $6.5 \times 10^5$  cell/ml in RPMI medium and 100 ng/ml phorbol 12-myristate-13-acetate (PMA) for 24 hours. Macrophage became adherent, facilitating their distinction from undifferentiated monocytes.

#### 3.3.2. Bacteria culture and fractions preparation

We used these bacterial strains: *E. coli* DH5 $\alpha$ , *Salmonella enterica* serovar *typhimurium* SV501 [231], *M. tuberculosis* H37Rv [232] and *M. smegmatis* mc<sup>2</sup>155 [233]. *E. coli* and *S. typhimurium* was grown in Luria-Bertani (LB) broth; and *M. tuberculosis* and *M. smegmatis* in Middlebrook 7H9 broth supplemented with 10% (vol/vol) of ADC (0.5% bovine serum albumin, 0.2% dextrose, 0.085% NaCl and 0.0003% beef catalase) and 0.05% (vol/vol) Tween-80.

Four bacterial fractions were prepared for the migration assays: secreted protein, bacteria inactivated by PFA treatment, bacterial lysate and bacteria inactivated by heat. For their preparation, bacteria were grown at a concentration of  $10^9$  cfu/ml and then separated in four tubes used for the different treatments. To obtain the secreted protein, a trichloroacetic acid (TCA) precipitation was performed. Briefly, the sample was centrifuged

and the bacterial pellet was discarded. The supernatant was incubated with 10% TCA for 1 hour on ice and centrifuged. The pellet containing secreted proteins was washed in acetone, and the pellet was resuspended in distilled water. To inactivate bacteria by PFA treatment, the bacterial pellet was washed twice with PBS to remove extracellular components, resuspended in 4% PFA, and incubated for 1 hour at room temperature. To obtain bacterial lysates, bacterial pellets were washed twice with PBS and then resuspended in 1 ml of cold PBS. Bacterial suspensions were disrupted by sonication using the BioRuptor (Diagenode, Belgium) for 15 min (30 s pulse at high power), allowing cooling in an ice-water bath for 30 s between pulses. The samples were centrifuged at 4.000 g for 10 min at 4 °C, and the supernatant containing whole-cell bacterial extracts was filtered through a 0.22 µm-pore-size low protein-binding filter (Pall, New York, NY, United States). For inactivating bacteria by heat treatment, bacterial pellets were washed twice with PBS, and then incubated at 100°C for 10 minutes.

### 3.3.3. Manufacturing of microfluidic device

Microfluidic devices were fabricated following the protocol published by Shin *et al.* in 2012 [63]. A PDMS mixture made of the base and curing agent of Sylgard 184 silicone elastomer in a 10:1 ratio was poured onto the printed wafer and incubated for 24 hours at 80°C. Then, PDMS molds were cut independently, perforated and autoclaved. Finally, both PDMS devices and 35 mm diameter glass bottom plates were treated with plasma to achieve a good seal between them. To increase the adherence of PDMS to the collagen hydrogel which is subsequently to be introduced, devices were filled with 1 mg/ml PDL for 4 hours at 37°C and then washed with sterile water.

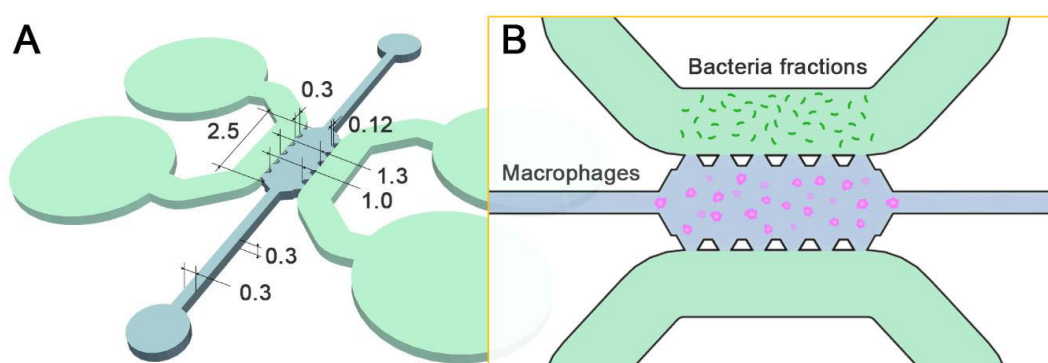
### 3.3.4. Migration assays

A suspension of THP-1, at a final concentration of  $3 \times 10^5$  cell/ml, was embedded in collagen hydrogels. These hydrogels were made of a predefined concentration of type I collagen, to obtain the desired matrix stiffness, and an optimal NaOH/H<sub>2</sub>O balance to achieve a pH of 7. By working with the most abundant protein of the ECM and a

physiological pH [234], it was possible to realistically recreate the extracellular environment in which macrophages migrate.

This hydrogel was introduced into the central channel of the microfluidic device (Figure 3.1) and polymerized at 37°C for at least 20 minutes in a humid box. Devices were turned around every 5 minutes to avoid adhesions between the cells and the PDMS or glass surface and to prevent them from passing into a two-dimensional plane. Subsequently, the reservoirs and side channels were filled with RPMI culture medium and the devices were incubated 24 hours at 37°C to let the macrophages to adapt to their three-dimensional environment before performing the migration assay.

Next day, the medium in the reservoirs was removed and the reservoirs were refilled differentially. In the case of the upper reservoir and channel, the fraction of bacteria of study diluted to  $10^{-4}$  in medium was added, and the lower one was filled with only RPMI medium. In this way, a gradient was generated where the stimulus came from the upper part of the device. The devices were visualized in a phase contrast microscopy which included an incubation chamber to maintain optimal culture conditions, taking pictures every 20 minutes for 24 hours with 10x objective lenses. Subsequently, individual cells migration were analyzed with a custom cell tracker algorithm for use in MatLab [214] and statistical results were performed with one-way Anova test.



**Figure 3.1. Microfluidic device**

A) Dimensioned top view of the microfluidic device consisting of a central channel (blue) and two side channels (gray), each with corresponding loading ports at the ends of the channel. B) Schematic drawing of the migration experiment design. Macrophages (pink) are embedded in a collagen gel in the central channel, while a gradient with bacterial fractions (green) is generated in the upper side channel.

## 3.4. Results

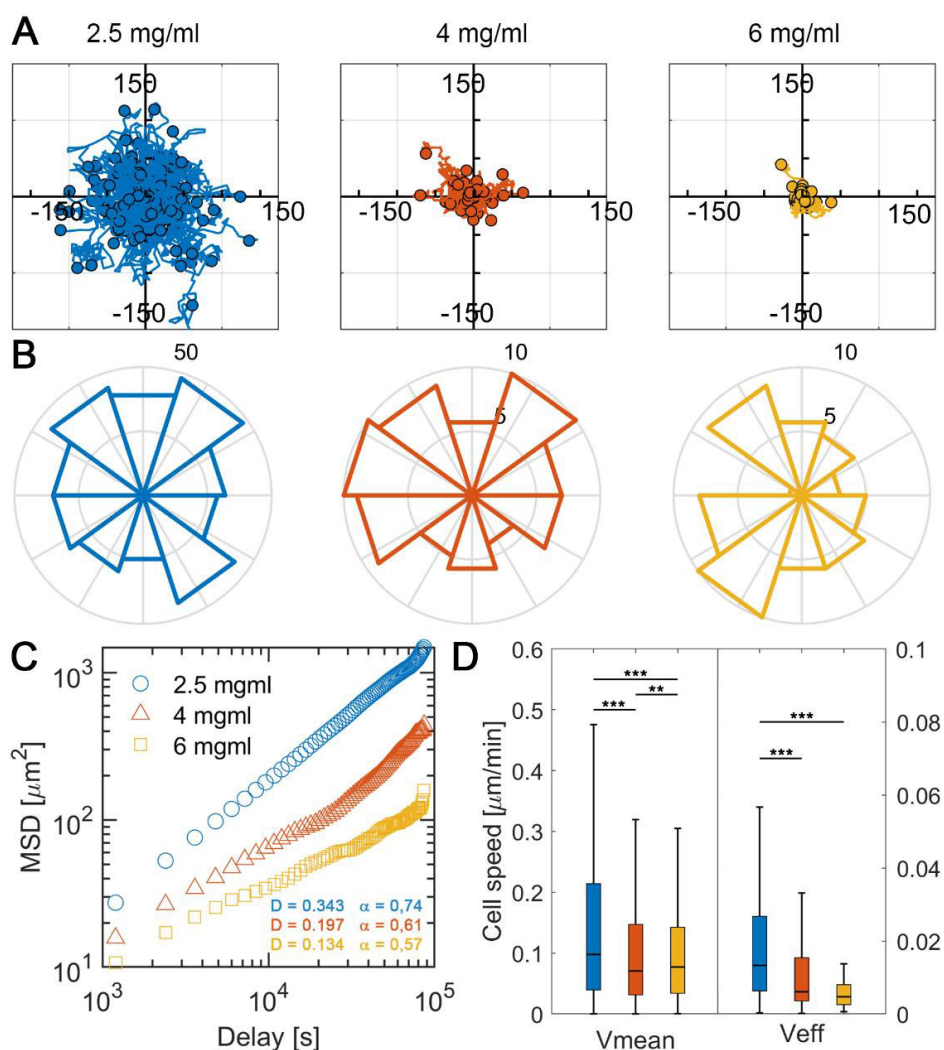
### 3.4.1. Macrophage migration and velocity are inversely proportional to collagen concentration in the microfluidic device

Macrophages are motile cells that migrate through the ECM to sites of infection and inflammation. Since previous literature has demonstrated differences between cell migration in two-dimensional and three-dimensional environments [235], in this study, we recreated the ECM by confining a hydrogel of collagen I, in which macrophages were embedded three-dimensionally. In addition, we analyzed macrophage migration in gels of different collagen concentration, at 2.5, 4 and 6 mg/ml. These concentration changes imply structural changes in the hydrogel, such as smaller pore size or porosity, higher storage shear modulus and a decreasing hydraulic permeability with increasing collagen concentration [236].

As the concentration of collagen in the hydrogels increases, macrophages migrate shorter total distances (Figure 3.2A). In 2.5 mg/ml gels, some macrophages are able to overcome total distances of 100  $\mu\text{m}$  from their point of origin, whereas as the concentration increases to 4 mg/ml, macrophages have more difficulty moving forward and their maximum migration distances are around 50  $\mu\text{m}$ . In the case of the highest collagen concentration (6 mg/ml), macrophages do not reach distances greater than 25  $\mu\text{m}$ . In all conditions, macrophages migrate radially without observing a directional movement, which is consistent with the absence of external stimulus (Figure 3.2B).

The analysis of the Mean Squared Displacement (MSD) of the macrophage trajectories provides information on the persistence of migration, reflected in the diffusive coefficient ( $D$ ), and the type of movement that the cells have in this environment depending on the motion angle ( $\alpha$ ) that they show (Figure 3.2C). The increase in the concentration of collagen in the gels implies a decrease in the diffusive coefficient, indicating a lower persistence in the migration of macrophages. In 2.5 mg/ml gels, macrophages show a diffusive coefficient of 0.343  $\mu\text{m}^2/\text{min}$ , which decreases to 0.197  $\mu\text{m}^2/\text{min}$  in 4 mg/ml gels,

and to  $0.134 \mu\text{m}/\text{min}^2$  in higher concentration gels at 6 mg/ml. In addition, in all the conditions a  $\alpha$  value lower than 1 is obtained, indicating that macrophages have a confined-type subdiffusive movement, whose biological interpretation is continuous-time random walk [237].



**Figure 3.2. Macrophage migration in collagen gels of different concentrations: 2.5 mg/ml (blue), 4 mg/ml (orange) and 6 mg/ml (yellow).**

A) Representation of the relative trajectories of macrophages, each line being the individual trajectory of a cell. B) Directionality of migration considering the length of the radius as the number of cells that migrated in that direction. C) Mean squared displacement (MSD) of the tracked trajectories, where  $D$  is the diffusive coefficient and  $\alpha$  is the angle of motion. D) Mean and effective velocity, where mean velocity is the total distance migrated divided by the time spent, and effective velocity is the distance between the starting and final point of the cell divided by the time spent.  $**p < 0.01$ ,  $***p < 0.005$ .  $n$  (devices) = 10 (2.5 mg/ml gels), 3 (4 mg/ml gels) and 6 (6 mg/ml gels), with an average of 25 cells per device.

As the collagen concentration increases, the mean and effective velocities decrease significantly (Figure 3.2D). However, comparing the obtained values of mean velocities with those published in previous literature, we observe that our values are clearly lower. In our collagen hydrogels, macrophages tend to migrate in a range of 0.05-0.2  $\mu\text{m}/\text{min}$ , reaching velocities of 0.5  $\mu\text{m}/\text{min}$  in the lowest concentration gels. In contrast, *in vitro* assays where macrophages migrated on 2D surfaces, velocities around 1  $\mu\text{m}/\text{min}$  have been observed [238]. *In vivo* fish models, similar results have been obtained, with velocities in the range of 1-2.5  $\mu\text{m}/\text{min}$  [239], which can increase over 10  $\mu\text{m}/\text{min}$  in the presence of a wound [240].

The literature defines two types of macrophage migration movements: amoeboid and mesenchymal migration. Amoeboid motility is characterized by rounded cell bodies with short protrusions and high velocities. In contrast, during mesenchymal movement, macrophages present more elongated shapes stretching their protrusions, but migrating more slowly. It has been observed that surrounding matrix influence the type of migration shown by macrophages. In a 3D low-concentration ECM, macrophages tend to migrate in an amoeboid manner, whereas in denser ECM, they show mesenchymal migration [241]. In our case, in 2.5 mg/ml gels, greater distances traveled at higher velocities are observed, so we may be in presence of an amoeboid migration. In contrast, in 6 mg/ml gels, the distance and speed of migration decreases significantly, characteristic of mesenchymal movement. However, confirming the type of movement shown by our macrophages would require a staining and quantification of cell adhesions to the ECM. For subsequent experiments with bacterial fractions we will work with 2.5 mg/ml collagen gels, because under these conditions they migrate longer distances and will allow us to follow cell trajectories more easily and with greater differentiation.

### 3.4.2. 2.5 mg/ml collagen hydrogels allow gradient of all molecules of the bacterial fractions

For providing directional migration, a stimulus must first be present. Subsequently, this stimulus is sensed and a signaling cascade is generated that activates the cytoskeleton machinery so that the macrophage migrates towards the received signal [242]. Although



there are numerous stimuli of different nature in cell migration, such as chemical or mechanical [243], the current literature on macrophage migration has only described stimuli of biochemical origin. This implies that a physical contact must be established between the signaling molecule and the sensitive macrophage receptor [244]. The design of the microfluidic device used in this study allows the generation of a chemical gradient from the side channel where the molecules of interest are introduced to the central chamber where the three-dimensional cell culture is located [245]. The diffusive coefficient of a particle in a hydrogel is defined by the Stokes-Einstein equation modified to take into account the porosity of the matrix. Thus, the effective diffusion coefficient (D) is calculated from the following formula:

$$D = \frac{k_B T}{6\pi\eta r} \cdot \exp\left(-\left[\sqrt{\varphi} \cdot \left(1 + \frac{r}{r_f}\right)\right]\right)$$

Where  $k_B$  is Boltzmann's constant, T is the absolute temperature,  $\eta$  is the viscosity of the fluid, r is the radius of the diffusing molecule,  $\varphi$  is the void ratio of the matrix and  $r_f$  is the radius of the fiber [245]. Thus, we hypothesize that the components of the bacterial fractions diffuse into the hydrogel until they come into contact with macrophages.

The bacterial fractions used in the present study consist on a great variety of molecules of different sizes, which makes it impossible to calculate the diffusion coefficient of each individual component. However, the size of the largest component, which is the intact bacterium after fixation with PFA, is known. Typically, a prokaryotic bacteria has an average length of 1-5 microns [246]. Therefore, for the calculation of the effective diffusive coefficient we are going to use as study molecule a particle of 3 microns in diameter. The fractions are dissolved in RPMI medium supplemented with 10% fetal bovine serum, which assumes a dynamic viscosity of the medium of approximately 0.95 mPa·s [247]. Migration assays are carried out on 2.5 mg/ml collagen gels, whose three-dimensional structure has been studied by Olivares *et al.* determining that the void ratio is 85.01% and the approximate radius of the collagen fibers is 0.12  $\mu\text{m}$  [218]. Applying these data to the previously described formula, we obtain an effective diffusion coefficient of  $1.77 \cdot 10^{-14} \text{ m}^2 \cdot \text{s}^{-1}$ . This indicates that the whole bacterium is able to diffuse through the hydrogel and will

come into contact with the macrophages, stimulating them. Therefore, we hypothesize that if the largest component of the fractions is able to diffuse, the remaining molecules, which are smaller in size, will be also able to diffuse towards the macrophages.

### 3.4.3. Macrophages show directional migration towards bacterial fractions of *S. typhimurium*

Once characterized the optimal conditions for macrophage migration in our microfluidic device, we prompted to simulate macrophage stimulation with *S. typhimurium* bacterial fractions (Figure 3.3A). Each fraction presents a different composition. On the one hand, the secreted protein exclusively contains those proteins released by the bacteria to the extracellular milieu. When bacteria are inactivated by PFA, a cross-linking reaction preserves bacterial surface macrostructures [248]. The cell lysate contains either the cytosolic components, or the membrane fractions from lysed bacteria, but not the secreted protein fraction. Finally, when bacteria are inactivated by heat, their composition is similar to the cell lysate, but protein denaturation is expected as a consequence of the thermal treatment [249]. A gradient was generated individually with each bacterial fraction in the microfluidic devices, and the macrophage migration was monitored for 24 h.

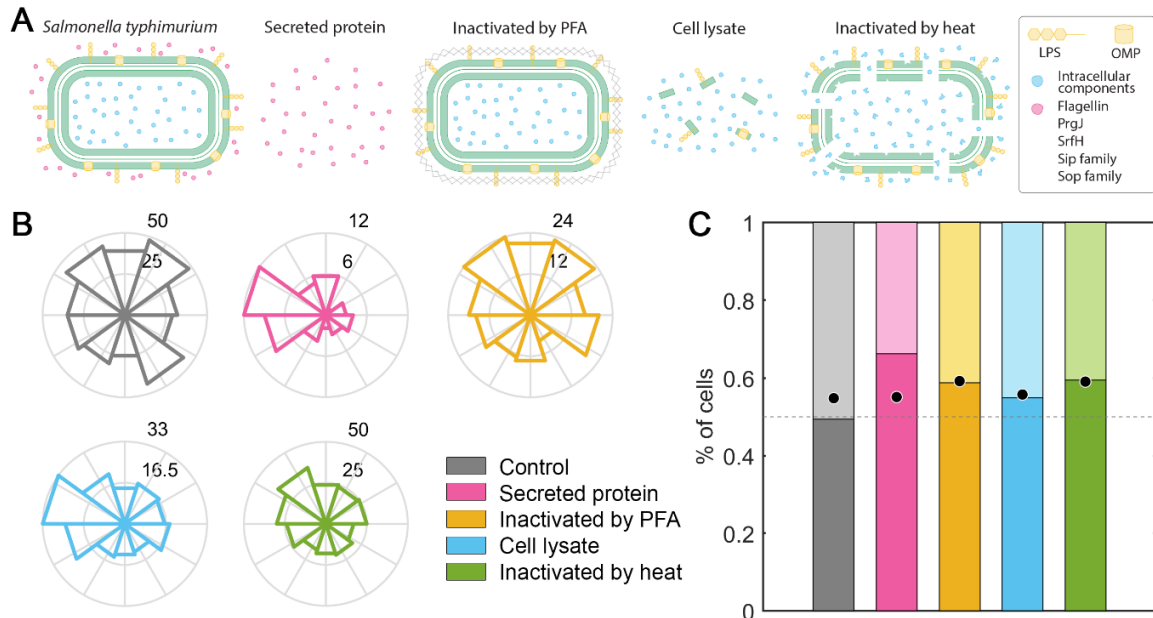
Next, we quantified the number of macrophages that migrated in each direction from their point of origin, and represented this migration in a rosette plot (Figure 3.3B). Since the gradient with bacterial stimulus is generated in the upper part of the devices, it provides qualitative information on whether the macrophages have migrated directionally towards these bacterial extracts. This qualitative information is transformed into quantitative information enumerating the percentage of macrophages whose final position was above or below their initial position, normalized by the effective distance traveled (Figure 3.3C).

Qualitatively, it is observed that macrophages preferentially migrate towards the *S. typhimurium* fractions, since the areas of the upper portions in the rosette plot are higher than in bottom portions. In contrast, in the absence of bacterial stimulus, macrophage

migrate in the same proportion to the upper or the lower area of the microfluidic device (Figure 3.3B). Analyzing the quantitative information, the randomness in the migration of macrophages without the presence of stimulus is demonstrated, since the percentage of cells migrating towards the top or the bottom of the hydrogel, with respect to their original position and weighted by the distance traveled, is similar. However, when generating a gradient with any of the *S. typhimurium* fractions, the percentage of macrophages that migrate towards the top of the device, where the stimulus is located, always exceeds the 0.5 baseline. Migration towards secreted protein results in the highest macrophage migration relative to the remaining fractions, exceeding 0.65 value. Therefore, from these results it can be deduced that macrophages are attracted to *S. typhimurium* due to either their extracellular, superficial or intracellular components (Figure 3.3C).

The bacterial fractions used in our study contains well-known proteins and lipids, whose interaction with macrophages has been previously described. *S. typhimurium* is characterized by a series of virulence-associated genes that are divided into 17 pathogenicity islands (SPI) throughout its genome, with SPI-1 being the most important. The best-known virulence system of *Salmonella* is the T3SS, which translocates effector proteins, both to the ECM and to the cytoplasm of host cells thanks to its needle-like structure [250]. Among the secreted effectors, flagellin together with the rod component PrgJ is able to interact with the NOD-like receptor 4 of macrophages, activating the formation of the inflammasome. Inflammasomes are large cytoplasmic complexes that detect the presence of microbes and induce the activation of caspases and production of proinflammatory interleukins with a protective effect [251]. Another effector to take into account is SrfH that interacts with the TRIP6 protein of macrophages stimulating their migration [252]. Finally, two important families of effector proteins are *Salmonella* invasive proteins (Sip A-D) and *Salmonella* outer proteins (Sop) that regulate host cell adhesion and invasion by binding to actin and reorganization of the cytoskeleton [253]. Peptidoglycans and lipopolysaccharides are well-known constituent of the *Salmonella* cell wall, which activate TLR and induce macrophage migration via iNOS/Src/FAK [254]. Another surface component that activates TLR receptors, in this case TLR2 and TLR4, are Omp porins.

Specifically, OmpC and OmpD that mediate adherence to macrophages, thus considered to be involved in host-pathogen recognition [255,256].



**Figure 3.3. Macrophage facing *S. typhimurium* stimuli.**

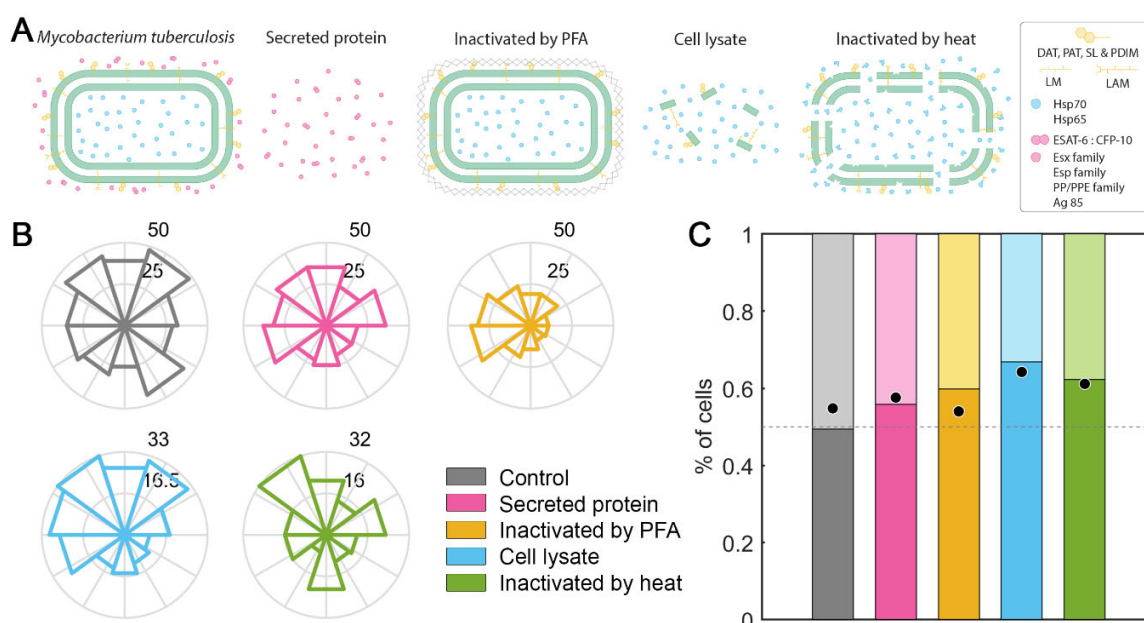
A) Treatments applied to *S. typhimurium* in order to obtain the different fractions subsequently tested. Intact bacteria consist of a gram-negative membrane (green) with superficial components such as LPS or OMP porines (yellow). Intracellular components are represented in blue, whereas extracellular secreted protein, like flagellin, PrgJ, SrfH, Sip and Sop family, are indicated in pink. Four treatments were performed to *S. typhimurium*: secreted protein where only extracellular molecules were collected; inactivation by PFA that generates a crosslinking (grey mesh) preserving the superficial components; a cell lysate to break the cell and release superficial and intracellular components; and an inactivation by heat that damages the membrane (green) and denatures proteins (amorphous blue balls). B) Migration of macrophages in 2.5 mg/ml collagen gels towards a gradient generated at the top with *S. typhimurium* bacterial fractions: control (gray), secreted protein (pink), inactivated by PFA (yellow), cell lysate (blue) and inactivated by heat (green). Directionality of migration, where the radius is the number of cells migrating in each direction. C) Percentage of macrophages as a function of the verticality of their migration and normalized by the total distance traveled. Those macrophages whose final position is above their initial position contribute to the bar graph exceeding the dashed line set at 0.5. The dots in each bar graph correspond to the percentage of macrophages whose final position is above or below their starting position, but not weighted by the total distance migrated. n (devices) = 10 (control), 5 (secreted protein), 5 (inactivated by PFA) and 5 (cell lysate) and 5 (inactivated by heat).

#### 3.4.4. Macrophages show directional migration towards bacterial fractions of *M. tuberculosis*

We applied those conditions tested in *S. typhimurium* to *M. tuberculosis*, since both bacteria are intracellular pathogens targeted by macrophages (Figure 3.4A). Macrophage migration was analyzed in 2.5 mg/ml collagen gels for 24 hours. When exposing macrophages to *M. tuberculosis* fractions, a clear directional migration toward the secreted protein, its cell lysate, and bacteria inactivated by heat treatment is observed (Figure 3.4B). By weighting the number of macrophages migrating toward the gradients generated with the *Mycobacterium* fractions, it is observed that all *M. tuberculosis* fractions exert an effect on macrophages by attracting them directionally (Figure 3.4C). The fractions promoting the higher migration were the cell lysate and bacterial extracts inactivated by heat, inducing more than 60% macrophages effectively migrating towards the stimuli.

*M. tuberculosis* contains in its genome five specialized secretion systems, known as ESX1-5 [257]. Among them, the ESX-1, which secretes ESAT-6 and CFP-10 is finely characterized. These genes are found in the RD1 region, which is lacking in the BCG tuberculosis vaccine, indicating their essentiality in the virulence of this bacterium [258]. ESAT-6 and CFP-10 each contains a dense repertoire of T-cell epitopes and are known for their immunogenicity; indeed, they are used as vaccine candidates [259]. Both proteins induce recruitment of macrophages to infected areas by interacting with beta-2-microglobulin ( $\beta$ 2M) and binding to the surface of primary macrophages [260]. ESAT-6 and CFP-10, also named as EsxA and EsxB, respectively, belong to the Esx family of antigens known for their immunogenicity and potential as vaccine candidates [261]. EspC, which is involved in ESAT-6 secretion, also interacts with TLR4 receptors resulting in macrophage activation [262]. The PP/PPE family of proteins secreted by *M. tuberculosis* is also documented to have a role in macrophage surface binding. For example, PE9-10 and PPE39 interact with TLR4, and PE11 and PE\_PGR60 bind to fibronectin promoting invasion into host cells [263]. Finally, another immunologically potent secreted protein is the antigen 85 (Ag85) complex that can bind to ECM fibronectin and elastin [264]. Macrophage TLR also

recognize lipid and glycoproteins components of the bacterial wall, such as lipoarabinomannan (LAM), its precursor lipomannan (LM) and the 38-kDa glycoprotein [265]. However, *M. tuberculosis* also possesses strategies to mask these PAMPs and go unnoticed by macrophages, such as the use of cell-surface-associated lipids like mannosylated phosphatidylinositol (PIM) and PDIM that negatively regulate TLR receptors [266,267]. At the intracellular level, heat shock protein 65 and 70 also activate TLR receptors and induce macrophage recruitment via a host chemokine receptor 2 (CCR2)-mediated pathway and myeloid differentiation primary response protein 88 (MyD88) [268].

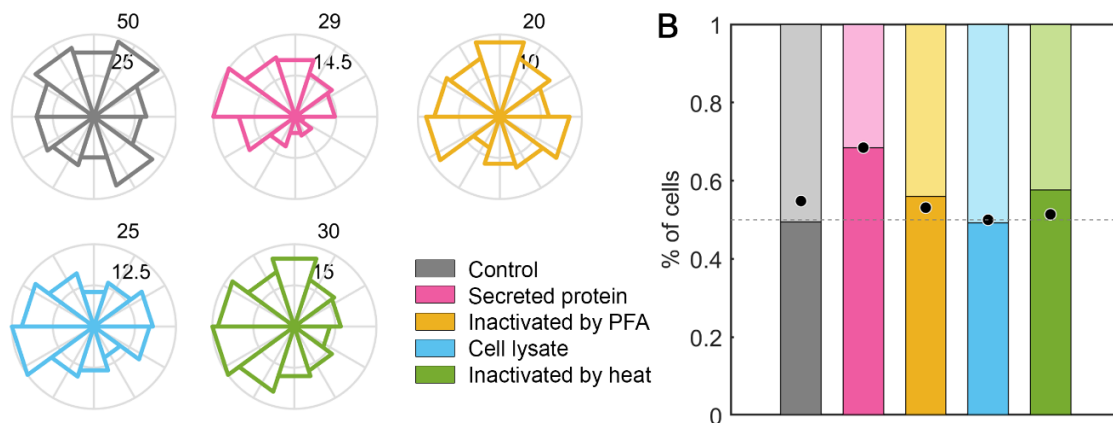


**Figure 3.4. Macrophage facing *M. tuberculosis* stimuli.**

A) Treatments applied to *M. tuberculosis* in order to obtain the different fractions subsequently tested. Bacteria components are represented in colors mycobacterial membrane (green) with superficial components such as DAT, PAT, SL, PDIM, LM and LAM (yellow), intracellular molecules like Hsp70 and Hsp65 (blue), and extracellular secreted protein, like ESAT-6:CFP-10, Esp, PP and PPE family and Ag85 (pink). Four treatments were performed to *M. tuberculosis*: secreted protein; inactivation by PFA that generates a crosslinking (grey mesh); a cell lysate; and an inactivation by heat that damages the membrane and denatures proteins (amorphous blue balls). B) Migration of macrophages in 2.5 mg/ml collagen gels towards a gradient generated at the top with *M. tuberculosis* bacterial fractions: control (gray), secreted protein (pink), inactivated by PFA (yellow), cell lysate (blue) and inactivated by heat (green). Directionality of migration, where the radius is the number of cells migrating in each direction. C) Percentage of macrophages as a function of the verticality of their migration and normalized by the total distance traveled. Dashed line set at 0.5. The dots in each bar graph correspond to the percentage of macrophages migrating above or below their starting position, but not weighted by the total distance migrated. n (devices) = 10 (control), 8 (secreted protein), 6 (inactivated by PFA), 6 (cell lysate) and 5 (inactivated by heat).

### 3.4.5. Macrophages migrate towards fractions of non-pathogenic *E. coli* and *M. smegmatis*

The response of macrophages to *E. coli* DH5 $\alpha$  bacteria was also tested. This *E. coli* strain is a non-pathogenic bacterium, routinely used in laboratories as a genetic model. Qualitatively, macrophages preferentially migrate toward the secreted protein and the PFA-fixed bacteria (Figure 3.5A). However, quantitatively, it is observed that macrophages, not only sense attraction to these two fractions, but also to bacteria inactivated by heat (Figure 3.5B). Overall, the chemotactic response generated by the secreted protein fraction results in up to 70% macrophage recruitment.

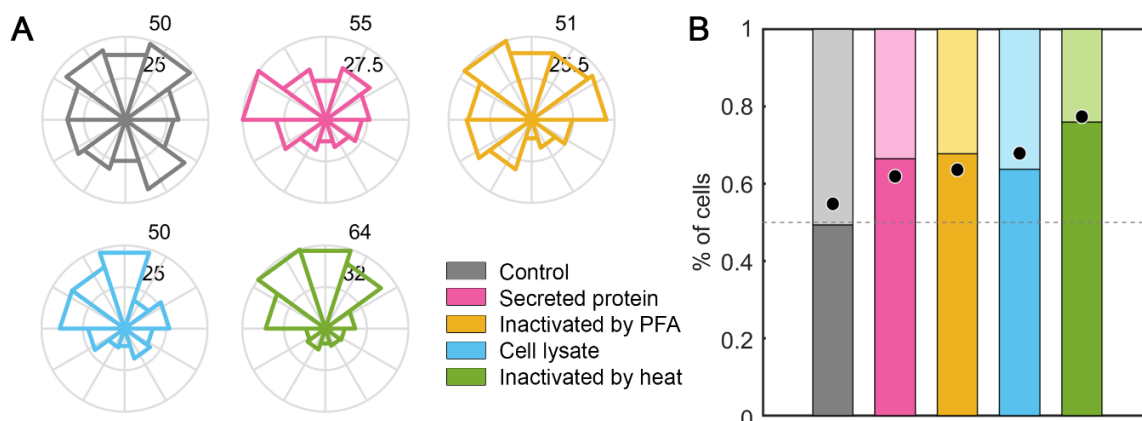


**Figure 3.5. Macrophage facing *E. coli* stimuli.**

Migration of macrophages in 2.5 mg/ml collagen gels towards a gradient generated at the top with *E. coli* bacterial fractions: control (gray), secreted protein (pink), inactivated by PFA (yellow), cell lysate (blue) and inactivated by heat (green). A) Directionality of migration, where the radius is the number of cells migrating in each direction. B) Percentage of macrophages as a function of the verticality of their migration and normalized by the total distance traveled. Those macrophages whose final position is above their initial position contribute to the bar graph exceeding the dashed line set at 0.5. The dots in each bar graph correspond to the percentage of macrophages whose final position is above or below their starting position, but not weighted by the total distance migrated. n (devices) = 10 (control), 4 (secreted protein), 5 (inactivated by PFA), 5 (cell lysate) and 5 (inactivated by heat).

Migration assays were also performed in response to stimuli from *M. smegmatis*, a mycobacterium commonly used as a non-pathogenic model of *M. tuberculosis*. Both qualitatively and quantitatively, a clear directional attraction of macrophages upon exposure to all bacterial fractions of *M. smegmatis* was observed (Figure 3.6A and 3.6B).

Specifically, the fraction that recruits the most macrophages is the heat-inactivated bacterium, with more than three quarters of the leukocytes migrating towards it.



**Figure 3.6. Macrophage facing *M. smegmatis* stimuli.**

Migration of macrophages in 2.5 mg/ml collagen gels towards a gradient generated at the top with *M. smegmatis* bacterial fractions: control (gray), secreted protein (pink), inactivated by PFA (yellow), cell lysate (blue) and inactivated by heat (green). A) Directionality of migration, where the radius is the number of cells migrating in each direction. B) Percentage of macrophages as a function of the verticality of their migration and normalized by the total distance traveled. Those macrophages whose final position is above their initial position contribute to the bar graph exceeding the dashed line set at 0.5. The dots in each bar graph correspond to the percentage of macrophages whose final position is above or below their starting position, but not weighted by the total distance migrated. n (devices) = 10 (control), 5 (secreted protein), 5 (inactivated by PFA), 5 (cell lysate) and 5 (inactivated by heat).

These results confirmed that fractions from non-virulent *E. coli* and *M. smegmatis* bacteria also promote a macrophage migration. These data are in agreement with existing literature indicating that they are even capable of infecting leukocytes [269,270]. However, it is key to remember that its fate within the macrophage differs from that of pathogenic *S. typhimurium* and *M. tuberculosis*, which unlike *E. coli DH5 $\alpha$*  possess intracellular survival mechanisms [271,272]. For example, *S. typhimurium* secretes effector proteins through T3SS that alter intracellular signaling, prevent fusion of the phagosome with the lysosome or induce macrophage apoptosis [38]. On the other hand, *M. tuberculosis* has strategies that allow it to inhibit oxidative and nitrosative stresses mediated by Acr chaperones [44], promote wall integrity thanks to cyclopropane rings [45]. *M. tuberculosis* can also release anti-apoptotic factors, like katG and sodA, [46] or arrest the phagosome maturation to which contributes LAM and GTPase Rabs [273].



### 3.5. Discussion

Pathogen-host interaction has been studied by molecular- and cellular-based methods. However, despite having contributed invaluable knowledge, these methods still show difficulties in mimicking a physiological infection. For example, *in vitro* or *ex vivo* models do not include the incorporation of realistic flow or biomechanical environments and culture conditions are sometimes not suitable for the growth of all microorganisms. This leads to results obtained that do not always correlate with *in vivo* models [58]. The emergence of new technologies, such as microfluidics, allows overcoming some of these limitations [274]. Specifically, the microfluidic device used in this article allows us to generate a three-dimensional biomechanical environment that recreates the ECM through which macrophages physiologically migrate. This is of utmost importance, since it has been shown that the two-dimensional and three-dimensional migration of this cell type presents differences, such as greater variation in cell dynamics and morphology in 3D environments [241].

We demonstrated that macrophages recognize proximal stimuli from bacterial components and migrate towards them. However, they also respond to chemo-attractant cytokines released at sites of infection [275]. Therefore, macrophages activated by the initial bacterial stimulus would be able to secrete molecules that induce the recruitment of neighboring macrophages [16]. For example, C-C motif chemokine ligand 2 (CCL2), also known as MCP1, is considered the most important anti-inflammatory cytokine in bacterial infections [276]. Another potent macrophage chemoattractant secreted by macrophages is colony-stimulating factor 1 (CSF1) [277].

Even if application of microfluidics to microbiology is an emerging field, recent studies show that this technique is gaining momentum. Kim *et al.* were able to grow intestinal microbiota bacteria and intracellular pathogens in a microfluidic device that recreated the gut. The composition of this device was based on the culture of a monolayer of intestinal epithelium on a hydrogel that recreates the ECM and the passage of fluid flow at low rate that mimics peristaltic movements [278,279]. Thacker *et al.* used a similar, but

more complex approach in which they co-cultured lung epithelium, along with endothelial cells and macrophages to recreate lung physiology. In this case, *M. tuberculosis* was introduced to mimic a realistic infection situation [280]. It should be also noted that the mechanical environment, such as stiffness, pH or hydrodynamics, also influences cell behavior [281]. Our microfluidic device would allow replacing the collagen-based matrix by other hydrogel options that bring new features to study macrophage motility characteristics. Scaffolds can be made sensitive to temperature, with polysaccharides such as hyaluronic acid or cellulose, to electric fields using sulfonated polystyrene, or to pH using polyacrylamide [282]. These perspectives show the great potential and versatility of the application of microfluidics in microbiology.

## 4. CONCLUSIONS

---



## 4.1. Conclusions

Throughout this PhD dissertation we have demonstrated the versatility of microfluidics, which has allowed us to introduce *in vitro* three-dimensionality in the environment, co-culture with various cell types and the application of biochemical and mechanical stimuli. As a consequence, we have been able to recreate *in vitro* different scenarios very similar to those presented in bacterial infections *in vivo*. Specifically, we have focused on two processes of the innate response involving macrophages: the extravasation of their precursors, the monocytes, into the ECM, and the migration of macrophages in response to bacterial stimuli. The conclusions obtained in each of the chapters are detailed below. However, as an overall conclusion of the thesis, I would highlight the potential of microfluidics as a tool to achieve a better understanding of the interaction between cells, microorganisms and their environment. In this case, it has allowed us to understand in detail the endothelium-monocyte interrelationship under the mechanical stimuli of flow and matrix stiffness, as well as the pattern changes in macrophage migration in the presence of bacterial molecules.

### 4.1.1. Monocytes extravasation

The monocyte extravasation assay consists of the development of an endothelial vessel through which monocytes are passed to study their extravasation. In addition, the effect of mechanical stimuli is determined: oscillatory flow and environmental stiffness. The conclusions obtained are presented below:

- The design of the microfluidic device allows the development of a functional endothelial vessel. We understand as functional a three-dimensional vessel of cylindrical shape; continuous monolayer with no gaps between cell junctions; and with actin aligned parallel to the direction of the vessel. In addition, the endothelial vessel is similar in diameter to venules and arterioles, areas of the circulatory system where extravasation occurs *in vivo*.

- The endothelial vessel is useful for the study of monocyte extravasation processes, and adhered and extravasated monocytes can be clearly observed.
- The application of oscillatory flow to the endothelial vessel increases its barrier integrity, reducing its permeability. Therefore, there is greater adherence of monocytes to the vessel, but less extravasation. This is because monocytes find more difficulties to cross the endothelial barrier due to the increased integrity.
- The concentration of collagen-based hydrogels presents effects on the fiber distribution and final properties. An increase in collagen concentration leads to an increase in the number of fibers in the gel, reducing its pores and increasing its rigidity.
- The culture of endothelial vessels in high stiffness gels significantly reduces their barrier integrity, increasing their permeability and, consequently, the monocyte extravasation.

#### 4.1.2. Macrophage migration in response to bacterial fractions

The macrophage migration assay tracks the movement of macrophages during 24 h in response to a gradient of bacterial fractions. It is studied the attracting effect of the fractions obtained from four bacteria: *Salmonella typhimurium*, *Mycobacterium tuberculosis*, *Escherichia coli* and *Mycobacterium smegmatis*. The conclusions of this work are detailed below:

- Macrophages embedded in hydrogels have a three-dimensional migration. In hydrogels with low collagen concentrations, they migrate longer distances and at higher speed.
- The design of the microfluidic device allows the generation of gradients by introducing the bacterial fractions through one of the reservoir channels. All components of these samples are able to diffuse through the pores of 2.5 mg/ml collagen gels.
- Macrophages migrate directionally attracted to the bacterial fractions of the pathogens *Salmonella typhimurium* and *Mycobacterium tuberculosis*. Both bacteria

possess molecules that interact with macrophage receptors, activating signaling pathways that modify their migratory behavior.

- Macrophages are also attracted to the bacterial fractions of the environmental and non-pathogenic *Escherichia coli* and *Mycobacterium smegmatis*. However, the final fate of these bacteria inside macrophages is very different from that of their pathogenic counterparts, since they do not possess survival mechanisms.

## 4.2. Conclusiones

A lo largo de esta tesis se ha demostrado la versatilidad de la microfluídica, que nos ha permitido introducir tridimensionalidad en el entorno de los experimentos *in vitro*, cocultivo con varios tipos celulares y la aplicación de estímulos bioquímicos y mecánicos. Como consecuencia, hemos podido recrear *in vitro* distintos escenarios muy similares a los presentes en infecciones bacterianas *in vivo*. En concreto, dos procesos de la respuesta innata que involucran a los macrófagos se han tenido en cuenta: la extravasación de sus precursores, los monocitos, a la matriz extracelular, y la migración de los macrófagos en respuesta a fracciones bacterianas. A continuación, se detallan las conclusiones obtenidas en cada uno de los trabajos. Sin embargo, como conclusión global de la tesis, destacaría el potencial de la microfluídica como una herramienta para lograr un mayor entendimiento de la interacción entre células, microorganismos y su entorno. En este caso, nos ha permitido comprender con mayor detalle la interrelación endotelio-monocito bajo los estímulos mecánicos de flujo y rigidez de la matriz, así como los cambios de patrón en la migración de los macrófagos en presencia de moléculas bacterianas.

### 4.2.1. Extravasación de monocitos

El ensayo de extravasación de monocitos consiste en el desarrollo de un vaso endotelial a través del cual se hacen pasar monocitos para estudiar su extravasación. Además, se determina el efecto de estímulos mecánicos: flujo oscilatorio y rigidez del entorno. A continuación se exponen las conclusiones obtenidas:

- El diseño del dispositivo microfluídico permite el desarrollo *in vitro* de un vaso endotelial funcional. Se entiende como funcional un vaso tridimensional de forma cilíndrica, de monocapa continua sin huecos entre uniones celulares y con la actina alineada paralelamente a la dirección del vaso. Además, el vaso endotelial tiene el diámetro similar a las vénulas y arteriolas, zonas del sistema circulatorio donde ocurre la extravasación *in vivo*.



- El vaso endotelial es útil para el estudio de procesos de extravasación de monocitos, pudiendo observarse con claridad los monocitos adheridos y extravasados a la matriz extracelular.
- La aplicación de flujo oscilatorio al vaso endotelial aumenta su integridad de barrera, haciéndolo menos impermeable. Como consecuencia, hay una mayor adherencia de los monocitos al vaso, pero una menor extravasación. Esto se debe a que los monocitos encuentran mayores dificultades para atravesar la barrera endotelial debido al aumento de integridad.
- La concentración de colágeno utilizada en el hidrogel tiene efectos en la distribución y propiedades del hidrogel formado. Un aumento en la concentración de colágeno conlleva un aumento en el número de fibras del gel, reduciendo sus poros y aumentando su rigidez.
- El cultivo de vasos endoteliales en geles de alta rigidez reduce significativamente su integridad, haciéndolos mucho más permeables y aumentando la extravasación de monocitos.

#### 4.2.2. Migración de macrófagos en respuesta a estímulos bacterianos

El ensayo de migración de macrófagos sigue el movimiento de los macrófagos durante 24 h en respuesta a un gradiente de fracciones bacterianas. Se estudia el efecto atrayente de las fracciones obtenidas por cuatro bacterias: *Salmonella typhimurium*, *Mycobacterium tuberculosis*, *Escherichia coli* y *Mycobacterium smegmatis*. A continuación se detallan las conclusiones de este trabajo:

- Los macrófagos embebidos en hidrogeles tienen una migración tridimensional. En hidrogeles con bajas concentraciones de colágeno, migran mayores distancias y a mayor velocidad
- El diseño del dispositivo microfluídico permite la generación de gradientes introduciendo las fracciones bacterianas por uno de los canales reservorios. Todos los componentes de estas muestras son capaces de difundir a través de los poros de geles de 2.5 mg/ml de colágeno.

- Los macrófagos migran direccionalmente atraídos hacia las fracciones bacterianas de los patógenos *Salmonella typhimurium* y *Mycobacterium tuberculosis*. Ambas bacterias poseen moléculas que interactúan con receptores de los macrófagos, activando rutas de señalización que modifican su comportamiento migratorio.
- Los macrófagos también se sienten atraídos hacia las fracciones bacterianas de las bacterias inocuas *Escherichia coli* y *Mycobacterium smegmatis*. Sin embargo, el resultado final de estas bacterias en el interior de los macrófagos será muy diferente al de sus similares patógenas, ya que no poseen mecanismos de supervivencia.

## 5. FUTURE WORK

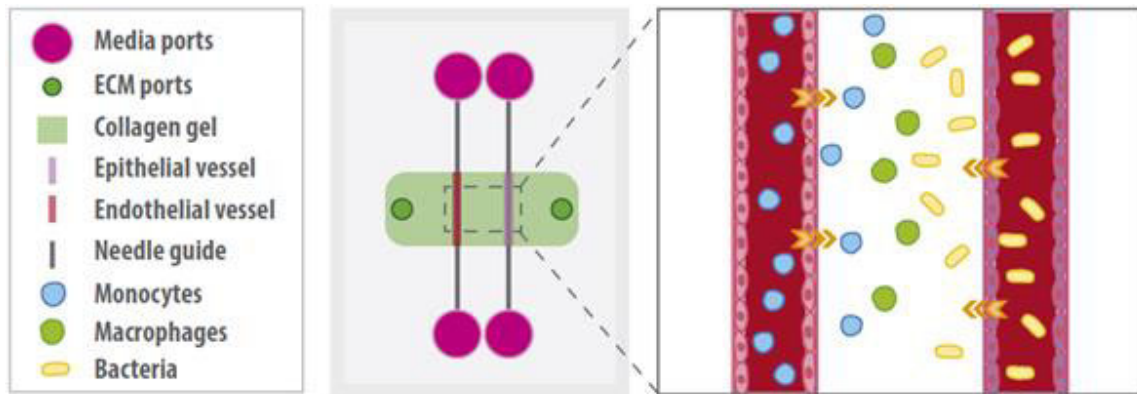
---



This project has demonstrated the versatility of microfluidics and the contribution that this technique can have in biomedical studies. However, the microfluidic devices used are still incomplete and do not recreate the complete infection process. The integration of several stages in the same platform, as well as more cell types, is necessary to achieve a more realistic model that includes the multiple interactions that occur. Therefore, as future work, I make a proposal for a microfluidic device in which the two processes discussed in this thesis are integrated: interaction of monocytes and endothelial cells in extravasation, and macrophage migration in response to bacterial stimuli. In addition, intestinal and alveolar epithelia can be also included, allowing the interaction between epithelium and the pathogens as a route of entry into the body.

The proposed microfluidic device is similar to the one used in [Chapter 2](#), but with two transversal channels for the insertion of acupuncture needles ([Figure 5.1](#)). In this way, two cylindrical monolayers embedded in a collagen hydrogel can be developed. In one of the channels, an endothelial vessel would be generated, through which monocytes would be passed. In the other channel, an epithelial vessel of intestinal or alveolar cells would be developed, which would recreate the lumen of the intestine or alveolus, respectively. The bacterial fractions will be passed through this epithelial channel.

The overall approach of this proposal is to recreate the entry of bacteria via oral and respiratory, by passing bacterial fractions or live bacteria through the epithelial vessel. These fractions would interact with the epithelium, activating signaling pathways, which may affect the nearby endothelial vessel, to induce monocyte recruitment. The monocytes would extravasate from the endothelial vessel and migrate toward the bacterial fractions. At some point after their extravasation, the monocytes differentiate into macrophages, their specialized cell form for phagocytosis. To determine and visualize the time at which monocytes differentiate into macrophages, a genetic modification would be performed whereby green fluorescent protein (GFP) will be expressed only in macrophages, but not in monocytes.



**Figure 5.1. Graphical representation for the device proposed for the study of the monocyte-bacteria extravasation and interaction.**

This device (not to scale) consists of a central chamber confining the collagen gel (light green) crossed by two transverse channels (gray). The ends of both channels connect with media ports (purple) that act as reservoirs. In one of these channels an endothelial vessel (light pink) will be developed and in the other, an epithelial vessel (dark pink). Monocytes (blue) will pass through the endothelial vessel and bacteria through the epithelial vessel. Both monocytes and bacteria will interact with their respective vessels and extravasate into the collagen gel. Upon bacterial stimulus, monocytes will differentiate into macrophages, expressing GFP (green)

## 6. BIBLIOGRAPHICAL NOTE

---





## 6.1. Publications obtained from this PhD Dissertation

**Pérez-Rodríguez, S.**; Borau, C.; García-Aznar, JM.; Gonzalo-Asencio, J.; **A microfluidic-based analysis of 3D macrophage migration after stimulation by *Mycobacterium*, *Salmonella* and *Escherichia*.** Under review.

**Pérez-Rodríguez, S.**; Huang, S.A.; Borau, C.; García-Aznar, JM.; Polacheck, W.J.; **Microfluidic model of monocyte extravasation reveals the role of hemodynamics and subendothelial matrix mechanics in regulating endothelial integrity.** *Biomicrofluidics*. 2021, 15(5):054102. doi: 10.1063/5.0061997.

**Pérez-Rodríguez, S.**; García-Aznar, JM.; Gonzalo-Asencio, J.; **Microfluidic devices for studying bacterial taxis, drug testing and biofilm formation.** *Microbial Biotechnology*. 2021. doi: 10.1111/1751-7915.13775.

**Pérez-Rodríguez, S.**; Tomás-González, E.; García-Aznar, JM.; **3D Cell Migration Studies for Chemotaxis on Microfluidic-Based Chips: A Comparison between Cardiac and Dermal Fibroblasts.** *Bioengineering*. 2018, 5(45). doi: 10.3390/bioengineering5020045

## 6.2. Participation in conferences and congresses

**Pérez-Rodríguez, S.**; Huang, S.A.; Borau, C.; García-Aznar, JM.; Polacheck, W.J.; **Microfluidics-based analysis of monocyte extravasation: the role of oscillating vessel flow and collagen stiffness.** Oral presentation. *X Reunión del Capítulo Español de la Sociedad Europea de Biomecánica (ESB)*. 2021, Granada (Spain).

**Pérez-Rodríguez, S.**; Huang, S.A.; Borau, C.; García-Aznar, JM.; Polacheck, W.J.; **Microfluidic model of monocyte extravasation reveals the role of hemodynamics and subendothelial matrix mechanics in regulating endothelial integrity.** Poster presentation. *VII Edición de las Jornadas Doctorales del Campus Iberus*. 2021, Jaca (Spain).

**Pérez-Rodríguez, S.**; Attendance and organization. *Virtual Physiological Human Conference*. 2018, Zaragoza (Spain).

**Pérez-Rodríguez, S.** and Juste, Y.; **Pasión por la ciencia, más allá del doctorado**. Mesa redonda Actividades por y para doctorados. *V Edición de las Jornadas Doctorales del Campus Iberus*. 2018, Jaca (Spain).

### 6.3. Research stay

Microfluidic model of monocyte extravasation reveals the role of hemodynamics and subendothelial matrix mechanics in regulating endothelial integrity. **William Polackek's Group. The Joint Department of Biomedical Engineering - University of North Carolina at Chapel Hill, NC, (United States)**. 01/08/2019 – 22/12/2019. *Grant: Ministerio de Educación, Cultura y Deporte. Ayudas a la movilidad para estancias breves y traslados temporales (EST18/00319)*

### 6.4. Teaching activities

**Microbial Biotechnology** (Degree in Biotechnology). *Departamento de Microbiología, Pediatría, Radiología y Salud Pública*.

- Academic year 2020/2021: 40 h

**Biotechnology applied to immunology and microbiology** (Degree in Biotechnology). *Departamento de Microbiología, Pediatría, Radiología y Salud Pública*.

- Academic year 2020/2021: 20 h

**Microbiology** (Degree in Biotechnology). *Departamento de Microbiología, Pediatría, Radiología y Salud Pública.*

- Academic year 2018/2019: 40 h
- Academic year 2019/2020: 40 h

**Genetic Engineering** (Degree in Biotechnology). *Departamento de Microbiología, Pediatría, Radiología y Salud Pública.*

- Academic year 2018/2019: 20 h
- Academic year 2019/2020: 20 h



# APPENDIX

---



In this appendix it is included certain advances that have been made in the methodology of the proposal explained in the chapter of [Future work](#).

## A.1. Selection of cell lines

The human cell lines used so far will be maintained, working with HUVEC endothelial cells and THP-1 leukocytes. To simulate the intestinal and pulmonary epithelium, the commercial cells Caco-2 and A549, respectively, have been selected. Both cell lines have been used as models for the study of intestinal and alveolar functions [283,284].

## A.2. Genetic modification

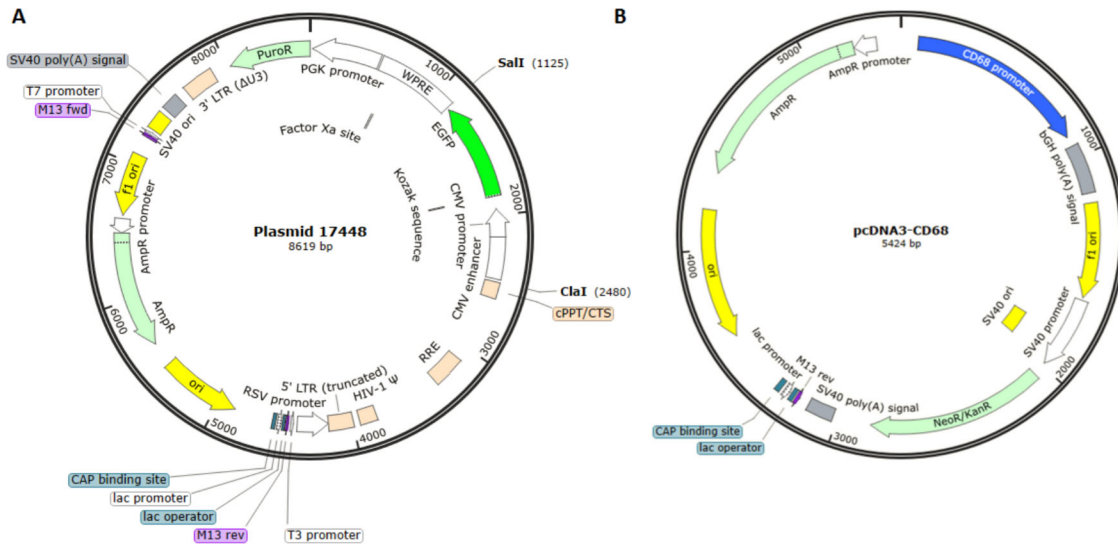
To achieve the genetic modification that would allow the observation of the differentiation of monocytes to macrophages, we based our strategy on the study performed by Igbal *et al.* in mice. In this study, they conducted a genetic construct consisting of the fusion of the CD68 promoter to the GFP gene. The CD68 gene is a molecular biomarker that is expressed in macrophages, but not in monocytes. Therefore, by placing CD68 promoter previous to GFP gene, this protein will be expressed when monocytes differentiate into macrophages, turning cells fluorescent and allowing their visualization [285].

As our objective is similar to that of Igbal *et al.* we decided to perform an equivalent construction but adapted to human cells. For this purpose, we selected the necessary plasmids, designed the primers and planned a possible protocol to follow.

### A.2.1. Selection of plasmids

Thanks to the addgene tool, the plasmids necessary for this modification were selected. On the one hand, plasmid 17448 ([Figure A.1](#)) was selected to express the final construct, since it contains the SV40 origin for expression in mammalian cells and the GFP gene of interest. However, the GFP gene is preceded by the constitutive mouse-specific cytomegalovirus early gene (CMV) promoter. Therefore, for our final construct, we need to replace the

mouse CMV promoter with the human CD68 promoter. This human CD68 promoter will be obtained from the pcDNA3-CD68 plasmid (Figure A.1).



**Figure A.1. Structure of plasmids 17448 and pcDNA-CD68.**

A) Plasmid 17448 has a total length of 8619 bp, in which it integrates the SV40 origin site for mammalian replication, the EGFP gene (green) preceded by the CMV promoter and surrounded by the restriction enzymes *Sall* and *ClaI* and several constructs with selective genes, such as puromycin (PuroR) to ampicillin (AmpR) resistance. B) The plasmid pcDNA-CD68 has a length of 5424 bp including the human CD68 promoter (blue) of interest for this project. Images taken from snapgene.

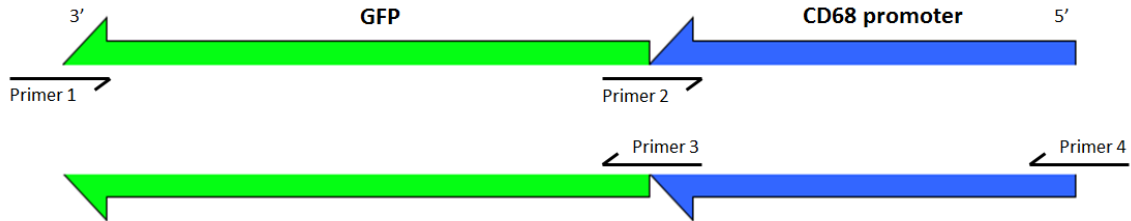
### A.2.2. Primers design

The primers design is based on amplifying the CD68 promoter of plasmid pcDNA3-CD68 and overlapping it with the GFP gene of plasmid 17448. This gene construct will be introduced into the plasmid 17448 vector, replacing the current CMV promoter + GFP. For this purpose, the restriction enzymes *Sall* and *ClaI* are used. The use of these two restriction enzymes has been decided because they are single-cutting and surround the construct of interest (Figure A.1). Therefore, the tails of the primers designed for the CD68 + GFP construct are overlapping the ends of plasmid 17448 after treatment with the restriction enzymes.

To perform the final construction, four primers have been designed (Figure A.2 and Table A.1). Primer 1 overlaps the *Sall*-cut plasmid 17448 with the 3' end of the GFP gene.



Primers 2 and 3 fuse the CD68 promoter with the GFP gene. Finally, primer 4 overlaps the *Clal*-cut plasmid17448 with the 5' end of the CD68 promoter.



**Figure A.2. Visual map of primer design.**

To achieve the construction of the CD68 promoter (blue) and GFP gene (green) fused to plasmid 17448 cut with *Sall* and *Clal*, the design of four primers was proposed. Primer 1 fuses the GFP gene to plasmid 17448, primers 2 and 3 fuse CD68 promoter and GFP gene, and primer 4 fuses CD68 promoter to plasmid 17448.

The sequences of the four primers are detailed in the following table:

Primer	Fusion	Sequence
Primer 1	Plasmid17448 + GFP	5'- CACAAATTTTGTAAATCCAGAGGTTGATTGTCGACGCGGCCGCTTTACTTGACAGC-3'
Primer 2	GFP + CD68	5'-CCAGGCGATCTGACGGTTCACTAAACGGGCGCTGAGTCCCCTGGGC-3'
Primer 3	CD68 + GFP	5'-GCCAGGGGACTCAGCGGCCGTTTGTAGTGAACCGTCAGATCGCCTGG-3'
Primer 4	Plasmid17448 + CD68	5'- AGAATTACAAAAACAAATTACAAAATTCAAAATTTTATGCAGATATCAAAGTGCCTGT TTGGGCT-3'

**Table A.1. Primers sequences**

Sequences of the four designed primers are detailed in this table. Overlapping with plasmid 17448 is shown in black, with GFP in green and with CD68 in blue.

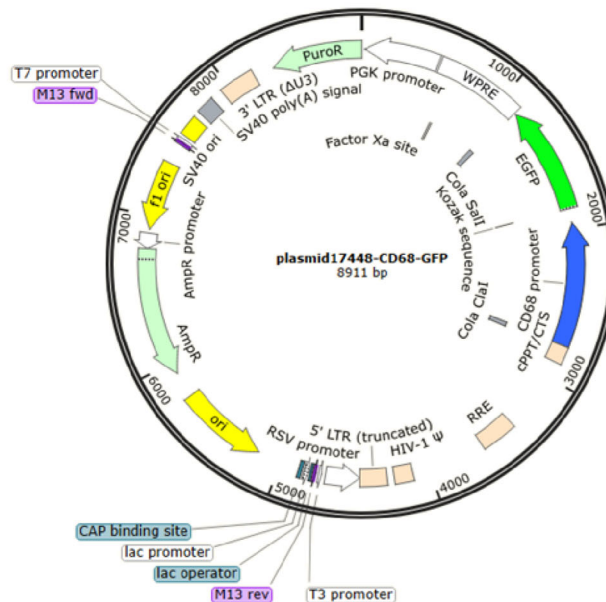
### A.2.3. Gibson Assembly Protocol

The primers have been designed to be fused by Gibson assembly. This requires overlapping DNA fragments and the presence of a DNA polymerase, a T5 exonuclease and a thermostable DNA ligase. A simplified protocol of the steps to be followed to carry out this construction has been established:

1. Amplify CD68 promoter using the plasmid pcDNA3-CD68 with oligos 2 and 4 as a template. Purify it.

2. Amplify GFP by taking plasmid 17448 with oligos 1 and 3 as a template. Purify it.
3. Cut the plasmid of interest with *Sall* and *Clal*. Purify it.
4. Assemble CD68 promoter and GFP.
5. Amplify the CD68 + GFP construct with oligos 1 and 4.
6. Assemble the CD68 + GFP construct with the plasmid 17448 cut with *Sall* and *Clal*.

The final product we expect to obtain will be plasmid 17448 with the GFP protein preceded by the CD68 promoter (Figure A.3).



**Figure A.3. Final plasmid after genetic modification**

Final construction of plasmid 17448 in which the CMV promoter has been replaced by the CD68 promoter (blue) preceding the GFP gene (green).

#### A.2.4. Cloning in monocyte

Plasmid 17448 is derived from lentivirus, so a lentivirus transduction protocol would be used for its incorporation into the monocyte. The selection and purification of modified cells would be performed by puromycin resistance (PuroR). However, the PGK promoter that precedes this gene is mouse-specific, so planning a new genetic modification to replace it with a human promoter would be necessary.

### A.3. Microfluidic device

The microfluidic device was designed by William Polacheck's research group as a modification of the device used in [Chapter 2](#). The novelty of this device is the addition of a second channel for vessel formation parallel to the existing one. Different designs were made that vary in the distance between the two channels. Optimization trials should be performed to determine which device is suitable for these studies. Their fabrication follows the same protocol previously applied and established by Polacheck *et al.* [167].



# REFERENCES

---



1. Balloux, F.; van Dorp, L. Q&A: What are pathogens, and what have they done to and for us? *BMC Biol.* **2017**, *15*, 4–9, doi:10.1186/s12915-017-0433-z.
2. Microbiology by numbers. *Nat. Rev. Microbiol.* **2011**, *9*, 628, doi:10.1038/nrmicro2644.
3. Chan, J. F.; Kok, K. Genomic characterization of the 2019 novel human-pathogenic coronavirus isolated from a patient with atypical pneumonia after visiting Wuhan. *Emerg. Microbes Infect.* **2020**, *9*, 540, doi:10.1080/22221751.2020.1737364.
4. Vouga, M.; Greub, G. Emerging bacterial pathogens: The past and beyond. *Clin. Microbiol. Infect.* **2016**, *22*, 12–21, doi:10.1016/j.cmi.2015.10.010.
5. Bartoli, C.; Roux, F.; Lamichhane, J. R. Molecular mechanisms underlying the emergence of bacterial pathogens: An ecological perspective. *Mol. Plant Pathol.* **2016**, *17*, 303–310, doi:10.1111/mpp.12284.
6. Hameed, S.; Xie, L.; Ying, Y. Conventional and emerging detection techniques for pathogenic bacteria in food science: A review. *Trends Food Sci. Technol.* **2018**, *81*, 61–73.
7. Váradi, L.; Luo, J. L.; Hibbs, D. E.; Perry, J. D.; Anderson, R. J.; Orega, S.; Groundwater, P. W. Methods for the detection and identification of pathogenic bacteria: Past, present, and future. *Chem. Soc. Rev.* **2017**, *46*, 4818–4832, doi:10.1039/c6cs00693k.
8. McArthur, D. B. Emerging Infectious Diseases. *Nurs Clin North Am* **2019**, *54*, 297–311.
9. Alberts, B.; Johnson, A.; Lewis, J.; Raff, M.; Roberts, K.; Walter, P. Introduction to Pathogens. In *Molecular Biology of the Cell. 4th edition.*; 2002.
10. Doron, S.; Gorbach, S. L. Bacterial Infections. *Int. Encycl. Public Heal.* **2008**, 273–282, doi:10.1016/B978-0-323-01199-0.50123-7.
11. Chaplin, D. D. Overview of the immune response. *J. Allergy Clin. Immunol.* **2010**, *125*, S3-23, doi:10.1016/j.jaci.2010.01.002.
12. Lowell, A. Immunology Overview: How does our immune system protect us?
13. WHO *WHO estimates of the global burden of foodborne diseases*; 2015;
14. WHO *Global Health Estimates*; 2019;
15. WHO *Global Tuberculosis Report*; 2021;
16. Mosser, D. M.; Edwards, J. P. Exploring the full spectrum of macrophage activation. *Nat. Rev. Immunol.* **2008**, *8*, 958–969.
17. Ginhoux, F.; Jung, S. Monocytes and macrophages: Developmental pathways and tissue homeostasis. *Nat. Rev. Immunol.* **2014**, *14*, 392–404, doi:10.1038/nri3671.
18. Silva, M. T. When two is better than one: macrophages and neutrophils work in concert in innate immunity as complementary and cooperative partners of a myeloid phagocyte system. *J. Leukoc. Biol.* **2010**, *87*, 93–106, doi:10.1189/jlb.0809549.
19. Akira, S.; Uematsu, S.; Takeuchi, O. Pathogen recognition and innate immunity. *Cell* **2006**, *124*, 783–801, doi:10.1016/j.cell.2006.02.015.
20. Kaufmann, S. H. E. The contribution of immunology to the rational design of novel antibacterial vaccines. *Nat. Rev. Microbiol.* **2007**, *5*, 491–504, doi:10.1038/nrmicro1688.
21. Chang, D. T.; Jones, J. A.; Meyerson, H.; Colton, E.; Kwon, I. K.; Matsuda, T.; Anderson, J. M. Lymphocyte/Macrophage Interactions: Biomaterial Surface- Dependent Cytokine, Chemokine, and Matrix Protein Production. *J Biomed Mater Res A.* **2008**, *87*, doi:10.1002/jbm.a.31630.Lymphocyte/Macrophage.
22. WHO *Salmonella (non-typhoidal)*; 2018;
23. Galán, J. E. Salmonella Typhimurium and inflammation: a pathogen-centric affair. *Nat. Rev. Microbiol.* **2021**, *19*, 716–725, doi:10.1038/s41579-021-00561-4.
24. Duan, Y.; Liao, A. P.; Kuppireddi, S.; Ye, Z.; Ciancio, M. J.; Sun, J.  $\beta$ -Catenin activity negatively regulates bacteria-induced inflammation. *Lab. Invest.* **2007**, *87*, 613–624, doi:10.1038/labinvest.3700545.
25. Eckmann, L.; Stenson, W. F.; Savidge, T. C.; Lowe, D. C.; Barrett, K. E.; Fierer, J.; Smith, J. R.; Kagnoff, M. F. Role of intestinal epithelial cells in the host secretory response to infection by invasive bacteria: Bacterial entry induces epithelial prostaglandin H synthase-2 expression and prostaglandin E2 and F(2 $\alpha$ ) production. *J. Clin. Invest.* **1997**, *100*, 296–309, doi:10.1172/JCI119535.
26. CDC *Salmonella Symptoms*; 2019;
27. Groschwitz, K. R.; Hogan, S. P. Intestinal Barrier Function: Molecular Regulation and Disease Pathogenesis. *J Allergy Clin Immuno* **2009**, *124*, 3–22, doi:10.1016/j.jaci.2009.05.038.

28. Thursby, E.; Juge, N. Introduction to the human gut microbiota. *Biochem. J.* **2017**, *474*, 1823–1836, doi:10.1042/BCJ20160510.
29. Kamada, N.; Chen, G. Y.; Inohara, N.; Núñez, G. Control of pathogens and pathobionts by the gut microbiota. *Nat. Immunol.* **2013**, *14*, 685–690, doi:10.1038/ni.2608.
30. Kobayashi, N.; Takahashi, D.; Takano, S.; Kimura, S.; Hase, K. The Roles of Peyer's Patches and Microfold Cells in the Gut Immune System: Relevance to Autoimmune Diseases. *Front. Immunol.* **2019**, *10*, 1–15, doi:10.3389/fimmu.2019.02345.
31. Batista, F. D.; Harwood, N. E. The who, how and where of antigen presentation to B cells. *Nat. Rev. Immunol.* **2009**, *9*, 15–27, doi:10.1038/nri2454.
32. Nagl, M.; Kacani, L.; Müllauer, B.; Lemberger, E. M.; Stoiber, H.; Sprinzl, G. M.; Schennach, H.; Dierich, M. P. Phagocytosis and killing of bacteria by professional phagocytes and dendritic cells. *Clin. Diagn. Lab. Immunol.* **2002**, *9*, 1165–1168, doi:10.1128/CDLI.9.6.1165-1168.2002.
33. Hirayama, D.; Iida, T.; Nakase, H. The phagocytic function of macrophage-enforcing innate immunity and tissue homeostasis. *Int. J. Mol. Sci.* **2018**, *19*, doi:10.3390/ijms19010092.
34. Griebel, P. J. *B Cell Development in Mucosa-Associated Lymphoid Tissues*; Elsevier, 2016; Vol. 1; ISBN 9780080921525.
35. Lupp, C.; Robertson, M. L.; Wickham, M. E.; Sekirov, I.; Champion, O. L.; Gaynor, E. C.; Finlay, B. B. Host-Mediated Inflammation Disrupts the Intestinal Microbiota and Promotes the Overgrowth of Enterobacteriaceae. *Cell Host Microbe* **2007**, *2*, 119–129, doi:10.1016/j.chom.2007.06.010.
36. Lim, J. S.; Na, H. S.; Lee, H. C.; Choy, H. E.; Park, S. C.; Han, J. M.; Cho, K. A. Caveolae-mediated entry of Salmonella typhimurium in a human M-cell model. *Biochem. Biophys. Res. Commun.* **2009**, *390*, 1322–1327, doi:10.1016/j.bbrc.2009.10.145.
37. Knodler, L. A.; Vallance, B. A.; Celli, J.; Winfree, S.; Hansen, B.; Montero, M.; Steele-Mortimer, O. Dissemination of invasive Salmonella via bacterial-induced extrusion of mucosal epithelia. *Proc. Natl. Acad. Sci. U. S. A.* **2010**, *107*, 17733–17738, doi:10.1073/pnas.1006098107.
38. Wang, M.; Qazi, I. H.; Wang, L.; Zhou, G.; Han, H. Salmonella virulence and immune escape. *Microorganisms* **2020**, *8*, 1–25, doi:10.3390/microorganisms8030407.
39. Pai, M.; Behr, M. A.; Dowdy, D.; Dheda, K.; Divangahi, M.; Boehme, C. C.; Ginsberg, A.; Swaminathan, S.; Spigelman, M.; Getahun, H.; Menzies, D.; Raviglione, M. Tuberculosis. *Nat. Rev. Dis. Prim.* **2016**, *2*, doi:10.1038/nrdp.2016.76.
40. Fogel, N. Tuberculosis: A disease without boundaries. *Tuberculosis* **2015**, *95*, 527–531, doi:10.1016/j.tube.2015.05.017.
41. Ramakrishnan, L. Revisiting the role of the granuloma in tuberculosis. *Nat. Rev. Immunol.* **2012**, *12*, 352–366, doi:10.1038/nri3211.
42. Dulberger, C. L.; Rubin, E. J.; Boutte, C. C. The mycobacterial cell envelope — a moving target. *Nat. Rev. Microbiol.* **2020**, *18*, 47–59, doi:10.1038/s41579-019-0273-7.
43. Simeone, R.; Sayes, F.; Lawarée, E.; Brosch, R. Breaching the phagosome, the case of the tuberculosis agent. *Cell. Microbiol.* **2021**, *23*, 1–11, doi:10.1111/cmi.13344.
44. Forrellad, M. A.; Klepp, L. I.; Gioffré, A.; García, J. S.; Morbidoni, H. R.; de la Paz Santangelo, M.; Cataldi, A. A.; Bigi, F. Virulence factors of the mycobacterium tuberculosis complex. *Virulence* **2013**, *4*, 3–66, doi:10.4161/viru.22329.
45. Singh, P.; Rameshwaram, N. R.; Ghosh, S.; Mukhopadhyay, S. Cell envelope lipids in the pathophysiology of Mycobacterium tuberculosis. *Future Microbiol.* **2018**, *13*, 689–710, doi:10.2217/fmb-2017-0135.
46. Gabriela Echeverria-Valencia; Flores-Villalva, S.; Espitia, C. I. Virulence Factors and Pathogenicity of Mycobacterium. In *Mycobacterium - Research and Development*; 2017; Vol. 12, pp. 231–255 ISBN 9781626239777.
47. FDA The Drug Development Process.
48. Alexandra Boussommier-Calleja; Li, R.; Chen, M. B.; Wong, S. C.; Kamm, R. D. Microfluidics: A new tool for modeling cancer-immune interactions. *Trends Cancer* **2017**, *176*, 139-148-, doi:doi:10.1016/j.trecan.2015.12.003.
49. Houpiqian, P.; Raoult, D. Traditional and molecular techniques for the study of emerging bacterial diseases: One laboratory's perspective. *Emerg. Infect. Dis.* **2002**, *8*, 122–131,



- doi:10.3201/eid0802.010141.
50. Balouiri, M.; Sadiki, M.; Ibensouda, S. K. Methods for in vitro evaluating antimicrobial activity: A review. *J. Pharm. Anal.* **2016**, *6*, 71–79, doi:10.1016/j.jpha.2015.11.005.
  51. Stevenson, M.; Baillie, A. J.; Richards, R. M. An in-vitro model of intracellular bacterial infection using the murine macrophage cell line J774.2. *J Pharm Pharmacol* **1984**, *36*, 90–94.
  52. Götz, R.; Kunz, T. C.; Fink, J.; Solger, F.; Schlegel, J.; Seibel, J.; Kozjak-Pavlovic, V.; Rudel, T.; Sauer, M. Nanoscale imaging of bacterial infections by sphingolipid expansion microscopy. *Nat. Commun.* **2020**, *11*, 1–9, doi:10.1038/s41467-020-19897-1.
  53. Kim, J.; Hegde, M.; Jayaraman, A. Co-culture of epithelial cells and bacteria for investigating host-pathogen interactions. *Lab Chip* **2010**, *10*, 43–50, doi:10.1039/b911367c.
  54. Kämpfer, A. A. M.; Urbán, P.; Gioria, S.; Kanase, N.; Stone, V.; Kinsner-Ovaskainen, A. Development of an in vitro co-culture model to mimic the human intestine in healthy and diseased state. *Toxicol. Vitro.* **2017**, *45*, 31–43, doi:10.1016/j.tiv.2017.08.011.
  55. Schweppe, D. K.; Harding, C.; Chavez, J. D.; Wu, X.; Ramage, E.; Singh, P. K.; Manoil, C.; Bruce, J. E. Host-Microbe Protein Interactions during Bacterial Infection. *Chem. Biol.* **2015**, *22*, 1521–1530, doi:10.1016/j.chembiol.2015.09.015.
  56. K.Schoolnik, G. Microarray analysis of bacterial pathogenicity. *Adv. Microb. Physiol.* **2002**, *46*, 1–45.
  57. Ito, T.; Sekizuka, T.; Kishi, N.; Yamashita, A.; Kuroda, M. Conventional culture methods with commercially available media unveil the presence of novel culturable bacteria. *Gut Microbes* **2019**, *10*, 77–91, doi:10.1080/19490976.2018.1491265.
  58. Bodor, A.; Bounedjoum, N.; Vincze, G. E.; Erdeiné Kis, Á.; Laczi, K.; Bende, G.; Szilágyi, Á.; Kovács, T.; Perei, K.; Rákhely, G. Challenges of unculturable bacteria: environmental perspectives. *Rev. Environ. Sci. Biotechnol.* **2020**, *19*, 1–22, doi:10.1007/s11157-020-09522-4.
  59. Vinderola, G.; Gueimonde, M.; Gomez-Gallego, C.; Delfederico, L.; Salminen, S. Correlation between in vitro and in vivo assays in selection of probiotics from traditional species of bacteria. *Trends Food Sci. Technol.* **2017**, *68*, 83–90, doi:10.1016/j.tifs.2017.08.005.
  60. Lebeaux, D.; Chauhan, A.; Rendueles, O.; Beloin, C. From in vitro to in vivo models of bacterial biofilm-related infections. *Pathogens* **2013**, *2*, 288–356, doi:10.3390/pathogens2020288.
  61. Sackmann, E. K.; Fulton, A. L.; Beebe, D. J. The present and future role of microfluidics in biomedical research. *Nature* **2014**, *507*, 181–189, doi:10.1038/nature13118.
  62. Halldorsson, S.; Lucumi, E.; Gómez-Sjöberg, R.; Fleming, R. M. T. Advantages and challenges of microfluidic cell culture in polydimethylsiloxane devices. *Biosens. Bioelectron.* **2015**, *63*, 218–231, doi:10.1016/j.bios.2014.07.029.
  63. Shin, Y.; Han, S.; Jeon, J. S.; Yamamoto, K.; K., I.; Zervantonakis; Sudo, R.; Kamm, R. D.; Chung, S. Microfluidic assay for simultaneous culture of multiple cell types on surfaces or within hydrogels. *Nat Protoc* **2012**, *7*, 1247–1259, doi:10.1080/10810730902873927.Testing.
  64. Huang, M.; Fan, S.; Xing, W.; Liu, C. Microfluidic cell culture system studies and computational fluid dynamics. *Math. Comput. Model.* **2010**, *52*, 2036–2042, doi:10.1016/j.mcm.2010.01.024.
  65. Velve-Casquillas, G.; Le Berre, M.; Piel, M.; Tran, P. T. Microfluidic tools for cell biological research. *Nano Today* **2010**, *5*, 28–47, doi:10.1016/j.nantod.2009.12.001.
  66. Friend, J.; Yeo, L. Fabrication of microfluidic devices using polydimethylsiloxane. *Biomicrofluidics* **2010**, *4*, 1–5, doi:10.1063/1.3259624.
  67. Weibel, D. B.; DiLuzio, W. R.; Whitesides, G. M. Microfabrication meets microbiology. *Nat. Rev. Microbiol.* **2007**, *5*, 209–218, doi:10.1038/nrmicro1616.
  68. Krell, T.; Lacal, J.; Muñoz-Martínez, F.; Reyes-Darias, J. A.; Cadirci, B. H.; García-Fontana, C.; Ramos, J. L. Diversity at its best: Bacterial taxis. *Environ. Microbiol.* **2011**, *13*, 1115–1124, doi:10.1111/j.1462-2920.2010.02383.x.
  69. Mirzaei, R.; Mohammadzadeh, R.; Sholeh, M.; Karampoor, S.; Abdi, M.; Dogan, E.; Moghadam, M. S.; Kazemi, S.; Jalalifar, S.; Dalir, A.; Yousefimashouf, R.; Mirzaei, E.; Khodavirdipour, A.; Alikhani, M. Y. The importance of intracellular bacterial biofilm in infectious diseases. *Microb. Pathog.* **2020**, *147*, doi:10.1016/j.micpath.2020.104393.
  70. Long, T.; Ford, R. M. Enhanced transverse migration of bacteria by chemotaxis in a porous T-sensor. *Environ. Sci. Technol.* **2009**, *43*, 1546–1552, doi:10.1021/es802558j.

71. Wright, E.; Neethirajan, S.; Warriner, K.; Retterer, S.; Srijanto, B. Single cell swimming dynamics of *Listeria monocytogenes* using a nanoporous microfluidic platform. *Lab Chip* **2014**, *14*, 938–946, doi:10.1039/c3lc51138c.
72. Englert, D. L.; Manson, M. D.; Jayaraman, A. Flow-based microfluidic device for quantifying bacterial chemotaxis in stable, competing gradients. *Appl. Environ. Microbiol.* **2009**, *75*, 4557–4564, doi:10.1128/AEM.02952-08.
73. Mao, H.; Cremer, P. S.; Manson, M. D. A sensitive, versatile microfluidic assay for bacterial chemotaxis. *Proc. Natl. Acad. Sci. U. S. A.* **2003**, *100*, 5449–5454, doi:10.1073/pnas.0931258100.
74. Ahmed, T.; Stocker, R. Experimental verification of the behavioral foundation of bacterial transport parameters using microfluidics. *Biophys. J.* **2008**, *95*, 4481–4493, doi:10.1529/biophysj.108.134510.
75. Lanning, L. M.; Ford, R. M.; Long, T. Bacterial chemotaxis transverse to axial flow in a microfluidic channel. *Biotechnol. Bioeng.* **2008**, *100*, 653–663, doi:10.1002/bit.21814.
76. Roggo, C.; Picioreanu, C.; Richard, X.; Mazza, C.; van Lintel, H.; van der Meer, J. R. Quantitative chemical biosensing by bacterial chemotaxis in microfluidic chips. *Environ. Microbiol.* **2018**, *20*, 241–258, doi:10.1111/1462-2920.13982.
77. Cheng, S. Y.; Heilman, S.; Wasserman, M.; Archer, S.; Shuler, M. L.; Wu, M. A hydrogel-based microfluidic device for the studies of directed cell migration. *Lab Chip* **2007**, *7*, 763–769, doi:10.1039/b618463d.
78. Adler, M.; Erickstad, M.; Gutierrez, E.; Groisman, A. Studies of bacterial aerotaxis in a microfluidic device. *Lab Chip* **2012**, *12*, 4835–4847, doi:10.1039/c2lc21006a.
79. Golchin, S. A.; Stratford, J.; Curry, R. J.; McFadden, J. A microfluidic system for long-term time-lapse microscopy studies of mycobacteria. *Tuberculosis* **2012**, *92*, 489–496, doi:10.1016/j.tube.2012.06.006.
80. Lam, R. H. W.; Kim, M. C.; Thorsen, T. Culturing aerobic and anaerobic bacteria and mammalian cells with a microfluidic differential oxygenator. *Anal. Chem.* **2009**, *81*, 5918–5924, doi:10.1021/ac9006864.
81. Stricker, L.; Guido, I.; Breithaupt, T.; Mazza, M. G.; Vollmer, J. Hybrid sideways/longitudinal swimming in the monoflagellate *Shewanella oneidensis*: from aerotactic band to biofilm. *Physics (College. Park. Md.)* **2019**.
82. Menolascina, F.; Rusconi, R.; Fernandez, V. I.; Smriga, S.; Aminzare, Z.; Sontag, E. D.; Stocker, R. Logarithmic sensing in *Bacillus subtilis* aerotaxis. *npj Syst. Biol. Appl.* **2017**, *3*, doi:10.1038/npjbsa.2016.36.
83. Kim, B. J.; Chu, I.; Jusuf, S.; Kuo, T.; TerAvest, M. A.; Angenent, L. T.; Wu, M. Oxygen tension and riboflavin gradients cooperatively regulate the migration of *Shewanella oneidensis* MR-1 revealed by a hydrogel-based microfluidic device. *Front. Microbiol.* **2016**, *7*, 1–12, doi:10.3389/fmicb.2016.01438.
84. Marcos, Fu, H. C.; Powers, T. R.; Stocker, R. Separation of microscale chiral objects by shear flow. *Phys. Rev. Lett.* **2009**, *102*, doi:10.1103/PhysRevLett.102.158103.
85. Rusconi, R.; Lecuyer, S.; Guglielmini, L.; Stone, H. A. Laminar flow around corners triggers the formation of biofilm streamers. *J. R. Soc. Interface* **2010**, *7*, 1293–1299, doi:10.1098/rsif.2010.0096.
86. Ishikawa, T.; Shioiri, T.; Numayama-Tsuruta, K.; Ueno, H.; Imaia, Y.; Yamaguchi, T. Separation of motile bacteria using drift velocity in a microchannel. *Lab Chip* **2014**, 1023–1032, doi:10.1039/c2lc41193h.
87. Yazdi, S.; Ardekani, A. M. Bacterial aggregation and biofilm formation in a vortical flow. *Biomicrofluidics* **2012**, *6*, doi:10.1063/1.4771407.
88. Zhang, X. Y.; Sun, K.; Abulimiti, A.; Xu, P. P.; Li, Z. Y. Microfluidic system for observation of bacterial culture and effects on biofilm formation at microscale. *Micromachines* **2019**, *10*, doi:10.3390/mi10090606.
89. Marty, A.; Causserand, C.; Roques, C.; Bacchin, P. Impact of tortuous flow on bacteria streamer development in microfluidic system during filtration. *Biomicrofluidics* **2014**, *8*, doi:10.1063/1.4863724.
90. Dehkharghani, A.; Waisbord, N.; Dunkel, J.; Guasto, J. S. Bacterial scattering in microfluidic crystal flows reveals giant active Taylor–Aris dispersion. *Proc. Natl. Acad. Sci. U. S. A.* **2019**, *166*, 11119–11124, doi:10.1073/pnas.1819613116.
91. Durham, W. M.; Tranzer, O.; Leombruni, A.; Stocker, R. Division by fluid incision: Biofilm patch

- development in porous media. *Phys. Fluids* **2012**, *24*, doi:10.1063/1.4747154.
92. Kaya, T.; Koser, H. Direct upstream motility in Escherichia coli. *Biophys. J.* **2012**, *102*, 1514–1523, doi:10.1016/j.bpj.2012.03.001.
  93. Caspi, Y. Deformation of filamentous Escherichia coli cells in a microfluidic device: A new technique to study cell mechanics. *PLoS One* **2014**, *9*, doi:10.1371/journal.pone.0083775.
  94. Rismani Yazdi, S.; Nosrati, R.; Stevens, C. A.; Vogel, D.; Escobedo, C. Migration of magnetotactic bacteria in porous media. *Biomicrofluidics* **2018**, *12*, doi:10.1063/1.5024508.
  95. Myklatun, A.; Cappetta, M.; Winklhofer, M.; Ntziachristos, V.; Westmeyer, G. G. Microfluidic sorting of intrinsically magnetic cells under visual control. *Sci. Rep.* **2017**, *7*, 1–8, doi:10.1038/s41598-017-06946-x.
  96. Miller, S.; Weiss, A. A.; Heineman, W. R.; Banerjee, R. K. Electroosmotic flow driven microfluidic device for bacteria isolation using magnetic microbeads. *Sci. Rep.* **2019**, *9*, 1–11, doi:10.1038/s41598-019-50713-z.
  97. Rismani Yazdi, S.; Nosrati, R.; Stevens, C. A.; Vogel, D.; Davies, P. L.; Escobedo, C. Magnetotaxis Enables Magnetotactic Bacteria to Navigate in Flow. *Small* **2018**, *14*, 1–10, doi:10.1002/sml.201702982.
  98. Demir, M.; Salman, H. Bacterial thermotaxis by speed modulation. *Biophys. J.* **2012**, *103*, 1683–1690, doi:10.1016/j.bpj.2012.09.005.
  99. Salman, H.; Zilman, A.; Loverdo, C.; Jeffroy, M.; Libchaber, A. Solitary modes of bacterial culture in a temperature gradient. *Phys. Rev. Lett.* **2006**, *97*, 1–5, doi:10.1103/PhysRevLett.97.118101.
  100. Murugesan, N.; Dhar, P.; Panda, T.; Das, S. K. Interplay of chemical and thermal gradient on bacterial migration in a diffusive microfluidic device. *Biomicrofluidics* **2017**, *11*, 1–13, doi:10.1063/1.4979103.
  101. Paulick, A.; Jakovljevic, V.; Zhang, S.; Erickstad, M.; Groisman, A.; Meir, Y.; Ryu, W. S.; Wingreen, N. S.; Sourjik, V. Mechanism of bidirectional thermotaxis in Escherichia coli. *Elife* **2017**, *6*, doi:10.7554/eLife.26607.
  102. Jeong, H. H.; Jeong, S. G.; Park, A.; Jang, S. C.; Hong, S. G.; Lee, C. S. Effect of temperature on biofilm formation by Antarctic marine bacteria in a microfluidic device. *Anal. Biochem.* **2014**, *446*, 90–95, doi:10.1016/j.ab.2013.10.027.
  103. Parvinezadeh Gashti, M.; Asselin, J.; Barbeau, J.; Boudreau, D.; Greener, J. A microfluidic platform with pH imaging for chemical and hydrodynamic stimulation of intact oral biofilms. *Lab Chip* **2016**, *16*, 1412–1419, doi:10.1039/c5lc01540e.
  104. Zhuang, J.; Carlsen, R. W.; Sitti, M. PH-taxis of biohybrid microsystems. *Sci. Rep.* **2015**, *5*, doi:10.1038/srep11403.
  105. Cao, J.; Nagl, S.; Kothe, E.; Köhler, J. M. Oxygen sensor nanoparticles for monitoring bacterial growth and characterization of dose-response functions in microfluidic screenings. *Microchim. Acta* **2015**, *182*, 385–394, doi:10.1007/s00604-014-1341-3.
  106. Kaushik, A. M.; Hsieha, K.; Chena, L.; Shina, D. J.; Liaob, J. C.; Wang, T.-H. Accelerating bacterial growth detection and antimicrobial susceptibility assessment in integrated picoliter droplet platform. *Biosens Bioelectron* **2017**, *97*, 260–266, doi:10.1016/j.physbeh.2017.03.040.
  107. Mahler, L.; Niehs, S.; Martin, K.; Weber, T.; Scherlach, K.; Agler-Rosenbaum, M.; Hertweck, C.; Roth, M. Highly parallelized microfluidic droplet cultivation and prioritization on antibiotic producers from complex natural microbial communities. **2019**, doi:10.1101/2019.12.18.877530.
  108. Takeuchi, S.; DiLuzio, W. R.; Weibel, D. B.; Whitesides, G. M. Controlling the Shape of Filamentous Cells of Escherichia Coli. *Nano Lett* **2005**, *5*, 1819–1823, doi:10.1038/jid.2014.371.
  109. Cho, H. J.; Jönsson, H.; Campbell, K.; Melke, P.; Williams, J. W.; Jedynek, B.; Stevens, A. M.; Groisman, A.; Levchenko, A. Self-organization in high-density bacterial colonies: Efficient crowd control. *PLoS Biol.* **2007**, *5*, 2614–2623, doi:10.1371/journal.pbio.0050302.
  110. Hyun, J. K.; Boedicker, J. Q.; Jang, W. C.; Ismagilov, R. F. Defined spatial structure stabilizes a synthetic multispecies bacterial community. *Proc. Natl. Acad. Sci. U. S. A.* **2008**, *105*, 18188–18193, doi:10.1073/pnas.0807935105.
  111. Li, H.; Torab, P.; Mach, K. E.; Surette, C.; England, M. R.; Craft, D. W.; Thomas, N. J.; Liao, J. C.; Puleo, C.; Wong, P. K. Adaptable microfluidic system for single-cell pathogen classification and antimicrobial susceptibility testing. *Proc. Natl. Acad. Sci. U. S. A.* **2019**, *116*, 10270–10279, doi:10.1073/pnas.1819569116.

112. Balaban, N. Q.; Merrin, J.; Chait, R.; Kowalik, L.; Leibler, S. Bacterial persistence as a phenotypic switch. *Science (80-. )* **2004**, *305*, 1622–1625, doi:10.1126/science.1099390.
113. Wang, P.; Robert, L.; Pelletier, J.; Dang, W. L.; Taddei, F.; Wright, A.; Jun, S. Robust growth of *Escherichia coli*. *Curr. Biol.* **2010**, *20*, 1099–1103, doi:10.1016/j.cub.2010.04.045.
114. Simmons, E. L.; Bond, M. C.; Koskella, B.; Drescher, K.; Bucci, V.; Nadella, C. D. Biofilm Structure Promotes Coexistence of Phage-Resistant and Phage-Susceptible Bacteria. *mSystems* **2020**, *5*, 1–17.
115. Kim, S.; Lee, S.; Kim, J. K.; Chung, H. J.; Jeon, J. S. Microfluidic-based observation of local bacterial density under antimicrobial concentration gradient for rapid antibiotic susceptibility testing. *Biomicrofluidics* **2019**, *13*, doi:10.1063/1.5066558.
116. Matsumoto, Y.; Sakakihara, S.; Grushnikov, A.; Kikuchi, K.; Noji, H.; Yamaguchi, A.; Iino, R.; Yagi, Y.; Nishino, K. A microfluidic channel method for rapid drug-susceptibility testing of *Pseudomonas aeruginosa*. *PLoS One* **2016**, *11*, 1–17, doi:10.1371/journal.pone.0148797.
117. Lambert, G.; Kussel, E. Memory and Fitness Optimization of Bacteria under Fluctuating Environments. *PLoS Genet.* **2014**, *10*, doi:10.1371/journal.pgen.1004556.
118. Aldridge, B. B.; Fernandez-Suarez, M.; Heller, D.; Ambravaneswaran, V.; Irimia, D.; Toner, M.; Fortune, S. M. Asymmetry and aging of mycobacterial cells lead to variable growth and antibiotic susceptibility. *Science (80-. )* **2012**, *335*, 100–104, doi:10.1126/science.1216166.
119. Chang, C. B.; Wilking, J. N.; Kim, S. H.; Shum, H. C.; Weitz, D. A. Monodisperse Emulsion Drop Microenvironments for Bacterial Biofilm Growth. *Small* **2015**, *11*, 3954–3961, doi:10.1002/smll.201403125.
120. Jin, Z.; Nie, M.; Hu, R.; Zhao, T.; Xu, J.; Chen, D.; Yun, J.; Ma, L. Z.; Du, W. Dynamic Sessile-Droplet Habitats for Controllable Cultivation of Bacterial Biofilm. *Small* **2018**, *14*, 1–8, doi:10.1002/smll.201800658.
121. White, A. R.; Jalali, M.; Sheng, J. A new ecology-on-a-chip microfluidic platform to study interactions of microbes with a rising oil droplet. *Sci. Rep.* **2019**, *9*, 1–11, doi:10.1038/s41598-019-50153-9.
122. Rath, H.; Stumpp, N.; Stiesch, M. Development of a flow chamber system for the reproducible in vitro analysis of biofilm formation on implant materials. *PLoS One* **2017**, 1–12, doi:10.5281/zenodo.259314.
123. Hansen, R. H.; Timm, A. C.; Timm, C. M.; Bible, A. N.; Morrell-Falvey, J. L.; Pelletier, D. A.; Simpson, M. L.; Doktycz, M. J.; Retterer, S. T. Stochastic assembly of bacteria in microwell arrays reveals the importance of confinement in community development. *PLoS One* **2016**, *11*, 1–18, doi:10.1371/journal.pone.0155080.
124. Aufrecht, J. A.; Fowlkes, J. D.; Bible, A. N.; Morrell-Falvey, J.; Doktycz, M. J.; Retterer, S. T. Pore-scale hydrodynamics influence the spatial evolution of bacterial biofilms in a microfluidic porous network. *PLoS One* **2019**, *14*, 1–17, doi:10.1371/journal.pone.0218316.
125. Kaminski, T. S.; Scheler, O.; Garstecki, P. Droplet microfluidics for microbiology: Techniques, applications and challenges. *Lab Chip* **2016**, *16*, 2168–2187, doi:10.1039/c6lc00367b.
126. Collins, D. J.; Neild, A.; deMello, A.; Liu, A. Q.; Ai, Y. The Poisson distribution and beyond: Methods for microfluidic droplet production and single cell encapsulation. *Lab Chip* **2015**, *15*, 3439–3459, doi:10.1039/c5lc00614g.
127. Adler, J. A method for measuring chemotaxis and use of the method to determine optimum conditions for chemotaxis by *Escherichia coli*. *J. Gen. Microbiol.* **1973**, *74*, 77–91, doi:10.1099/00221287-74-1-77.
128. Mesibov, R.; Adler, J. Chemotaxis toward amino acids in *Escherichia coli*. *J. Bacteriol.* **1972**, *112*, 315–326, doi:10.1128/jb.112.1.315-326.1972.
129. Wolfe, A. J.; Berg, H. C. Migration of bacteria in semisolid agar. *Proc. Natl. Acad. Sci. U. S. A.* **1989**, *86*, 6973–6977, doi:10.1073/pnas.86.18.6973.
130. Partridge, J. D.; Nhu, N. T. Q.; Dufour, Y. S.; Harshey, R. M. *Escherichia coli* remodels the chemotaxis pathway for swarming. *MBio* **2019**, *10*, 1–16, doi:10.1128/mBio.00316-19.
131. Bible, A. N.; Fletcher, S. J.; Pelletier, D. A.; Schadt, C. W.; Jawdy, S. S.; Weston, D. J.; Engle, N. L.; Tschaplinski, T.; Masyuko, R.; Polisetti, S.; Bohn, P. W.; Coutinho, T. A.; Doktycz, M. J.; Morrell-Falvey, J. L. A carotenoid-deficient mutant in *Pantoea* sp. YR343, a bacteria isolated from the Rhizosphere of *Populus deltoides*, is defective in root colonization. *Front. Microbiol.* **2016**, *7*, 1–15, doi:10.3389/fmicb.2016.00491.
132. Overmann, J.; Abt, B.; Sikorski, J. Present and Future of Culturing Bacteria. *Annu. Rev. Microbiol.* **2017**,

- 71, 711–730, doi:10.1146/annurev-micro-090816-093449.
133. Phillips, K. N.; Castillo, G.; Wünsche, A.; Cooper, T. F. Adaptation of *Escherichia coli* to glucose promotes evolvability in lactose. *Evolution (N. Y.)* **2016**, *70*, 465–470, doi:10.1111/evo.12849.
  134. Bauer, A. W.; Kirby, W. M. M.; Sherris, J. C.; Turck, M. Antibiotic susceptibility testing by a standardized single disk method. *Am. J. Clin. Pathol.* **1966**, *45*, 493–496, doi:10.1308/rscann.2013.95.7.532.
  135. Kibret, M.; Abera, B. Antimicrobial susceptibility patterns of *E. coli* from clinical sources in northeast Ethiopia. *Afr. Health Sci.* **2011**, *11*, doi:10.4314/ahs.v11i3.70069.
  136. van Meer, B. J.; de Vries, H.; Firth, K. S. A.; van Weerd, J.; Tertoolen, L. G. J.; Karperien, H. B. J.; Jonkheijm, P.; Denning, C.; IJzerman, A. P.; Mummery, C. L. Small molecule absorption by PDMS in the context of drug response bioassays. *Biochem. Biophys. Res. Commun.* **2017**, *482*, 323–328, doi:10.1016/j.bbrc.2016.11.062.
  137. Dangla, R.; Gallaire, F.; Baroud, C. N. Microchannel deformations due to solvent-induced PDMS swelling. *Lab Chip* **2010**, *10*, 2972–2978, doi:10.1039/c003504a.
  138. Shin, S.; Kim, N.; Hong, J. W. Comparison of Surface Modification Techniques on Polydimethylsiloxane to Prevent Protein Adsorption. *Biochip J.* **2018**, *12*, 123–127, doi:10.1007/s13206-017-2210-z.
  139. Gökaltun, A.; Kang, Y. B. (Abraham); Yarmush, M. L.; Usta, O. B.; Asatekin, A. Simple Surface Modification of Poly(dimethylsiloxane) via Surface Segregating Smart Polymers for Biomicrofluidics. *Sci. Rep.* **2019**, *9*, 1–14, doi:10.1038/s41598-019-43625-5.
  140. You, J. B.; Lee, B.; Choi, Y.; Lee, C. S.; Peter, M.; Im, S. G.; Lee, S. S. Nanoadhesive layer to prevent protein adsorption in a poly(dimethylsiloxane) microfluidic device. *Biotechniques* **2020**, *69*, 47–52, doi:10.2144/BTN-2020-0025.
  141. Subramanian, S.; Huiszoon, R. C.; Chu, S.; Bentley, W. E.; Ghodssi, R. Microsystems for biofilm characterization and sensing – A review. *Biofilm* **2020**, *2*, 100015, doi:10.1016/j.biofilm.2019.100015.
  142. Julich, S.; Hotzel, H.; Gärtner, C.; Trouchet, D.; Fawzy El Metwaly Ahmed, M.; Kemper, N.; Tomaso, H. Evaluation of a microfluidic chip system for preparation of bacterial DNA from swabs, air, and surface water samples. *Biologicals* **2016**, *44*, 574–580, doi:10.1016/j.biologicals.2016.06.013.
  143. Oblath, E. A.; Henley, W. H.; Alarie, J. P.; Ramsey, J. M. A microfluidic chip integrating DNA extraction and real-time PCR for the detection of bacteria in saliva. *Lab Chip* **2013**, *13*, 1325–1332, doi:10.1039/c3lc40961a.A.
  144. Schilling, E. A.; Kamholz, A. E.; Yager, P. Cell Lysis and Protein Extraction in a Microfluidic Device with Detection by a Fluorogenic Enzyme Assay. *Anal. Chem.* **2002**, *74*, 1798–1804.
  145. Hosokawa, M.; Nishikawa, Y.; Kogawa, M.; Takeyama, H. Massively parallel whole genome amplification for single-cell sequencing using droplet microfluidics. *Sci. Rep.* **2017**, *7*, 3–4, doi:10.1038/s41598-017-05436-4.
  146. Kim, H. J.; Ingber, D. E. Gut-on-a-Chip microenvironment induces human intestinal cells to undergo villus differentiation. *Integr. Biol. (United Kingdom)* **2013**, *5*, 1130–1140, doi:10.1039/c3ib40126j.
  147. Huh, D. A human breathing lung-on-a-chip. *Ann. Am. Thorac. Soc.* **2015**, *12*, S42–S44, doi:10.1513/AnnalsATS.201410-442MG.
  148. Ho, C. T.; Lin, R. Z.; Chang, W. Y.; Chang, H. Y.; Liu, C. H. Rapid heterogeneous liver-cell on-chip patterning via the enhanced field-induced dielectrophoresis trap. *Lab Chip* **2006**, *6*, 724–734, doi:10.1039/b602036d.
  149. Polacheck, W. J.; Kutys, M. L.; Tefft, J. B.; Chen, C. S. *Microfabricated blood vessels for modeling the vascular transport barrier*; Springer US, 2019; Vol. 14; ISBN 4159601901448.
  150. Bang, S.; Jeong, S.; Choi, N.; Kim, H. N. Brain-on-a-chip: A history of development and future perspective. *Biomicrofluidics* **2019**, *13*, doi:10.1063/1.5120555.
  151. Goutos, I.; Cogswell, L. K.; Giele, H. Extravasation injuries: A review. *J. Hand Surg. Eur. Vol.* **2014**, *39*, 808–818, doi:10.1177/1753193413511921.
  152. Reglero-Real, N.; García-Weber, D.; Millán, J. Cellular Barriers after Extravasation: Leukocyte Interactions with Polarized Epithelia in the Inflamed Tissue. *Mediators Inflamm.* **2016**, *2016*, doi:10.1155/2016/7650260.
  153. Gerhardt, T.; Ley, K. Monocyte trafficking across the vessel wall. *Cardiovasc. Res.* **2015**, *107*, 321–330, doi:10.1093/cvr/cvv147.

154. Wettschureck, N.; Strilic, B.; Offermanns, S. Passing the vascular barrier: Endothelial signaling processes controlling extravasation. *Physiol. Rev.* **2019**, *99*, 1467–1525, doi:10.1152/physrev.00037.2018.
155. Min, J.-K.; Kim, Y.-M.; Kim, S. W.; Kwon, M.-C.; Kong, Y.-Y.; Hwang, I. K.; Won, M. H.; Rho, J.; Kwon, Y.-G. TNF-Related Activation-Induced Cytokine Enhances Leukocyte Adhesiveness: Induction of ICAM-1 and VCAM-1 via TNF Receptor-Associated Factor and Protein Kinase C-Dependent NF- $\kappa$ B Activation in Endothelial Cells. *J. Immunol.* **2005**, *175*, 531–540, doi:10.4049/jimmunol.175.1.531.
156. Hsu, W. Y.; Chao, Y. W.; Tsai, Y. L.; Lien, C. C.; Chang, C. F.; Deng, M. C.; Ho, L. T.; Kwok, C. F.; Juan, C. C. Resistin induces monocyte-endothelial cell adhesion by increasing ICAM-1 and VCAM-1 expression in endothelial cells via p38MAPK-dependent pathway. *J. Cell. Physiol.* **2011**, *226*, 2181–2188, doi:10.1002/jcp.22555.
157. Schmitz, B.; Vischer, P.; Brand, E.; Schmidt-Petersen, K.; Korb-Pap, A.; Guske, K.; Nedele, J.; Schellekes, M.; Hillen, J.; Rötrige, A.; Simmet, T.; Paul, M.; Cambien, F.; Brand, S. M. Increased monocyte adhesion by endothelial expression of VCAM-1 missense variation invitro. *Atherosclerosis* **2013**, *230*, 185–190, doi:10.1016/j.atherosclerosis.2013.07.039.
158. León, B.; Ardavín, C. Monocyte migration to inflamed skin and lymph nodes is differentially controlled by L-selectin and PSGL-1. *Blood* **2008**, *111*, 3126–3130, doi:10.1182/blood-2007-07-100610.
159. Dudek, S. M.; Garcia, J. G. N. Cytoskeletal regulation of pulmonary vascular permeability. *J. Appl. Physiol.* **2001**, *91*, 1487–1500, doi:10.1016/j.envpol.2004.10.021.
160. Voisin, M. B.; Woodfin, A.; Nourshargh, S. Monocytes and neutrophils exhibit both distinct and common mechanisms in penetrating the vascular basement membrane in vivo. *Arterioscler. Thromb. Vasc. Biol.* **2009**, *29*, 1193–1199, doi:10.1161/ATVBAHA.109.187450.
161. Schenkel, A. R.; Mamdouh, Z.; Muller, W. A. Locomotion of monocytes on endothelium is a critical step during extravasation. *Nat. Immunol.* **2004**, *5*, 393–400, doi:10.1038/ni1051.
162. Rutledge, N. S.; Muller, W. A. Understanding Molecules that Mediate Leukocyte Extravasation. *Curr. Pathobiol. Rep.* **2020**, *8*, 25–35, doi:10.1007/s40139-020-00207-9.
163. Burns, M. P.; DePaola, N. Flow-conditioned HUVECs support clustered leukocyte adhesion by coexpressing ICAM-1 and E-selectin. *Am. J. Physiol. - Hear. Circ. Physiol.* **2005**, *288*, 194–204, doi:10.1152/ajpheart.01078.2003.
164. Chappell, D. C.; Varner, S. E.; Nerem, R. M.; Medford, R. M.; Alexander, R. W. Expression in Cultured Human Endothelium. *Circ. Res.* **1998**, *82*, 532–539.
165. Gonzales, R. S.; Ph.D., T. M. W. Hemodynamic modulation of monocytic cell adherence to vascular endothelium. *Ann. Biomed. Eng.* **1996**, *24*, 382–393.
166. Tzima, E.; Angel, M.; Pozo, D.; Kiosses, W. B.; Mohamed, S. A.; Li, S.; Chien, S.; Schwartz, M. A. Activation of Rac1 by shear stress in endothelial cells mediates both cytoskeletal reorganization and effects on gene expression. *EMBO J.* **2002**, *21*, 6791–6800.
167. Polacheck, W. J.; Kutys, M. L.; Tefft, J. B.; Chen, C. S. *Microfabricated blood vessels for modeling the vascular transport barrier*; Springer US, 2019; Vol. 14; ISBN 4159601901448.
168. Polacheck, W. J.; Kutys, M. L.; Yang, J.; Eyckmans, J.; Wu, Y.; Vasavada, H.; Hirschi, K. K.; Chen, C. S. A non-canonical Notch complex regulates adherens junctions and vascular barrier function. *Nature* **2017**, *552*, 258–262, doi:10.1038/nature24998.
169. Humphrey, J. D.; Dufresne, E. R.; Schwartz, M. A. Mechanotransduction and extracellular matrix homeostasis. *Nat Rev Mol Cell Biol.* **2014**, *15*, 802–812, doi:10.1038/nrm3896.
170. Mammoto, A.; Mammoto, T.; Kanopathipillai, M.; Yung, C. W.; Jiang, E.; Jiang, A.; Lofgren, K.; Gee, E. P. S.; Ingber, D. E. Control of lung vascular permeability and endotoxin-induced pulmonary oedema by changes in extracellular matrix mechanics. *Nat. Commun.* **2013**, *4*, doi:10.1038/ncomms2774.
171. MacKaya, J. L.; Hammer, D. A. Stiff substrates enhance monocytic cell capture through Eselectin but not P-selectin. *Integr Biol* **2016**, *8*, 62–72, doi:10.1039/c5ib00199d.
172. Schimmel, L.; van der Stoel, M.; Rianna, C.; van Stalborch, A. M.; de Ligt, A.; Hoogenboezem, M.; Tol, S.; van Rijssel, J.; Szulcek, R.; Bogaard, H. J.; Hofmann, P.; Boon, R.; Radmacher, M.; de Waard, V.; Huvneers, S.; van Buul, J. D. Stiffness-Induced Endothelial DLC-1 Expression Forces Leukocyte Spreading through Stabilization of the ICAM-1 Adhesome. *Cell Rep.* **2018**, *24*, 3115–3124, doi:10.1016/j.celrep.2018.08.045.

173. Dzenko, K. A.; Andjelkovic, A. V.; Kuziel, W. A.; Pachter, J. S. The chemokine receptor CCR2 mediates the binding and internalization of monocyte chemoattractant protein-1 along brain microvessels. *J. Neurosci.* **2001**, *21*, 9214–9223, doi:10.1523/jneurosci.21-23-09214.2001.
174. Gerszten, R. E.; Garcia-Zepeda, E. A.; Lim, Y. C.; Yoshida, M.; Ding, H. A.; Gimbrone, M. A.; Luster, A. D.; Lusinskas, F. W.; Rosenzweig, A. MCP-1 and IL-8 trigger firm adhesion of monocytes to vascular endothelium under flow conditions. *Nature* **1999**, *398*, 718–725, doi:10.1038/19546.
175. Sawa, Y.; Tsuruga, E. The expression of E-selectin and chemokines in the cultured human lymphatic endothelium with lipopolysaccharides. *J. Anat.* **2008**, *212*, 654–663, doi:10.1111/j.1469-7580.2008.00892.x.
176. Brown, Z.; Gerritsen, M. E.; Carley, W. W.; Strieter, R. M.; Kunkel, S. L.; Westwick, J. Chemokine gene expression and secretion by cytokine-activated human microvascular endothelial cells: Differential regulation of monocyte chemoattractant protein-1 and interleukin-8 in response to interferon- $\gamma$ . *Am. J. Pathol.* **1994**, *145*, 913–921.
177. Rollins, B. J.; Pober, J. S. Interleukin-4 induces the synthesis and secretion of MCP-1/JE by human endothelial cells. *Am. J. Pathol.* **1991**, *138*, 1315–1319.
178. Middleton, J.; Neil, S.; Wintle, J.; Clark-Lewis, I.; Moore, H.; Charles, L.; Auer, M.; Elin, H.; Antal, R. Transcytosis and surface presentation of IL-8 by venular endothelial cells. *Cell* **1997**, *91*, 385–395, doi:10.1016/S0092-8674(00)80422-5.
179. Muller, W. A. Mechanisms of Leukocyte Transendothelial Migration. *Annu Rev Pathol* **2011**, *6*, 323–344, doi:10.1161/CIRCULATIONAHA.110.956839.
180. Middleton, J.; Patterson, A. M.; Gardner, L.; Schmutz, C.; Ashton, B. A. Leukocyte extravasation: Chemokine transport and presentation by the endothelium. *Blood* **2002**, *100*, 3853–3860, doi:10.1182/blood.V100.12.3853.
181. Escribano, J.; Chen, M. B.; Moeendarbary, E.; Cao, X.; Shenoy, V.; Garcia-Aznar, J. M.; Kamm, R. D.; Spill, F. Balance of mechanical forces drives endothelial gap formation and may facilitate cancer and immune-cell extravasation. *PLoS Comput. Biol.* **2019**, *15*, 1–21, doi:10.1371/journal.pcbi.1006395.
182. Doherty, E. L.; Aw, W. Y.; Hickey, A. J.; Polacheck, W. J. Microfluidic and Organ-on-a-Chip Approaches to Investigate Cellular and Microenvironmental Contributions to Cardiovascular Function and Pathology. *Front. Bioeng. Biotechnol.* **2021**, *9*, 1–14, doi:10.3389/fbioe.2021.624435.
183. Molteni, R.; Bianchi, E.; Patete, P.; Fabbri, M.; Baroni, G.; Dubini, G.; Pardi, R. A novel device to concurrently assess leukocyte extravasation and interstitial migration within a defined 3D environment. *Lab Chip* **2015**, *15*, 195–207, doi:10.1039/c4lc00741g.
184. Bersini, S.; Jeon, J. S.; Moretti, M.; Kamm, R. D. In vitro models of the metastatic cascade: from local invasion to extravasation. *Drug Discov Today*. **2014**, *19*, 735–742, doi:10.1038/jid.2014.371.
185. Song, H. K.; Hwang, D. Y. Use of C57BL/6N mice on the variety of immunological researches. *Lab. Anim. Res.* **2017**, *33*, 119–123, doi:10.5625/lar.2017.33.2.119.
186. Muller, W. A. Getting Leukocytes to the Site of Inflammation. *Vet Pathol* **2013**, *50*, 7–22, doi:10.1038/jid.2014.371.
187. Gale, B. K.; Jafek, A. R.; Lambert, C. J.; Goenner, B. L.; Moghimifam, H.; Nze, U. C.; Kamarapu, S. K. A review of current methods in microfluidic device fabrication and future commercialization prospects. *Inventions* **2018**, *3*, doi:10.3390/inventions3030060.
188. Xu, H.; Li, Z.; Yu, Y.; Sizardkhani, S.; Ho, W. S.; Yin, F.; Wang, L.; Zhu, G.; Zhang, M.; Jiang, L.; Zhuang, Z.; Qin, J. A dynamic in vivo-like organotypic blood-brain barrier model to probe metastatic brain tumors. *Sci. Rep.* **2016**, *6*, 1–12, doi:10.1038/srep36670.
189. Jeon, J. S.; Bersini, S.; Gilardi, M.; Dubini, G.; Charest, J. L.; Moretti, M.; Kamm, R. D. Human 3D vascularized organotypic microfluidic assays to study breast cancer cell extravasation. *Proc. Natl. Acad. Sci. U. S. A.* **2015**, *112*, 214–219, doi:10.1073/pnas.1417115112.
190. Bersini, S.; Jeon, J. S.; Dubini, G.; Arrigoni, C.; Chung, S.; Charest, J. L.; Moretti, M.; Kamm, R. D. A microfluidic 3D invitro model for specificity of breast cancer metastasis to bone. *Biomaterials* **2014**, *35*, 2454–2461, doi:10.1016/j.biomaterials.2013.11.050.
191. Ma, Y.-H. V.; Middleton, K.; You, L.; Sun, Y. A review of microfluidic approaches for investigating cancer extravasation during metastasis. *Microsystems Nanoeng.* **2018**, *4*, doi:10.1038/micronano.2017.104.
192. Kühnbach, C.; da Luz, S.; Baganz, F.; Hass, V. C.; Mueller, M. M. A microfluidic system for the

- investigation of tumor cell extravasation. *Bioengineering* **2018**, *5*, doi:10.3390/bioengineering5020040.
193. Bianchi, E.; Molteni, R.; Pardi, R.; Dubini, G. Microfluidics for in vitro biomimetic shear stress-dependent leukocyte adhesion assays. *J. Biomech.* **2013**, *46*, 276–283, doi:10.1016/j.jbiomech.2012.10.024.
  194. Bersini, S.; Miermont, A.; Pavesi, A.; Kamm, R. D.; Thiery, J. P.; Moretti, M.; Adriani, G. A combined microfluidic-transcriptomic approach to characterize the extravasation potential of cancer cells. *Oncotarget* **2018**, *9*, 36110–36125, doi:10.18632/oncotarget.26306.
  195. Frantz, C.; Stewart, K. M.; Weaver, V. M. The extracellular matrix at a glance. *J. Cell Sci.* **2010**, *123*, 4195–4200, doi:10.1242/jcs.023820.
  196. Jones, C. M.; Baker-Groberg, S. M.; Cianchetti, F. A.; Glynn, J. J.; Healy, L. D.; Lam, W. Y.; Nelson, J. W.; Parrish, D. C.; Phillips, K. G.; Scott-Drechsel, D. E.; Tagge, I. J.; Zelaya, J. E.; Hinds, M. T.; McCarty, O. J. T. Measurement science in the circulatory system. *Cell. Mol. Bioeng.* **2014**, *7*, 1–14, doi:10.1007/s12195-013-0317-4.
  197. Ricci, S. Anatomy. In *Sclerotherapy*; 2017; pp. 1–16.
  198. Daniel Harris, BA, Lynn McNicoll, MD, Gary Epstein-Lubow, MD, and Kali S. Thomas, P. Vessel sampling and blood flow velocity distribution with vessel diameter for characterizing the human bulbar conjunctival microvasculature. *Physiol. Behav.* **2017**, *176*, 139–148, doi:10.1016/j.physbeh.2017.03.040.
  199. Park, S. E.; Georgescu, A.; Oh, J. M.; Kwon, K. W.; Huh, D. Polydopamine-Based Interfacial Engineering of Extracellular Matrix Hydrogels for the Construction and Long-Term Maintenance of Living Three-Dimensional Tissues. *ACS Appl. Mater. Interfaces* **2019**, *11*, 23919–23925, doi:10.1021/acsami.9b07912.
  200. Schindelin, J.; Arganda-Carrera, I.; Frise, E.; Verena, K.; Mark, L.; Tobias, P.; Stephan, P.; Curtis, R.; Stephan, S.; Benjamin, S.; Jean-Yves, T.; Daniel, J. W.; Volker, H.; Kevin, E.; Pavel, T.; Albert, C. Fiji - an Open platform for biological image analysis. *Nat. Methods* **2019**, *9*, doi:10.1038/nmeth.2019.Fiji.
  201. Liu, P. Y.; Chin, L. K.; Ser, W.; Chen, H. F.; Hsieh, C. M.; Lee, C. H.; Sung, K. B.; Ayi, T. C.; Yap, P. H.; Liedberg, B.; Wang, K.; Bourouina, T.; Leprince-Wang, Y. Cell refractive index for cell biology and disease diagnosis: Past, present and future. *Lab Chip* **2016**, *16*, 634–644, doi:10.1039/c5lc01445j.
  202. Dannhauser, D.; Rossi, D.; Memmolo, P.; Finizio, A.; Ferraro, P.; Netti, P. A.; Causa, F. Biophysical investigation of living monocytes in flow by collaborative coherent imaging techniques. *Biomed. Opt. Express* **2018**, *9*, 5194, doi:10.1364/boe.9.005194.
  203. Movilla, N.; Borau, C.; Valero, C.; García-Aznar, J. Degradation of extracellular matrix regulates osteoblast migration: A microfluidic-based study. *Bone* **2017**, *107*, 10–17, doi:10.1016/j.bone.2017.10.025.
  204. Sander, E. A.; Barocas, V. H. Comparison of 2D fiber network orientation measurement methods. *J. Biomed. Mater. Res.* **2008**, *88A*, 322–331.
  205. Tzima, E.; Irani-Tehrani, M.; Kiosses, W. B.; Dejana, E.; Schultz, D. A.; Engelhardt, B.; Cao, G.; DeLisser, H.; Schwartz, M. A. A mechanosensory complex that mediates the endothelial cell response to fluid shear stress. *Nature* **2005**, *437*, 426–31.
  206. Vestweber, D. VE-cadherin: The major endothelial adhesion molecule controlling cellular junctions and blood vessel formation. *Arterioscler. Thromb. Vasc. Biol.* **2008**, *28*, 223–232, doi:10.1161/ATVBAHA.107.158014.
  207. Harris, E. S.; Nelson, W. J. VE-Cadherin: At the Front, Center, and Sides of Endothelial Cell Organization and Function. *Curr Opin Cell Biol* **2010**, *2*, 651–658, doi:10.1016/j.ceb.2010.07.006.VE-Cadherin.
  208. Frost, T. S.; Jiang, L.; Lynch, R. M.; Zohar, Y. Permeability of epithelial/endothelial barriers in transwells and microfluidic bilayer devices. *Micromachines* **2019**, *10*, doi:10.3390/mi10080533.
  209. Rabodzey, A.; Yao, Y.; Luscinikas, F.; Shaw, S.; Dewey, C. F. Early response of endothelial cells to flow is mediated by VE-Cadherin. *Cell Commun. Adhes.* **2007**, *14*, 195–209, doi:10.1080/15419060701755792.
  210. Citi, S. The mechanobiology of tight junctions. *Biophys. Rev.* **2019**, *11*, 783–793, doi:10.1007/s12551-019-00582-7.
  211. Wallez, Y.; Huber, P. Endothelial adherens and tight junctions in vascular homeostasis, inflammation



- and angiogenesis. *Biochim. Biophys. Acta - Biomembr.* **2008**, *1778*, 794–809, doi:10.1016/j.bbamem.2007.09.003.
212. Boussommier-Calleja, A.; Atiyas, Y.; Haase, K.; Headley, M.; Lewis, C.; Kamm, R. The effects of monocytes on tumor cell extravasation in a 3D vascularized microfluidic model. *Biomaterials*. **2019**, *198*, 180–193, doi:10.1016/j.biomaterials.2018.03.005.The.
  213. Moreno-Arotzena, O.; Meier, J.; del Amo, C.; García-Aznar, J. Characterization of Fibrin and Collagen Gels for Engineering Wound Healing Models. *Materials (Basel)*. **2015**, *8*, 1636–1651, doi:10.3390/ma8041636.
  214. Moreno-Arotzena, O.; Borau, C.; Movilla, N.; Vicente-Manzanares, M.; García-Aznar, J. Fibroblast Migration in 3D is Controlled by Haptotaxis in a Non-muscle Myosin II-Dependent Manner. *Ann. Biomed. Eng.* **2015**, *43*, 3025–3039, doi:10.1007/s10439-015-1343-2.
  215. Kutys, M. L.; Chen, C. S. Forces and mechanotransduction in 3D vascular biology. *Curr. Opin. Cell Biol.* **2016**, *42*, 73–79, doi:10.1016/j.ceb.2016.04.011.
  216. Huynh, J.; Nishimura, N.; Rana, K.; Peloquin, J. M.; Califano, J. P.; Montague, C. R.; King, M. R.; Schaffer, C. B.; Reinhart-King, C. A. Age-related intimal stiffening enhances endothelial permeability and leukocyte transmigration. *Sci. Transl. Med.* **2011**, *3*, doi:10.1126/scitranslmed.3002761.
  217. Valero, C.; Amaveda, H.; Mora, M.; García-Aznar, J. M. Combined experimental and computational characterization of crosslinked collagen-based hydrogels. *PLoS One* **2018**, *13*, 1–16, doi:10.1371/journal.pone.0195820.
  218. Olivares, V.; Córdor, M.; Del Amo, C.; Asín, J.; Borau, C.; García-Aznar, J. M. Image-based characterization of 3d collagen networks and the effect of embedded cells. *Microsc. Microanal.* **2019**, *25*, 971–981, doi:10.1017/S1431927619014570.
  219. Nguyen, D. H. T.; Stapleton, S. C.; Yang, M. T.; Cha, S. S.; Choi, C. K.; Galie, P. A.; Chen, C. S. Biomimetic model to reconstitute angiogenic sprouting morphogenesis in vitro. *Proc. Natl. Acad. Sci. U. S. A.* **2013**, *110*, 6712–6717, doi:10.1073/pnas.1221526110.
  220. Trappmann, B.; Baker, B. M.; Polacheck, W. J.; Choi, C. K.; Burdick, J. A.; Chen, C. S. Matrix degradability controls multicellularity of 3D cell migration. *Nat. Commun.* **2017**, *8*, 1–8, doi:10.1038/s41467-017-00418-6.
  221. Gong, M. M.; Lugo-Cintrón, K. M.; White, B. R.; Kerr, S. C.; Harari, P. M.; Beebe, D. J. Human organotypic lymphatic vessel model elucidates microenvironment-dependent signaling and barrier function. *Biomaterials* **2019**, *214*, doi:10.1016/j.biomaterials.2019.119225.Human.
  222. Virumbrales-Muñoz, M.; Ayuso, J. M.; Gong, M. M.; Humayun, M.; Livingston, M. K.; Lugo-Cintrón, K. M.; McMinn, P.; Álvarez-García, Y. R.; Beebe, D. J. Microfluidic lumen-based systems for advancing tubular organ modeling. *Chem. Soc. Rev.* **2020**, *49*, 6402–6442, doi:10.1039/d0cs00705f.
  223. Kreuger, J.; Phillipson, M. Targeting vascular and leukocyte communication in angiogenesis, inflammation and fibrosis. *Nat. Rev. Drug Discov.* **2016**, *15*, 125–142, doi:10.1038/nrd.2015.2.
  224. Baxter, E. W.; Graham, A. E.; Re, N. A.; Carr, I. M.; Robinson, J. I.; Mackie, S. L.; Morgan, A. W. Standardized protocols for differentiation of THP-1 cells to macrophages with distinct M(IFN $\gamma$ +LPS), M(IL-4) and M(IL-10) phenotypes. *J. Immunol. Methods* **2020**, *478*, doi:10.1016/j.jim.2019.112721.
  225. Bah, A.; Vergne, I. Macrophage autophagy and bacterial infections. *Front. Immunol.* **2017**, *8*, 1–9, doi:10.3389/fimmu.2017.01483.
  226. Kutys, M. L.; Polacheck, W. J.; Welch, M. K.; Gagnon, K. A.; Koorman, T.; Kim, S.; Li, L.; McClatchey, A. I.; Chen, C. S. Uncovering mutation-specific morphogenic phenotypes and paracrine-mediated vessel dysfunction in a biomimetic vascularized mammary duct platform. *Nat. Commun.* **2020**, *11*, doi:10.1038/s41467-020-17102-x.
  227. Jalili-Firoozinezhad, S.; Gazzaniga, F. S.; Calamari, E. L.; Camacho, D. M.; Fadel, C. W.; Bein, A.; Swenor, B.; Nestor, B.; Cronce, M. J.; Tovaglieri, A.; Levy, O.; Gregory, K. E.; Breault, D. T.; Cabral, J. M. S.; Kasper, D. L.; Novak, R.; Ingber, D. E. A complex human gut microbiome cultured in an anaerobic intestine-on-a-chip. *Nat. Biomed. Eng.* **2019**, *3*, 520–531, doi:10.1038/s41551-019-0397-0.
  228. Ley, K.; Pramod, A. B.; Croft, M.; Ravichandran, K. S.; Ting, J. P. How mouse macrophages sense what is going on. *Front. Immunol.* **2016**, *7*, 1–17, doi:10.3389/fimmu.2016.00204.
  229. Underhill, D. M.; Ozinsky, A. Phagocytosis of microbes: Complexity in action. *Annu. Rev. Immunol.* **2002**, *20*, 825–852, doi:10.1146/annurev.immunol.20.103001.114744.

230. Pérez-Rodríguez, S.; Tomás-González, E.; García-Aznar, J. M. *3D cell migration studies for chemotaxis on microfluidic-based chips: a comparison between cardiac and dermal fibroblasts*; 2018;
231. Hoiseth, S. K.; Stocker, B. A. D. Aromatic-dependent Salmonella typhimurium are non-virulent and effective as live vaccines. *Nature* 1981, *291*, 238–239.
232. Cole, S. T.; Brosch, R.; Parkhill, J.; Garnier, T.; Churcher, C.; Harris, D.; Gordon, S. V.; Eiglmeier, K.; Gas, S.; Barry, C. E.; Tekaiia, F.; Badcock, K.; Basham, D.; Brown, D.; Chillingworth, T.; Connor, R.; Davies, R.; Devlin, K.; Feltwell, T.; Gentles, S.; Hamlin, N.; Holroyd, S.; Hornsby, T.; Jagels, K.; Krogh, A.; McLean, J.; Moule, S.; Murphy, L.; Oliver, K.; Osborne, J.; Quail, M. A.; Rajahdram, M. A.; Rogers, J.; Rutter, S.; Seeger, K.; Skelton, J.; Squares, R.; Squares, S.; Sulsten, J. E.; Taylor, K.; Whitehead, S.; Bartell, B. G. Deciphering the biology of Mycobacterium tuberculosis from the complete genome sequence. *Nature* 1998, *396*, 537–544, doi:10.1038/24206.
233. Snapper, S. B.; Melton, R. E.; Mustafa, S.; Kieser, T.; Jr, W. R. J. Isolation and characterization of efficient plasmid transformation mutants of Mycobacterium smegmatis. *Mol. Microbiol.* 1990, *4*, 1911–1919, doi:10.1111/j.1365-2958.1990.tb02040.x.
234. Frantz, C.; Stewart, K.; Weaver, V. The extracellular matrix at a glance. *J Cell Sci* 2010, *123*, 4195–4200, doi:10.1242/jcs.023820.
235. Duval, K.; Grover, H.; Han, L. H.; Mou, Y.; Pegoraro, A. F.; Fredberg, J.; Chen, Z. Modeling physiological events in 2D vs. 3D cell culture. *Physiology* 2017, *32*, 266–277, doi:10.1152/physiol.00036.2016.
236. Pérez-Rodríguez, S.; Huang, S. A.; Borau, C.; García-Aznar, J. M.; Polacheck, W. J. Microfluidic model of monocyte extravasation reveals the role of hemodynamics and subendothelial matrix mechanics in regulating endothelial integrity. *Biomicrofluidics* 2021, *15*, 054102, doi:10.1063/5.0061997.
237. Woringer, M.; Izeddin, I.; Favard, C.; Berry, H. Anomalous Subdiffusion in Living Cells: Bridging the Gap Between Experiments and Realistic Models Through Collaborative Challenges. *Front. Phys.* 2020, *8*, 1–9, doi:10.3389/fphy.2020.00134.
238. van den Bos, E.; Walbaum, S.; Horsthemke, M.; Bachg, A. C.; Hanley, P. J. Time-lapse imaging of mouse macrophage chemotaxis. *J. Vis. Exp.* 2020, 2020, doi:10.3791/60750.
239. Nguyen-Chi, M.; Laplace-Builhe, B.; Travnickova, J.; Luz-Crawford, P.; Tejedor, G.; Phan, Q. T.; Duroux-Richard, I.; Levraud, J. P.; Kissa, K.; Lutfalla, G.; Jorgensen, C.; Djouad, F. Identification of polarized macrophage subsets in zebrafish. *Elife* 2015, *4*, 1–14, doi:10.7554/eLife.07288.
240. Grabher, C.; Cliffe, A.; Miura, K.; Hayflick, J.; Pepperkok, R.; Rørth, P.; Wittbrodt, J. Birth and life of tissue macrophages and their migration in embryogenesis and inflammation in medaka. *J. Leukoc. Biol.* 2007, *81*, 263–271, doi:10.1189/jlb.0806526.
241. GAO, W. J.; LIU, J. X.; LIU, M. N.; YAO, Y. Da; LIU, Z. Q.; LIU, L.; HE, H. H.; ZHOU, H. Macrophage 3D migration: A potential therapeutic target for inflammation and deleterious progression in diseases. *Pharmacol. Res.* 2021, *167*, 105563, doi:10.1016/j.phrs.2021.105563.
242. SenGupta, S.; Parent, C. A.; Bear, J. E. The principles of directed cell migration. *Nat. Rev. Mol. Cell Biol.* 2021, *22*, 529–547, doi:10.1038/s41580-021-00366-6.
243. Del Amo, C.; Borau, C.; Movilla, N.; Asín, J.; García-Aznar, J. Quantifying 3D chemotaxis in microfluidic-based chips with step gradients of collagen hydrogel concentrations. *Integr. Biol.* 2017, *9*, 339–349, doi:10.1039/c7ib00022g.
244. Dianqing, W. U. Signaling Mechanisms for Regulation of Chemotaxis. *Cell Res.* 2005, *15*, 52–56.
245. Moreno-Arotzena, O.; Mendoza, G.; Córdor, M.; Rüberg, T.; García-Aznar, J. M. Inducing chemotactic and haptotactic cues in microfluidic devices for three-dimensional in vitro assays. *Biomicrofluidics* 2014, *8*, 1–15, doi:10.1063/1.4903948.
246. Stuart Hogg *Essential microbiology*; 2005;
247. Poon, C. Measuring the density and viscosity of culture media for optimized computational fluid dynamics analysis of in vitro devices. *bioRxiv* 2020, 2020.08.25.266221, doi:10.1101/2020.08.25.266221.
248. Chao, Y.; Zhang, T. Optimization of fixation methods for observation of bacterial cell morphology and surface ultrastructures by atomic force microscopy. *Appl. Microbiol. Biotechnol.* 2011, *92*, 381–392, doi:10.1007/s00253-011-3551-5.
249. Smelt, J. P. P. M.; Brul, S. Thermal Inactivation of Microorganisms. *Crit. Rev. Food Sci. Nutr.* 2014, *54*, 1371–1385, doi:10.1080/10408398.2011.637645.

250. Agbor, T. A.; McCormick, B. A. Salmonella effectors: Important players modulating host cell function during infection. *Cell. Microbiol.* **2011**, *13*, 1858–1869, doi:10.1111/j.1462-5822.2011.01701.x.
251. Zhao, Y.; Yang, J.; Shi, J.; Gong, Y. N.; Lu, Q.; Xu, H.; Liu, L.; Shao, F. The NLRC4 inflammasome receptors for bacterial flagellin and type III secretion apparatus. *Nature* **2011**, *477*, 596–602, doi:10.1038/nature10510.
252. Worley, M. J.; Nieman, G. S.; Geddes, K.; Heffron, F. Salmonella typhimurium disseminates within its host by manipulating the motility of infected cells. *Proc. Natl. Acad. Sci. U. S. A.* **2006**, *103*, 17915–17920, doi:10.1073/pnas.0604054103.
253. Lou, L.; Zhang, P.; Piao, R.; Wang, Y. Salmonella Pathogenicity Island 1 (SPI-1) and Its Complex Regulatory Network. *Front. Cell. Infect. Microbiol.* **2019**, *9*, 1–12, doi:10.3389/fcimb.2019.00270.
254. Maa, M. C.; Leu, T. H. Activation of Toll-like receptors induces macrophage migration via the iNOS/Src/FAK pathway. *BioMedicine* **2011**, *1*, 11–15, doi:10.1016/j.biomed.2011.10.002.
255. Pérez-Toledo, M.; Valero-Pacheco, N.; Pastelin-Palacios, R.; Gil-Cruz, C.; Perez-Shibayama, C.; Moreno-Eutimio, M. A.; Becker, I.; Pérez-Tapia, S. M.; Arriaga-Pizano, L.; Cunningham, A. F.; Isibasi, A.; Bonifaz, L. C.; López-Macías, C. Salmonella typhi porins OmpC and OmpF are potent adjuvants for T-dependent and T-independent antigens. *Front. Immunol.* **2017**, *8*, 1–10, doi:10.3389/fimmu.2017.00230.
256. Ipinza, F.; Collao, B.; Monsalva, D.; Bustamante, V. H.; Luraschi, R.; Alegría-Arcos, M.; Almonacid, D. E.; Aguayo, D.; Calderón, I. L.; Gil, F.; Santiviago, C. A.; Morales, E. H.; Calva, E.; Saavedra, C. P. Participation of the Salmonella OmpD porin in the infection of RAW264.7 macrophages and BALB/c mice. *PLoS One* **2014**, *9*, doi:10.1371/journal.pone.0111062.
257. Simeone, R.; Bottai, D.; Frigui, W.; Majlessi, L.; Brosch, R. ESX/type VII secretion systems of mycobacteria: Insights into evolution, pathogenicity and protection. *Tuberculosis* **2015**, *95*, S150–S154, doi:10.1016/j.tube.2015.02.019.
258. Lewis, K. N.; Liao, R.; Guinn, K. M.; Hickey, M. J.; Smith, S.; Behr, A.; Sherman, D. R. Deletion of RD1 from Mycobacterium tuberculosis Mimics Bacille Calmette-Guérin Attenuation. *J Infect Dis.* **2003**, *187*, 117–123.
259. Copin, R.; Coscollá, M.; Efstathiadis, E.; Gagneux, S.; Ernst, J. D. Impact of in vitro evolution on antigenic diversity of Mycobacterium bovis bacillus Calmette-Guérin (BCG). *Vaccine.* **2014**, *32*, 5998–6004, doi:10.1016/j.vaccine.2014.07.113.Impact.
260. Davis, J. M.; Ramakrishnan, L. The Role of the Granuloma in Expansion and Dissemination of Early Tuberculous Infection. *Cell* **2009**, *136*, 37–49, doi:10.1016/j.cell.2008.11.014.
261. Khademi, F.; Tafaghodi, M. Immunogenicity of ESX Family Antigens of Mycobacterium Tuberculosis : An Overview. *Austin Clin. Microbiol.* **2016**, *1*, 1–5.
262. Guo, Q.; Bi, J.; Li, M.; Ge, W.; Xu, Y.; Fan, W.; Wang, H.; Zhang, X. ESX secretion-associated protein C from mycobacterium tuberculosis induces macrophage activation through the toll-like receptor-4/mitogen-activated protein kinase signaling pathway. *Front. Cell. Infect. Microbiol.* **2019**, *9*, 1–14, doi:10.3389/fcimb.2019.00158.
263. Qian, J.; Chen, R.; Wang, H.; Zhang, X. Role of the PE/PPE Family in Host–Pathogen Interactions and Prospects for Anti-Tuberculosis Vaccine and Diagnostic Tool Design. *Front. Cell. Infect. Microbiol.* **2020**, *10*, 1–8, doi:10.3389/fcimb.2020.594288.
264. Karbalaee Zadeh Babaki, M.; Soleimanpour, S.; Rezaee, S. A. Antigen 85 complex as a powerful Mycobacterium tuberculosis immunogene: Biology, immune-pathogenicity, applications in diagnosis, and vaccine design. *Microb. Pathog.* **2017**, *112*, 20–29, doi:10.1016/j.micpath.2017.08.040.
265. Means, T. K.; Wang, S.; Lien, E.; Yoshimura, A.; Golenbock, D. T.; Fenton, M. J. Human toll-like receptors mediate cellular activation by Mycobacterium tuberculosis. *J. Immunol.* **1999**, *163*, 3920–7.
266. Cambier, C. J.; Takaki, K. K.; Larson, R. P.; Hernandez, R. E.; Tobin, D. M.; Urdahl, K. B.; Cosma, C. L.; Ramakrishnan, L. Mycobacteria manipulate macrophage recruitment through coordinated use of membrane lipids. *Nature* **2014**, *505*, 218–222, doi:10.1038/nature12799.
267. Doz, E.; Rose, S.; Court, N.; Front, S.; Vasseur, V.; Charron, S.; Gilleron, M.; Puzo, G.; Fremaux, I.; Delneste, Y.; Erard, F.; Ryffel, B.; Martin, O. R.; Quesniaux, V. F. J. Mycobacterial phosphatidylinositol mannosides negatively regulate host toll-like receptor 4, MyD88-dependent proinflammatory cytokines, and TRIF-dependent co-stimulatory molecule expression. *J. Biol. Chem.* **2009**, *284*, 23187–23196, doi:10.1074/jbc.M109.037846.

268. Bulut, Y.; Michelsen, K. S.; Hayrapetian, L.; Naiki, Y.; Spallek, R.; Singh, M.; Ardit, M. Mycobacterium tuberculosis heat shock proteins use diverse toll-like receptor pathways to activate pro-inflammatory signals. *J. Biol. Chem.* **2005**, *280*, 20961–20967, doi:10.1074/jbc.M411379200.
269. Auricchio, G.; Garg, S. K.; Martino, A.; Volpe, E.; Ciaramella, A.; De Vito, P.; Baldini, P. M.; Colizzi, V.; Fraziano, M. Role of macrophage phospholipase D in natural and CpG-induced antimycobacterial activity. *Cell. Microbiol.* **2003**, *5*, 913–920, doi:10.1046/j.1462-5822.2003.00330.x.
270. Peiser, L.; Gough, P. J.; Kodama, T.; Gordon, S. Macrophage class A scavenger receptor-mediated phagocytosis of Escherichia coli: Role of cell heterogeneity, microbial strain, and culture conditions in vitro. *Infect. Immun.* **2000**, *68*, 1953–1963, doi:10.1128/IAI.68.4.1953-1963.2000.
271. Ibarra, J. A.; Steele-Mortimer, O. Salmonella - the ultimate insider. Salmonella virulence factors that modulate intracellular survival. *Cell. Microbiol.* **2009**, *11*, 1579–1586, doi:10.1111/j.1462-5822.2009.01368.x.
272. Zhai, W.; Wu, F.; Zhang, Y.; Fu, Y.; Liu, Z. The immune escape mechanisms of Mycobacterium Tuberculosis. *Int. J. Mol. Sci.* **2019**, *20*, doi:10.3390/ijms20020340.
273. Vergne, I.; Chua, J.; Deretic, V. Mycobacterium tuberculosis phagosome maturation arrest: Selective targeting of PI3P-dependent membrane trafficking. *Traffic* **2003**, *4*, 600–606, doi:10.1034/j.1600-0854.2003.00120.x.
274. Pérez-Rodríguez, S.; García-Aznar, J. M.; Gonzalo-Asensio, J. Microfluidic devices for studying bacterial taxis, drug testing and biofilm formation. *Microb. Biotechnol.* **2021**, doi:10.1111/1751-7915.13775.
275. Turner, M. D.; Nedjai, B.; Hurst, T.; Pennington, D. J. Cytokines and chemokines: At the crossroads of cell signalling and inflammatory disease. *Biochim. Biophys. Acta - Mol. Cell Res.* **2014**, *1843*, 2563–2582, doi:10.1016/j.bbamcr.2014.05.014.
276. Deshmane, S. L.; Kremlev, S.; Amini, S.; Sawaya, B. E. Monocyte chemoattractant protein-1 (MCP-1): An overview. *J. Interf. Cytokine Res.* **2009**, *29*, 313–325, doi:10.1089/jir.2008.0027.
277. Zhang, T.; Yu, J.; Zhang, Y.; Li, L.; Chen, Y.; Li, D.; Liu, F.; Zhang, C. Y.; Gu, H.; Zen, K. Salmonella enterica serovar enteritidis modulates intestinal epithelial mir-128 levels to decrease macrophage recruitment via macrophage colony-stimulating factor. *J. Infect. Dis.* **2014**, *209*, 2000–2011, doi:10.1093/infdis/jiu006.
278. Kim, H. J.; Huh, D.; Hamilton, G.; Ingber, D. E. Human gut-on-a-chip inhabited by microbial flora that experiences intestinal peristalsis-like motions and flow. *Lab Chip* **2012**, *12*, 2165–2174, doi:10.1039/c2lc40074j.
279. Kim, H. J.; Li, H.; Collins, J. J.; Ingber, D. E. Contributions of microbiome and mechanical deformation to intestinal bacterial overgrowth and inflammation in a human gut-on-a-chip. *Proc. Natl. Acad. Sci. U. S. A.* **2016**, *113*, E7–E15, doi:10.1073/pnas.1522193112.
280. Thacker, V. V.; Dhar, N.; Sharma, K.; Barrille, R.; Karalis, K.; McKinney, J. D. A lung-on-chip model of early M. tuberculosis infection reveals an essential role for alveolar epithelial cells in controlling bacterial growth. *Elife* **2020**, *9*, 1–22, doi:10.7554/elife.59961.
281. Persat, A.; Nadell, C. D.; Kim, M. K.; Ingremeau, F.; Siryaporn, A.; Drescher, K.; Wingreen, N. S.; Bassler, B. L.; Gitai, Z.; Stone, H. A. The mechanical world of bacteria. *Cell* **2015**, *161*, 988–997, doi:10.1016/j.cell.2015.05.005.
282. Mantha, S.; Pillai, S.; Khayambashi, P.; Upadhyay, A.; Zhang, Y.; Tao, O.; Pham, H. M.; Tran, S. D. Smart Hydrogels in Tissue Engineering and Regenerative Medicine. *Materials (Basel)*. **2019**, *12*, 33.
283. de Angelis, I.; Turco, L. Caco-2 cells as a model for intestinal absorption. *Curr. Protoc. Toxicol.* **2011**, 1–15, doi:10.1002/0471140856.tx2006s47.
284. Smith, B. T. Cell line A 549: A model system for the study of alveolar type II cell function. *Am. Rev. Respir. Dis.* **1977**, *115*, 285–293, doi:10.1164/arrd.1977.115.2.285.
285. Iqbal, A. J.; McNeill, E.; Kapellos, T. S.; Regan-Komito, D.; Norman, S.; Burd, S.; Smart, N.; Machemer, D. E. W.; Stylianou, E.; McShane, H.; Channon, K. M.; Chawla, A.; Greaves, D. R. Human CD68 promoter GFP transgenic mice allow analysis of monocyte to macrophage differentiation in vivo. *Blood* **2014**, *124*, e33–e44, doi:10.1182/blood-2014-04-568691.